Spring 2009

Study of the DNA Damage Complexes Within the HTLV-1 Tax Oncoprotein Interactome

Sidi Mehdi Belgnaoui
Old Dominion University

STUDY OF THE DNA DAMAGE COMPLEXES WITHIN THE HTLV-1 TAX ONCOPROTEIN INTERACTOME

by

Sidi Mehdi Belgnaoui
B.S. July 2004, Albright College

A Dissertation Submitted to the Faculty of
Eastern Virginia Medical School and Old Dominion University
in Partial Fulfillment of the
Requirement for the Degree of

DOCTOR OF PHILOSOPHY

BIOMEDICAL SCIENCES

EASTERN VIRGINIA MEDICAL SCHOOL
OLD DOMINION UNIVERSITY
December 2009

Approved by:

O. John Semmes (Director)

Richard Drake (Member)

Julie Kerry (Member)

Neel Krishna (Member)

ABSTRACT

STUDY OF THE DNA DAMAGE COMPLEXES WITHIN THE HTLV-1 TAX ONCOPROTEIN INTERACTOME

Sidi Mehdi Belgnaoui
Eastern Virginia Medical School and Old Dominion University, 2009
Director: Dr. O. John Semmes

Human T-cell leukemia virus type 1 (HTLV-1) is a transforming retrovirus that can give rise to adult T-cell leukemia (ATL) and HTLV-1 associated myelopathy/tropical spastic paraparesis (HAM/TSP). Tax is a virally encoded oncoprotein that is involved in HTLV-1 mediated cellular transformation. It has been hypothesized that Tax induces genomic instability via repression of the cellular DNA damage repair response. Our laboratory has previously shown that the interaction between Tax and various proteins involved in the DNA-damage response pathway impairs the ability of these proteins to mount an efficient repair response. As part of these observations, we proposed that Tax induces a constitutive phosphorylation state in the DNA-dependent Protein Kinase (DNA-PK) which effectively saturates the naive response to new DNA damage events.

In this study, using Liquid Chromatography-Mass Spectrometry, we determined that the mediator of DNA damage checkpoint protein 1 (MDC1) is also part of the Tax-bound complex. MDC1 is a DNA damage repair (DDR) protein that is found in nuclear foci called ionizing radiation-induced foci (IRIF) that form in response to DNA damage. In this study we show that MDC1, which is a part DNA-PK-MDC1 signaling pathway, is active in Tax expressing cells. In addition, we demonstrate that Tax recruits MDC1 to "Tax speckled structures" (TSS). The same observation was made when the localization of other DDR proteins such as DNA-PK were examined. These results suggest an ability

of Tax to generate a damage-independent DDR response. Here, we demonstrate that MDC1 is recruited away from the TSS to the IRIF following damage, whereas DNA-PK phosphorylated at threonine 2609, an activated form of DNA-PK, and BRCA1 were shared between the two entities. These results suggest that there is a limited amount of MDC1 in the cell that is competed for between TSS and IRIF. One potential impact of generating a damage independent DDR response is competitive sequestering of components of the DDR away from the actual sites of damage. This competitive recruitment of cellular DDR may explain the observation that Tax expression results in genomic instability.

This dissertation is dedicated to my father, mother, two brothers and, last but not least, to my wonderful wife.

ACKNOWLEDGMENTS

I would like to thank my committee members, Dr. Julie Kerry, Dr. Neel Krishna and Dr. Richard Drake, and especially my adviser Dr. O. John Semmes for their guidance and mentoring. I would also like to acknowledge current and past members of my laboratory, Dr. Abdelali Haoudi, Dr. Julius Nyalwidhe, Dr. Kimberly Fryrear, Dr. Xin Guo, Yvonne Oden, Michael Ward, Jessica Tiedebohl, and Robert Mitchell, who provided technical and moral support throughout my studies.

TABLE OF CONTENTS

Page

Page

LIST OF FIGURES

Figure Page

SECTION 1

INTRODUCTION

Retroviruses

The *Retroviridae*, or retroviruses, are RNA viruses that are capable of infecting all vertebrates. Retroviruses are enveloped viruses that possess a single stranded RNA genome, and replicate via a DNA intermediate. Each virion has two copies of the genome. They may be divided into simple and complex retroviruses according to the organization of their genomes. All retroviruses possess four virally encoded genes. These are the *gag* gene, which encodes the virion structural proteins, the *pol* gene, which encodes the various virion-associated enzymes (reverse transcriptase and integrase), the *env* gene, which encodes the envelope glycoprotein, and the *pro* gene, which encodes the virion protease. Simple retroviruses typically carry only this elementary information, while complex retroviruses incorporate in their genomes some additional regulatory genes (1). They are characterized by a very unique life cycle. Following the entry of the virion into the host cell, the genomic RNA is reverse transcribed into DNA, which is then incorporated into the host's genome. The integrated viral DNA is then called the *provirus*, and it will be used as a template for the production of new viral RNAs and proteins, ultimately leading to the formation of new virions. Immature virions, which are characterized by the presence of unprocessed precursor proteins, are first released from the infected cells. Maturation consists of the cleavage of these precursor proteins and leads to a change in structure and morphology of the virion (2). The cleavage of Gag, Pol

---

The model journal for this dissertation is *The Journal of Biological Chemistry.*

and Env precursor proteins eventually produces the proteins that will form the mature infectious virion (Fig. 1). Processing of the Gag precursor will give rise to the matrix protein (MA), the capsid protein (CA) and the nucleocapsid protein (NC). The cleavage of the Pol precursor gives rise to PR for protease, RT for reverse transcriptase and IN for integrase. Finally, processing of the Env precursor produces the surface protein (SU) and the transmembrane protein (TM) (3). In addition to the viral proteins, each virion contains two identical, positive-sense, single-stranded RNA molecules that are each 7 to 13 kilobases (kb). The last component of the virion is the envelope, which is a lipid bilayer that has been acquired from the host plasma membrane during the budding process.

Human T-Cell Leukemia Virus Type 1

Human T-Cell leukemia virus type 1 (HTLV-1) belongs to the family *Retroviridae* and was the first human retrovirus to be discovered (4). The life cycle of HTLV-1 is similar to that of other retroviruses. It starts with the interaction of the envelope glycoprotein on the virion with specific host-cell membrane proteins. This allows the viral envelope to fuse with the plasma membrane of the cell. The lipid membrane of the virus incorporates in the cell's membrane and the core enters the host cell. The core contains the viral genetic material as well as enzymes that participate in the first stages of viral replication. The viral reverse transcriptase allows the conversion of the viral RNA into double stranded DNA. The double stranded viral DNA then enters the nucleus and is integrated into the host cell's chromosomal DNA by the viral integrase. The *provirus* is then transcribed by the host cell RNA polymerase, generating mRNAs

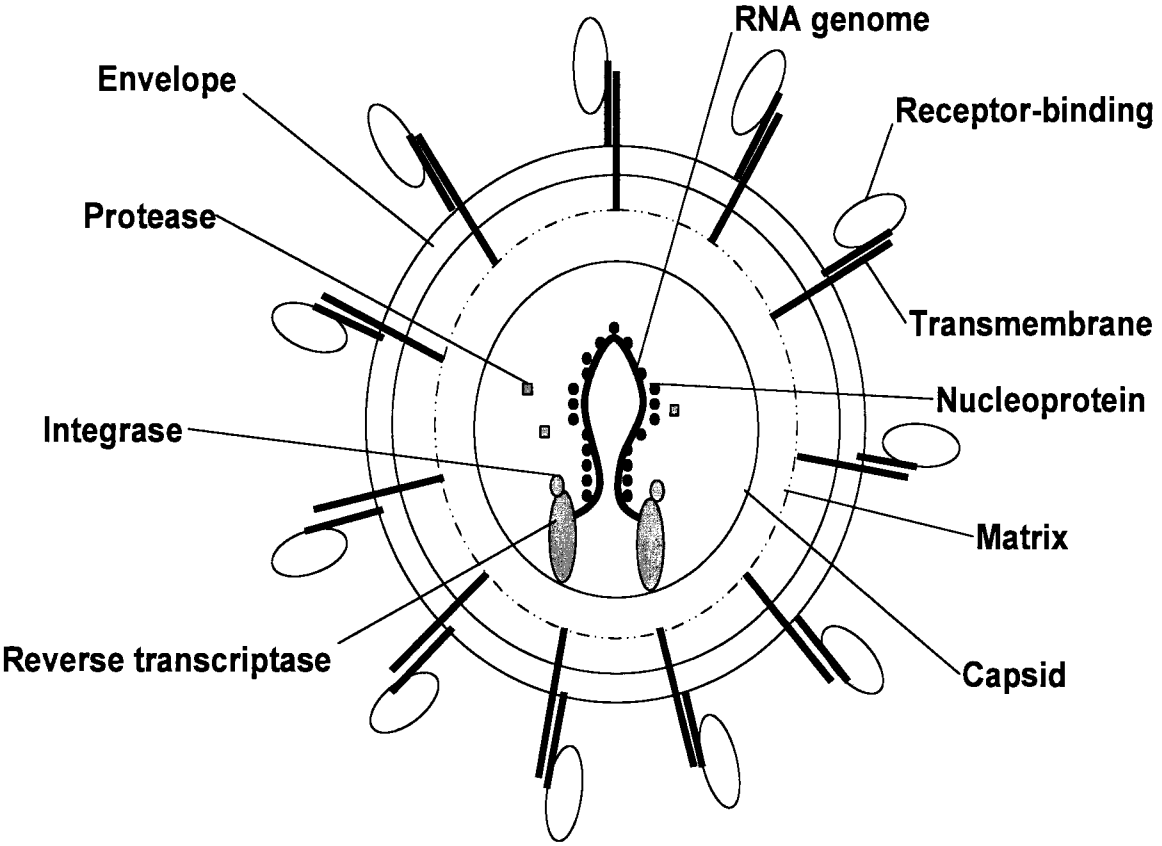

FIGURE 1. **General structure of a retrovirus.** Schematic representation of a mature retrovirus

and genomic RNA molecules. The host-cell machinery translates the viral mRNAs into virion proteins which assemble with genomic RNA to form progeny nucleocapsids. The nucleocapsids interact with the membrane-bound viral glycoproteins and bud from the host cell (1).

HTLV-I is a complex retrovirus and belongs to the delta-type retroviruses, which also include bovine leukemia virus, human T-cell leukemia virus type II (HTLV-II), and simian T-cell leukemia virus (5). In 1983, the virus was successfully cloned and the complete sequence of the 9 kb proviral genome was resolved (6). In addition to two long terminal repeats (LTRs), the HTLV-1 genome encodes *gag*, *pol*, and *env* genes, as well as a unique region, designated *pX* (Fig. 2*A*). Therefore, instead of the LTR-gag-pol-env-LTR genome organization of replication competent simple retroviruses, HTLV-1 has a LTR-gag-pol-env-pX-LTR genomic structure (7). The *pro* gene spans the 3' part of the *gag* region and the 5'part of the *pol* region, and a ribosomal frameshift is used to express the protease as part of the Gag polyprotein precursor (8). The *pX* region can encode multiple proteins using alternative open reading frames. These are the accessory proteins $p12^{I}$ expressed from ORF I, $p13^{II}$ and $p30^{II}$ from ORF II and the regulatory proteins Rex and Tax from ORF III and ORF IV, respectively (9). The accessory proteins are not essential for viral replication *in vitro*, but they appear to be crucial for viral persistence *in vivo* (9). On the other hand, Tax and Rex regulatory proteins are known to be critical for viral replication (9). The 27 kD Rex protein acts at the post-transcriptional level and modulates gene expression. The 40 kD Tax protein is a strong *trans*-activator of viral gene expression (10).

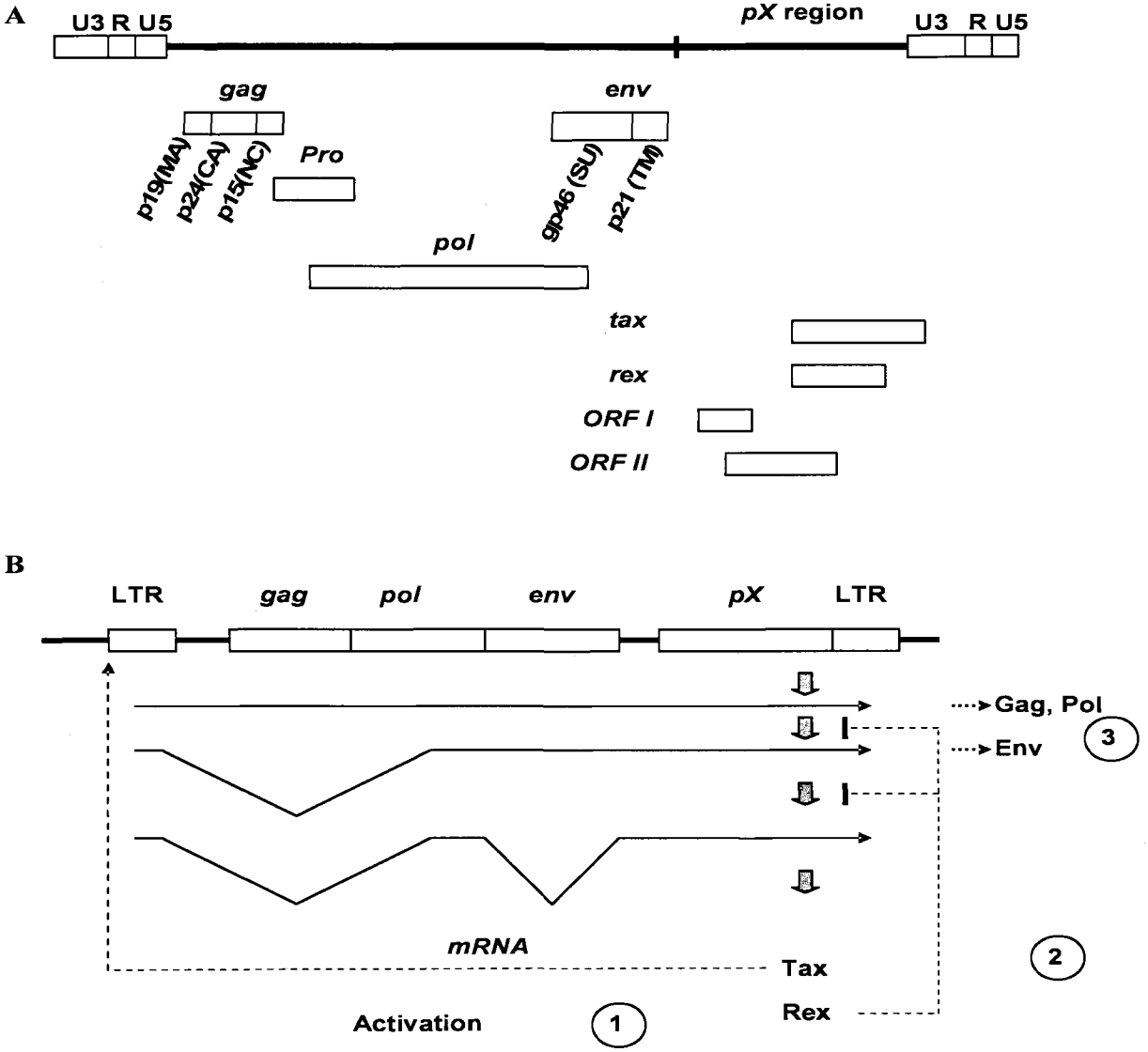

FIGURE 2. **The HTLV-1 genome.** *A*, structure of the HTLV-1 genome. *B*, feedback mechanism. Tax is spontaneously expressed from the doubly spliced viral transcript (1), Tax activates viral transcription (2), Rex which is expressed from the same mRNA as Tax inhibits splicing of viral RNA (3), causing the accumulation of unspliced mRNAs, thus leading to expression of Gag, Pol and Env proteins. This also induces a sharp decrease in Tax and Rex expression.

HTLV-1 has a unique mode of regulation of its viral replication (Fig. 2*B*). First, an initial HTLV-1 transcript is fully spliced into the *pX* region, thus leading to Tax and Rex expression. Tax induces the *trans*-activation of the viral genome. This causes an accumulation of Rex, which inhibits the splicing of the viral transcripts. Consequently, unspliced *gag-pol-env* and *env* mRNAs are produced, leading to the expression of the viral structural proteins. In addition, inhibition of viral RNA splicing causes a decrease in fully spliced *pX* mRNA, resulting in a sharp decrease in Tax expression and ultimately to a downregulation of viral gene expression. This feedback mechanism ensures efficient viral gene expression at the initial stage of infection, and the subsequent decrease in gene expression allows the virus to escape detection by the host immune system (7).

Cellular Tropism and Viral Entry

A variety of cell types can be infected by HTLV-1, such as T-lymphocytes, B-lymphocytes, monocytes and fibroblasts (11). It has been determined that glucose transporter-1 (GLUT-1), which is a ubiquitous cell surface receptor, is a receptor for HTLV-1 (12). HTLV-1 provirus is mostly detected in $CD4^+$ T lymphocytes and to a lesser extent in $CD8^+$ T cells (13). This might be explained by the fact that Tax causes an increase in CD4+ T cell proliferation and inhibits apoptosis in those same cells (14). It is believed that HLTV-1 spreads through cell-to-cell transmission. This hypothesis is supported by the fact that no virions can be detected in the serum of HTLV-1-infected individuals. Moreover, infectivity of infected cells is much higher than that of free virions (15-17). *In vitro* studies have shown that HTLV-1-infected cells form "virological synapses" with uninfected cells. These structures allow contact between infected and

uninfected cells and cause the accumulation of the viral proteins Gag and Env as well as viral RNA. Ultimately, this leads to the transfer of the virus to the uninfected cells through the "virological synapses" (16).

Epidemiology

About 10 to 20 million people worldwide are currently infected with HTLV-1 (18). HTLV-I is endemic in southwestern Japan, the Caribbean islands, the areas surrounding the Caribbean basin, and Central Africa. In addition, there are HTLV-I carriers in South America, Papua New Guinea, and the Solomon Islands (19). Japan has approximately 1.2 million individuals infected with HTLV-1 (20).

There are three major routes of HTLV-1 infection. The infection is spread primarily from mothers to their children, most commonly through milk (21-25). HTLV-1 can also be transmitted sexually from infected men to women via virus-infected cells present in semen (26, 27). Transmission from women to men is very rare (1). Parenteral transmission is the third route of transmission (1). This mode of transmission accounts for the high frequency of intravenous drug users that have become infected (28-33).

Diseases of HTLV-I Infection

HTLV-1 was the first retrovirus to be shown to cause a human cancer, adult T-cell leukemia (ATL) (19). HTLV-1 infection induces another incurable life threatening disease called HTLV-1–associated myelopathy and tropical spastic parapesis (HAM/TSP) (34).

Adult T-cell leukemia

In the 1970s, adult T-cell Leukemia (ATL) was first described due to a geographical clustering of leukemias in southwestern Japan (19). In 1980 and 1981, human T-cell Leukemia virus was isolated and identified as the exclusive causal agent of ATL (4). The link between ATL and HTLV-1 was established by showing the presence of an antibody against HTLV-1 in sera from a patient with ATL and the finding of proviral DNA in ATL cell lines (35, 36). Soon after infection, the virus goes into a latent state, making the infected individuals asymptomatic seropositive carriers. About 5% of these individuals develop one of the viral-associated diseases 10 to 40 years after infection (37). In Japan, 800 to 1000 new ATL cases are diagnosed every year (20). Despite intensive chemotherapy, aggressive ATL is a disease with a poor prognosis (38). Study of the molecular pathogenesis of HTLV-1-mediated T-cell transformation is crucial to improve ATL treatment regimen.

The viral Tax protein is considered to play a central role in the process leading to ATL (37). It is thought that Tax causes transformation through various mechanisms which include the induction of chromosomal instability and the abrogation of DNA repair (20). ATL's mean age of onset of disease is 55 (39). There are four clinical subtypes of ATL: acute, chronic, smoldering and lymphoma types. The subtypes are determined according to the following criteria: the number of abnormal T cells in peripheral blood, serum lactic acid dehydrogenase (LDH) level, tumor lesions in various organs, and clinical course (40-42). Symptoms of the acute type of ATL, which represents 55% of all cases, include general malaise, fever, cough, dyspnea, abdominal fullness, thirst,

drowsiness, lymph node enlargement, hepatosplenomegaly and jaundice, as well as abnormal laboratory findings such as marked leukocytosis, hypercalemia, high serum levels of LDH, a soluble form of interleukin-2 receptor (IL-2R) α chain, and the presence of distinctive leukemic cells with lobulated nuclei (39, 40, 43). Following onset of ATL, combination chemotherapy often leads to transient remission of the disease. The median survival time for patients diagnosed with the acute type of ATL is only 6.2 months (40).

HTLV-1 associated myelopathy/tropical spastic paraparesis and other diseases

HAM/TSP was first diagnosed in 1985 by two independent groups (44, 45). HAM/TSP occurs in about 1 in 1646 HTLV-1-seropositive individuals, and the time between HLTV-1 infection and the onset of the disease range from months to decades (46). Developing both ATL and HAM/TSP at the same is a very rare occurrence. Symptoms of HAM/TSP are spasticity of lower extremities, urinary bladder disturbance, lower muscle weakness, and sensory disturbance with poorly defined thoracic sensory levels (45). Furthermore, patients with HAM/TSP have HLTV-1 antibodies in the serum and cerebrospinal fluid (CSF), a mild lymphocyte pleocytosis in CSF, and lymphocytes with lobulated nuclei in the blood and/or CSF. The median survival time of patients who develop HAM/TSP is about 10 years, and death is in general due to complications like infections and cancers (44-46).

Other HTLV-1 associated diseases include HTLV-1 uveitis (HAU) and HTLV-1 associated arthropathy (HAAP) (47). Symptoms of HAU are blurred vision or myodysopsia with acute or sub-acute onset, iritis, vitreous opacities, retinal vasculitis, and retinal exudates and hemorrhages (48). In HAAP, HTLV-1 antibodies are detectable

in synovial fluids of the affected joints and HLTV-1 proviral DNA is found in both synovial tissue and in synovial fluid lymphocytes (49). Other diseases that have been linked to HTLV-1 infections are polymyositis, chronic respiratory diseases, lymphadenitis and dermatitis (47).

Diagnosis of HTLV-1 infection

Antibody screening is a commonly used method to diagnose HTLV-1 infection. Commercial enzyme immunoassay (EIA) or particle agglutination assays are available to detect HTLV-1 antibodies (50). When first introduced, EIAs generated a relatively high number of false positive results (51). However, more recent EIAs that use recombinant proteins and/ or synthetic HLTV-1 peptides have been much more reliable (52). Nonetheless, it is still recommended to perform a confirmatory assay following EIAs in order to discriminate between false positive and positive results (52). Confirmation tests include indirect immunofluorescence assays and western blots (52, 53). One issue with these confirmatory tests is that they cannot always distinguish between HTLV-1 and HTLV-2 (54). The assay of choice for detection of HLTV-1 infection is PCR. These PCR assays are often based on *tax*, which is the most conserved region of HTLV-1 (55, 56). In addition, real-time PCR, which allows quantifying the proviral load, is frequently used as a marker for prognosis and disease progression of infected people (57-61).

The Tax Oncoprotein

Tax is a viral oncoprotein that is crucial for the initial stages of viral mediated-transformation of T-cell after HTLV-1 infection (20). Tax can bind the Tax-responsive

element (TRE-1) in the viral long terminal repeats (LTRs) and *trans*-activate viral gene expression (62). In parallel, Tax can also *trans*-activate a variety of cellular genes, which leads to a variety of changes in the cell (62-66). Tax also interferes with cell function through interactions with proteins involved in different cellular functions, such as DNA damage repair and cell cycle (67). In the cell, Tax is mostly present in the nucleus and forms what are called Tax speckled structures (TSS) (68). However, it should be noted that a considerable portion of Tax is also present in the cytoplasm (69).

Transforming potential of Tax

The viral Tax protein is considered to play a crucial role in the process leading to ATL (37). Many studies on the oncogenic potential of Tax in cultured cells and animal models have been done. It was shown that Tax is able to induce neoplastic transformation of the rat fibroblast cell line Rat-1 (70) and the mouse fibroblast NIH/3T3 line (71). Furthermore, Tax can immortalize primary human T-cells derived from peripheral blood or cord blood (72, 73). This has been shown by transducing cells with Tax expressed from rhadinoviral (72) or retroviral (73) vectors. These results highlight the central role of Tax in the transformation process.

Genomic instability is thought to play a crucial role in the process of carcinogenesis (74). HTLV-1-transformed ATL cells show a variety of chromosomal abnormalities including duplication, deletions, translocations, rearrangement and aneuploidy (75). Due to the critical role of Tax in HTLV-1-induced oncogenesis, it is believed that Tax has a detrimental effect on the integrity and stability of the cellular genome. One proposed mechanism by which Tax induces genomic instability is the

abrogation of DNA repair. The association between Tax and the presence of DNA damage was first demonstrated using a micronucleus formation assay (76). It was shown that Tax induces micronuclei formation, which represents fragmented chromosomes indicative of DNA damage, or defects in DNA repair or in chromosomal segregation (76). Additionally, gene amplification was used to determine the effect of Tax on genomic stability. Gene amplification is a known indicator of genomic instability. It was shown that that there was a five-fold increase in gene amplification in Tax-expressing cells, which indicated that Tax expression contributes to genomic instability (77). Together, these results show that Tax induces genomic instability; however, the precise mechanism remains to be determined.

Tax affects a variety of cellular functions such as cell cycle regulation, transcription and the DNA damage repair pathway (75). Tax-mediated transformation is the result of its ability to both transcriptionally regulate cellular genes expression and to functionally inactivate proteins involved in cell-cycle progression and DNA repair (75). Tax oncogenic activity is accomplished through transcriptional activation and protein-protein interaction with cell cycle regulators (75).

Tax is a viral and cellular trans-activator

Tax was initially discovered as a *trans*-activator of HTLV-1 gene expression (78). Tax is able to *trans*-activate viral gene expression by *trans*-activating the viral long terminal repeats (LTR). In addition, Tax can also *trans*-activate various cellular genes through complex interaction with cyclic AMP-responsive element binding protein (CREB), CREB-response elements (CRE), and transcriptional coactivators CREB-

binding protein (CBP), p300 and P300/CBP-associated factor (PCAF) (62-66). Tax has also been shown to activate transcription from a number of critical cellular genes through the NF-κB pathway (79-81). Tax induces persistent activation of the NF-κB pathway by directly binding and stimulating IκB kinase γ (IKKγ), which in turn phosphorylates IκB, causing its degradation (79-81). The role of IκB is to sequester NF-κB in the cytoplasm, but Tax causes its degradation, thus allowing NF-κB to enter the nucleus and cause the activation of the NF-κB pathway.

Tax dysregulates the cell cycle

Tax-induced genomic instability is partly the result of cell cycle dysregulation. Progression through cell cycle is a tightly controlled process which is crucial for proper replication and chromosomal segregation (82). Impairment of these two mechanisms can cause genomic instability. Tax affects the cell cycle through transcriptional activation and direct interaction with cell cycle regulatory proteins (75). The effects of Tax on the cell cycle lead to accelerated progression through G1 phase, coupled with defects in G1/S, S, G2/M and M checkpoints (83-87). Tax activates cyclin-dependent kinases (Cdks) such as Cdk 4 and 6 through direct interaction which results in retinoblastoma (Rb) protein hyperphosphorylation (88, 89). Once phosphorylated, Rb releases the E2F1 transcription factor, leading to accelerated cell-cycle transition from G1 to S (90, 91). In addition, our laboratory showed that Tax expression causes an accumulation of cells in G2/M, which suggested that Tax abrogates the G2/M checkpoint (92). In fact, our laboratory also established in the same study that Tax colocalizes and interacts with Chk2, causing its activation which leads to the observed G2/M accumulation. These examples show that

Tax is able to dysregulate different stages of the cell cycle which ultimately can lead to genomic instability.

Tax and the DNA repair machinery

Loss of genomic integrity through Tax is partly due to its effect on the cell cycle. Tax also causes genomic instability through the impairment of the DNA damage repair pathway. DNA damage repair is crucial to maintain the integrity of the genome. As cells divide, DNA can be damaged by environmental factors or as a result of nucleotide misincorporation during replication (75). A properly functioning DNA damage repair pathway ensures that daughter cells do not inherit any mutations (75). DNA damage can be repaired by different pathways such as nucleotide excision repair (NER), base excision repair (BER), mismatch repair (MMR), and double strand break repair (75). The first link between Tax and DNA repair was made when it was shown that Tax represses the transcription of the human DNA polymerase β (pol β) promoter (93), an enzyme involved in BER and MMR (94). In addition, Tax has also been shown to suppress NER (95), and this correlates with its ability to activate transcription of the proliferating cell nuclear antigen (PCNA) (96, 97).

Our laboratory has previously shown that Tax interacts with and functionally alters DNA-dependent Protein Kinase (DNA-PK) (98). The predominant DSB repair pathway in mammalian cells is the non-homologous end joining (NHEJ) pathway, in which broken DNA ends are rejoined. DNA-PK is the key enzyme in the NHEJ pathway of DSB repair (99-102). We found that the kinase activity of DNA-PK is increased in the presence of Tax (98). Furthermore, Tax induced hyperphosphorylation of DNA-PK at

S2056 and T2609, and co-localized with these phosphorylated forms in nuclear foci (98). We also demonstrated that DNA-PK activity mediates Tax activation of Chk2 (98), which is a known target of DNA-PK phosphorylation (103).

Another known target of DNA-PK is the histone protein H2AX. DNA damage induces histone H2AX phosphorylation by ATM, ATR and DNA-PK (104). Phosphorylated H2AX (termed γ-H2AX) contributes to DNA double strand break repair. The mechanism behind the role of γ-H2AX in DNA repair is not yet fully understood, but γ-H2AX is thought to be a sensor of damage and recruiter of DNA damage repair proteins (104). Another important aspect of γ-H2AX, which is not yet fully understood, is that it needs to be dephosphorylated once the repair has been completed (105, 106). Our laboratory has shown that, in the presence of Tax alone, there is dramatic increase in the level of γ-H2AX compared to cells that do not express Tax (98). At first, it seems that the presence of γ-H2AX would stimulate DNA repair, but as mentioned earlier, for proper repair γ-H2AX needs to also be dephosphorylated. This suggests that by causing persistent phosphorylation of H2AX, Tax does not allow the cell to detect and repair newly formed damage.

MDC1 is another crucial protein involved in the repair of DNA double strand breaks. In the studies described in this dissertation, we determined that Tax interacts with the mediator of DNA damage checkpoint protein 1 (MDC1). Following DNA damage, MDC1 binds directly to the phosphorylated form of H2AX at serine 139 and recruits downstream DNA damage repair proteins to the damage sites such as 53BP1 and NBS1 which is part of the MRE11–RAD50–NBS1 (MRN) complex (107, 108). MDC1 also recruits RNF8, a RING-finger ubiquitin ligase, which in turn ubiquitylates H2AX (109,

110). This induces a change in chromatin conformation causing the DNA to "open up", which allows the recruitment of downstream DNA damage repair proteins (109, 110). In addition, MDC1 knockdown cells display a shortened duration of H2AX phosphorylation, suggesting that it may protect H2AX from dephosphorylation (108). Furthermore, MDC1 directly interacts with DNA-PK and regulates its autophosphorylation at T2609 in response to DNA damage (111). Another study on MDC1 demonstrated that it not only binds Chk2 through the phosphorylated threonine 68 of Chk2, but this binding was shown to be essential for Chk2-mediated DNA damage responses (112). Finally, the central role of MDC1 is illustrated by the fact that MDC1 -/- mice demonstrate many phenotypes of H2AX -/- mice, including growth retardation, male infertility, immune defects, chromosome instability, DNA repair and radiation sensitivity (113). Tax interaction with such an essential protein of the DNA damage repair pathway suggests that it may alter MDC1's function, which could disrupt the entire pathway. This may partially explain the mechanism by which Tax interferes with the DNA damage repair machinery, which leads to genomic instability and cellular transformation.

SECTION 2

SPECIFIC AIMS

Human T-cell leukemia virus type 1 (HTLV-1) is a human transforming retrovirus. HTLV-1 is the causative agent of adult T-cell leukemia (ATL), and a neurodegenerative disease, HTLV-1 associated myelopathy/tropical spastic paraperesis (HAM/TSP) (19, 34). Research has shown that expression of the viral oncoprotein Tax alone can cause cellular transformation (114). Tax is a potent *trans*-activating protein of viral and cellular genes (62-66, 78). The mechanism behind Tax's oncogenic activity is not fully understood, but it is has been established that Tax directly interacts with many cellular proteins which affects various cellular processes (67).

One major characteristic of HTLV-1 transformed cells is genomic instability. It is thought to be a direct effect of Tax and an essential process for cellular transformation. Our laboratory has shown the interaction between Tax and various DNA damage repair (DDR) proteins such as Chk2 and DNA-PK (92, 98). These proteins interact with Tax in discrete nuclear foci called "Tax speckled structures" (TSS) (68, 115). In a normal cell, following DNA damage, DDR proteins get recruited to the DNA damage sites called ionizing radiation-induced nuclear foci (IRIF) (104). TSS and IRIF seem to share several proteins. One of these proteins is a DNA repair enzyme, DNA dependent protein kinase (DNA-PK) (98). It has been demonstrated that Tax induces DNA-PK activation which in turn causes phosphorylation of H2AX histone protein (called γ-H2AX) (98). Similarly, following DNA damage, DNA-PK gets recruited to the IRIF and phosphorylates H2AX

which induces a change in chromatin conformation allowing the recruitment of more DDR proteins (116, 117). This indicates that Tax mimics the DNA Damage repair pathway which may contribute to its dysregulation. Preliminary data have shown the presence of MDC1 (mediator of DNA damage checkpoint protein 1), another protein involved in the DNA damage response pathway, in the Tax interactome. Our study is the first one to directly link Tax and MDC1. MDC1 regulates various aspects of DNA damage response pathways and interacts with many proteins involved that same pathway such as DNA-PK and BRCA1 (107, 111, 112, 118, 119). MDC1 is crucial for IR-induced autophosphorylation of DNA-PK, which is important for H2AX phosphorylation and subsequent DNA damage repair (111). Additional evidence of the importance of MDC1 in H2AX phosphorylation is illustrated by the fact that the loss of MDC1 expression or the decrease of its cellular levels by short interfering RNA (siRNA) treatments leads to the reduction of H2AX phosphorylation in response to IR (107, 108, 113). MDC1 is also involved in the Chk2-mediated DNA damage response (112). MDC1 was found not only to bind Chk2 through the phosphorylated Thr68 of Chk2, but this binding was also shown to be essential for Chk2-mediated DNA damage responses (112). As mentioned earlier, MDC1 seems to play an important role in phosphorylation of H2AX, but in addition, it has also been demonstrated that MDC1 is crucial for H2AX ubiquitylation (109). H2AX ubiquitylation, though not as studied and known as H2AX phoshorylation, is a crucial step in the DNA damage repair mechanism (110). Knowing that MDC1 is present in the Tax interactome and that it has a central role in the DNA damage response pathway through its interaction with DNA-PK, Chk2 and H2AX, we will focus in this dissertation

on the role of MDC1 in the Tax induced dysregulation of the DNA damage response pathway.

Analysis of the functional and physical interactions of Tax can advance our understanding of the mechanism behind Tax-induced genomic instability. The *objective* of this proposal was to investigate the structural and functional characteristics of the DNA damage complexes within the Tax interactome. The *hypothesis* of the research was that Tax interacts with and functionally alters cellular proteins involved in the DNA damage response pathway. This study should make a significant contribution to our understanding of how Tax transforms cells.

The *objective* of this proposal was accomplished by pursuing the following specific aims:

AIM 1. Characterization of Tax-containing protein complexes involved in the DNA damage response.

To establish the different cellular process that are influenced by Tax, it is essential to determine the various proteins that are part of the Tax interactome. We will isolate Tax using a transient expression model followed by purification of Tax complexes. The components of the Tax complexes will be characterized using mass spectrometry.

AIM 2. Structural characterization of MDC1 within the Tax complexes.

We will determine whether Tax interacts with MDC1. We will also look at the localization of both Tax and MDC1 within the cell. Since Tax is a *trans*-activator, we will determine whether it has an effect on MDC1 expression. We will investigate the effect of Tax on known downstream targets of MDC1 such ubiquitylated γ-H2AX. Next, we will determine the effect of knocking down MDC1 in Tax-expressing cells. In

addition, studies of the structural modification of MDC1 will also be conducted in the presence or absence of Tax and DNA damage.

AIM 3. Determine the functional significance of the interaction of Tax with MDC1.

We will measure DNA damage in the presence of Tax after treatment with ionizing radiation (IR) and determine whether Tax impairs DNA repair. We will examine the biological consequence of the Tax-MDC1 interaction as it relates to genomic instability. We will also determine the localization of MDC1 and other DDR proteins in the Tax expressing cells in the presence of DNA damage.

SECTION 3

CHARACTERIZATION OF TAX-CONTAINING PROTEIN COMPLEXES INVOLVED IN THE DNA DAMAGE RESPONSE

Introduction

Human T cell leukemia virus-1 (HTLV-1) is the etiological agent of adult T-cell Leukemia (ATL) and HTLV-associated myelopathy/tropical spastic paraperisis (HAM/TSP) (19, 34). Tax, which is one of the HLTV-1 encoded proteins, plays a central role in viral transcription and cellular transformation (20, 114, 120, 121). All of these functions are carried out through a variety of protein-protein interactions. Tax was first discovered as a viral *trans*-activator (78). It is also known that Tax is a *trans*-activator for many cellular genes (122). In fact, Tax is able to deregulate expression of more than one hundred genes (122). Therefore, it is not surprising that Tax interacts with many transcriptional activators, basal transcription factors and proteins involved in chromatin remodeling (67). Briefly, the mechanism by which Tax *trans*-activates viral and cellular genes is as follows. In the viral genome, Tax alleviates transcriptional repression of the long terminal repeat (LTR) by directly interacting with histone deacetylases (HDAC1) and/or methyltransferases (HMT) (123-125). Next, Tax recruits via binding cAMP-responsive element/activating transcription factors (CREB/ATF), transcription factors, histone modifying enzymes and chromatin remodelers (SWI/SNF, P/CAF and CBP/p300) (67). Ultimately, this causes changes in the chromatin conformation, leading to the recruitment of basal transcription factors to the TATA box (67). In addition, Tax binds to the transcription factor IIA ($TF_{II}A$), transcription factor IID ($TF_{II}D$) and the TATA

binding protein (TBP) which stabilizes the initiation complex (126-128). This is followed by the recruitment by Tax of the positive transcription elongation factor b (P-TEFb) causing stimulation of elongation through the phosphorylation of the carboxy-terminal domain (CTD) of the RNA polymerase II (129). Furthermore, Tax also binds to SWI/SNF, which prevents stalling of transcription elongation (67, 130).

In addition to interacting with transcription factors and post-transcriptional regulators, it is also known that Tax binds a variety of proteins involved in cellular signaling (67). NF-κB signaling is one of the pathways that Tax influences via protein-protein interactions. There are two alternative NF-κB signaling pathways: the canonical and the non-canonical and both are stimulated by Tax (131-133). In the canonical pathway, Tax binds both IκB kinase γ/NF-κB essential modulator (IKKγ/NEMO) in the cytoplasm (80, 81). Tax also interacts and activates MAPK/ERK kinase kinase 1 (MEKK1) and TGF-β activating kinase 1 (TAK1) (134, 135). This leads to IKKα and IKKβ phosphorylation which in turn phosphorylate IκB, causing its proteosomal degradation (80, 81). Once degraded, IκB releases the NF-κB dimer, p50/RelA, which is then recruited to κB enhancers in the nucleus, ultimately leading to constant NF-κB activity (67). In the non-canonical pathway, Tax binds both IKKα and p100, causing p100 phosphorylation and subsequent ubiquitylation, allowing nuclear translocation of the p52/RelB dimer to the nucleus leading to NF-κB activation (131, 133).

Other signaling pathways affected by Tax through protein-protein interaction include JNK, AP-1 and TGF-β (67). In the JNK pathway, Tax binds G-protein pathway suppressor 2 (GPS2) which is an inhibitor of the JNK signaling. This leads to the inhibition of GPS-2 mediated inactivation of JNK signaling causing persistent activation

of the JNK pathway (136). In the AP-1 pathway, Tax binds and activates the phosphatidylinositol 3-kinase (PI3K) which in turn phosphorylates the Akt effector at serine 473 triggering the activation of AP-1 and cell proliferation (137). Finally, in the TGF-β signaling pathway, Tax interacts with Smad2, Smad3 and Smad4 (138). This ultimately leads to the inhibition of Smad3-Smad4 binding to TGF-β target genes thus inhibiting the induction of apoptosis by TGF-β (138, 139).

Lastly, Tax interacts with proteins involved in cell cycle and DNA damage repair (67). Tax can bind cyclin D1, cyclin D2, cyclin D3, CDK4 and CDK6 (88, 89, 140, 141). Tax interacts with and stabilizes the cyclinD2/CDK4 complex which then phosphorylates the retinoblastoma protein (Rb) (67). Tax also binds Rb directly and targets it for proteosomal degradation (142). E2F is then released by Rb which leads to an acceleration of G1/S transition (67). Finally, as mentioned earlier, Tax also interacts with proteins involved in the DNA damage repair pathway such as Rad51 (130), DNA topoisomerase 1 (143), Chk2 (92) and DNA-PK (98). Protein-protein interaction of DNA damage repair proteins with Tax can lead to the dysregulation of the DNA damage repair pathway. For instance, our laboratory determined that Tax not only binds DNA-PK but that it also causes its hyperphosphorylation at S2056 and T2609 (98). This leads to H2AX phosphorylation (termed γ-H2AX) which is an early double strand break marker. In Tax expressing cells, H2AX is maintained in a hyperphosphorylated state which interferes with the detection of new DNA breaks and the proper repair of these breaks (98). This process might contribute the Tax induced genomic instability.

The few examples mentioned above show that Tax interacts with numerous cellular proteins thus influencing various cellular processes such as transcription, cell

cycle regulation, DNA repair, and apoptosis (75, 130). It is clear that there are many more proteins present in the Tax interactome and identification of these Tax-binding proteins can give valuable information on the different pathways affected by Tax and on the mechanisms involved. The *objective* for this aim is to construct the Tax interactome. We accomplished this objective using the following experimental approaches. (1) We expressed and isolated Tax on beads; (2) We incubated the Tax isolate on beads with nuclear extracts in order to allow interaction of Tax with nuclear proteins; (3) We used mass spectrometry to identify proteins that interact with Tax. Using this approach, we found known Tax binding proteins (such as DNA-PK) and novel Tax binding proteins such as MDC1. We also found proteins involved in a variety of cellular pathways such as cell cycle, DNA damage repair and apoptosis. We attempted to classify the proteins according to their function in the cell.

Experimental Procedures

Cell culture and transient transfection

293T cells were maintained at 37°C in a humidified atmosphere of 5% CO_2 in air, in Iscove's modified Dulbecco's medium supplemented with 10% fetal bovine serum (Cambrex, East Rutherford, NJ) and 1% penicillin-streptomycin (Invitrogen, Carlsbad, CA).

Transfections of 293T cells were performed by standard calcium phosphate precipitation. Cells were plated at $1x10^5$ cells/ml. The following day, plasmid DNA in 2M $CaCl_2$ and 2X HBS were added dropwise to cells in fresh medium. Cells were incubated at 37°C overnight and fresh medium was added. The cells were harvested 48 h

post-transfection, following a single wash with 1X PBS, in 500 µl M-Per mammalian protein extraction reagent (Pierce, Rockford, IL) with protease inhibitor cocktail (Roche, Palo Alto, CA) and immediately frozen at –80°C.

Plasmids

Generation of the *STaxGFP* and *SGFP* plasmids have been described earlier (144). Briefly, the S-tagged expression vectors *STaxGFP* and *SGFP* were constructed by inserting the *tax-EGFP* fusion or *EGFP* ORF, respectively, into the *Sma*I site of *pTriEx4-Neo* (Novagen, Madison, WI) in frame with the amino-terminal S-tag and His-tag.

HPX Tax expression vector and *H2AX-GFP* vector were also used for the immunoprecipitation experiments. The *H2AX-GFP* vector was a gift from Dr. Tomilin (UC Davis School of Medicine, CA, USA).

Immunoblot analysis

Proteins separated by electrophoresis were transferred to Immobilon-P membranes (Millipore, Billerica, MA) using the semidry transfer method with 20 V applied for 1 hour. The membranes were then blocked for 1 hour at room temperature in 1x Odyssey blocking buffer (Li-Cor Biosciences, Lincoln, NE). Primary antibodies diluted in 1x Odyssey blocking buffer were applied to the membranes and allowed to interact at 4°C overnight on an orbital shaker. Membranes were washed four times for 5 minutes with PBS-1% Tween. Li-Cor Odyssey secondary antibodies were diluted to a concentration of 1/20,000 in 1x Odyssey blocking buffer containing 0.5% SDS and 0.5% Tween and then incubated for 1 hour at room temperature on an orbital shaker in the dark.

The membranes were washed four times for 5 minutes with PBS-1% Tween and then stored in PBS and in the dark until ready to be analyzed. Blots were scanned and analyzed with a Li-Cor Odyssey scanner and software (Li-Cor Biosciences, Lincoln, NE).

Antibodies

For immunofluorescence analysis the following antibodies were used: anti-IFI16 goat polyclonal (1/100, Santa Cruz Biotechnology, Santa Cruz, CA) and anti-MCM7 (1/100, Santa Cruz Biotechnology, Santa Cruz, CA). For immunoblot analysis, anti-GFP mouse monoclonal (1/500, Santa Cruz Biotechnology, Santa Cruz, CA) and anti-Tubulin mouse monoclonal (1/2000, Sigma, St. Louis, MO) were used.

Immunofluorescence

Cells that were plated on a coverslip were washed twice with ice cold PBS. Cells were then fixed with 4% paraformaldehyde for 12 minutes at room temperature. Next, cells were washed 3 times with PBS. Methanol was added and left on the cells for 2 minutes. Cells were washed 4 times with PBS. The primary antibody was diluted in 3% Bovine Serum Albumin (BSA) in PBS at the appropriate concentration. A 100 µl drop of the diluted primary antibody was then placed on parafilm in a wet chamber. The coverslip was then inverted onto the drop and left incubating at 4°C overnight. The next day, the coverslip was removed from the parafilm and placed back into the tissue culture dish. The cells were washed twice with PBS-1% Tween 20 and twice with PBS. Nuclei were counterstained with To-Pro-3 iodide (Invitrogen, Carlsbad, CA) diluted 1/1,000 in the 3% BSA in PBS by putting a 100 µl drop of the solution onto parafilm in a wet

chamber. The coverslip was inverted onto the drop and left incubating for 1 hour at room temperature in the dark. Next, the coverslip was put back into a tissue culture dish and washed twice with 3% BSA in PBS then twice with PBS. One drop of Vectashield mounting medium with DAPI (Vector Laboratories Inc, Burlingame, CA) was placed onto a slide. The coverslip was inverted onto the slide and left to air dry for one hour at room temperature in the dark. The coverslip was then sealed to the slide using nail polish. Confocal fluorescent images were acquired using a Zeiss LSM 510 confocal microscope at 63X magnification with a 2X zoom using Argon (488 nm), HeNe1 (543 nm), and HeNe2 (633 nm) lasers, and imaged with LSM Image Browser software (Carl Zeiss, Jena, Germany).

S-tag protein purification

Prepared cell lysate (750 µl) was incubated with 90 µl of 50% slurry of S-protein agarose (Novagen, Madison, WI) for 30 minutes rotating at room temperature, then washed 3 times with 1 ml Bind/Wash Buffer (20 mM Tris-HCl pH 7.5, 150 mM NaCl, 0.1% TritonX-100) by centrifugation at 4°C for 5 minutes each time at 500 *g* (2500 rpm). The washed beads were either eluted by resuspension in 45 µl Laemmli Sample Buffer (Bio-Rad, Hercules, CA) with β-mercaptoethanol, followed by boiling for 10 minutes or kept for incubation with Jurkat nuclear lysates. Beads that were eluted were then separated by electrophoresis in a 4%- to 12%-gradient sodium dodecyl sulfate (SDS) polyacrylamide gel. Following electrophoresis, the gel was stained with Biosafe™ Coomassie (Bio-Rad, Hercules, CA). Briefly, the gel was washed three times with sterile water for 5 minutes each, and then it was covered with Biosafe™ Coomassie and left

shaking for one hour. The gel was then washed twice with sterile water for 30 minutes each. The picture of the gel was then captured using Li-Cor Odyssey scanner and software (Li-Cor Biosciences, Lincoln, NE).

Tax bead nuclear lysate pull down

Freshly prepared STaxGFP/SGFP beads (200 µl) were thoroughly washed 3 times with 500 µl of ice cold incubation Buffer (IB; 25 mM HEPES, ph 6.5, 150 mM NaCl, 1% NP-40, 10 mM $MgCl_2$, 1 mM EDTA, 1% glycerol). The samples were spun at 5000 rpm at 4°C for each wash. After the final wash, enough IB was added to make a 50 % slurry. The resulting slurry was stored one ice. Next, the commercially available Jurkat nuclear lysate (Active motif, cat# 30614, 200 µg) was pre-cleared. To do so, 50 µl of unreacted S-beads were washed 3 times with ice cold incubation buffer. S-beads slurry (5 µl) was added to 25 µg of Jurkat nuclear lysate and incubated for 30 minutes at 4°C with mild shaking. The beads were centrifuged at 2000 *g* (5000 rpm) for 1 minute at 4°C and the supernatant was transferred to a fresh tube and 10 µl of STaxGFP or SGFP beads prepared earlier was added. The volume was brought to 50 µl with IB. Samples were then incubated for 60 minutes at 4°C with mild shaking. Next, the beads were centrifuged at 2000 *g* (5000 rpm) at 4°C for 3 minutes and the supernatant was carefully removed. Ice cold PBS (250 µl) was added and the beads resuspended by briefly vortexing. Samples were spun at 2000 *g* (5000 rpm) for 3 minutes at 4°C and the supernatant was discarded. The two last steps were repeated four more times. For LC-MS analysis, the supernatant was removed and 50 µl of 6.25 µg/µl of trypsin solution was added and left to incubate for 3 hours at 37°C.

In-Bead trypsin digestion and LC-MS/MS analysis

Beads were incubated with 50 µl of 6.25 µg/µl of trypsin solution and left to incubate for 3 hours at 37°C. The samples were then spun down at 2000 *g* (5000 rpm) for 5 minutes at 4°C. The supernatant was transferred to a new microcentrifuge tube and vortexed and dried using a vacuum concentrator. The sample was stored at -20°C until ready to use. For LC-MS/MS analysis the sample was resuspended in 11 µl of 5% Acetonitrile, 0.1% Formic acid and 0.005% Heptafluorobutyric acid (HFBA). Analysis was performed on a thermoElectron LTQ Linear Ion Trap tandem mass spectrometer. Protein identity was determined by sequence analysis with TurboSEQUEST™ (ThermoFinnigan, San Jose, CA) or MASCOT (Matrix Sciences, London GB) using an indexed viral subset database of the non-redundant protein database from National Center for Biotechnology Information (NCBI) web site (http://www.ncbi.nlm.nih.gov/).

Immunoprecipitation

Whole cell lysates (1500 µg in 1000 µl volume) from Mock transfected cells, cells transfected with *HPX* and *H2AX-GFP* vectors, *HPX* alone or *H2AX-GFP* alone were incubated with 15 µl anti-tax pep 3 rabbit polyclonal antibody at 4°C for 4 hours, with constant rotation. The lysate were then incubated with 90 µl Protein A/G plus Agarose beads (Zymed, San Francisco, CA) while rotating for overnight at 4°C. The beads were washed 3 times with 1 ml of 1X SNNTE buffer (5% sucrose, 500 mM NaCl, 1% Nonidet P-40, 50 mM Tris-HCl [pH 7.4], 5 mM EDTA) by centrifugation at 4°C for 5 minutes each time at 500 *g* (2500 rpm). Proteins were eluted from beads by

resuspension in 45 µl Laemmli sample buffer (Bio-Rad, Hercules, CA) with β-mercaptoethanol, and boiled for 10 minutes. The samples were the centrifuged at 4°C for 5 minutes at 500 *g* (2500 rpm) and the supernatant was transferred to a sterile eppendorf tube. The samples were either ran in a gel directly or frozen at -20°C.

Results

Efficient expression and purification of STaxGFP and SGFP

To identify the different proteins in the Tax interactome, we first needed to efficiently express Tax in mammalian cells. We decided to use the *STaxGFP* plasmid (Fig. 3*A*), which was previously described (144), for two main reasons. First, it has an amino-terminal S tag that allows protein isolation using the S-Tag purification system (Novagen), which is based on the interaction between a 15-amino acid S tag and S protein immobilized on agarose beads, both of which are derived from RNase S (145). Second, it also has a carboxy-terminal GFP tag which permits the monitoring of protein localization and transfection efficiency. Furthermore, it was previously shown that the *STaxGFP* plasmid expresses biological active full-length Tax protein (144). S-tagged GFP (*SGFP*) was our control plasmid (Fig. 3*A*). We chose to use human embryonic kidney 293T (293 T) cells because of their high transfection efficiency. We transiently transfected both plasmids into 293 T cells and determined expression levels of each protein by Western blotting and immunohistochemistry analysis. For Western blot analysis, a GFP antibody was used to detect both STaxGFP and SGFP. This permitted the

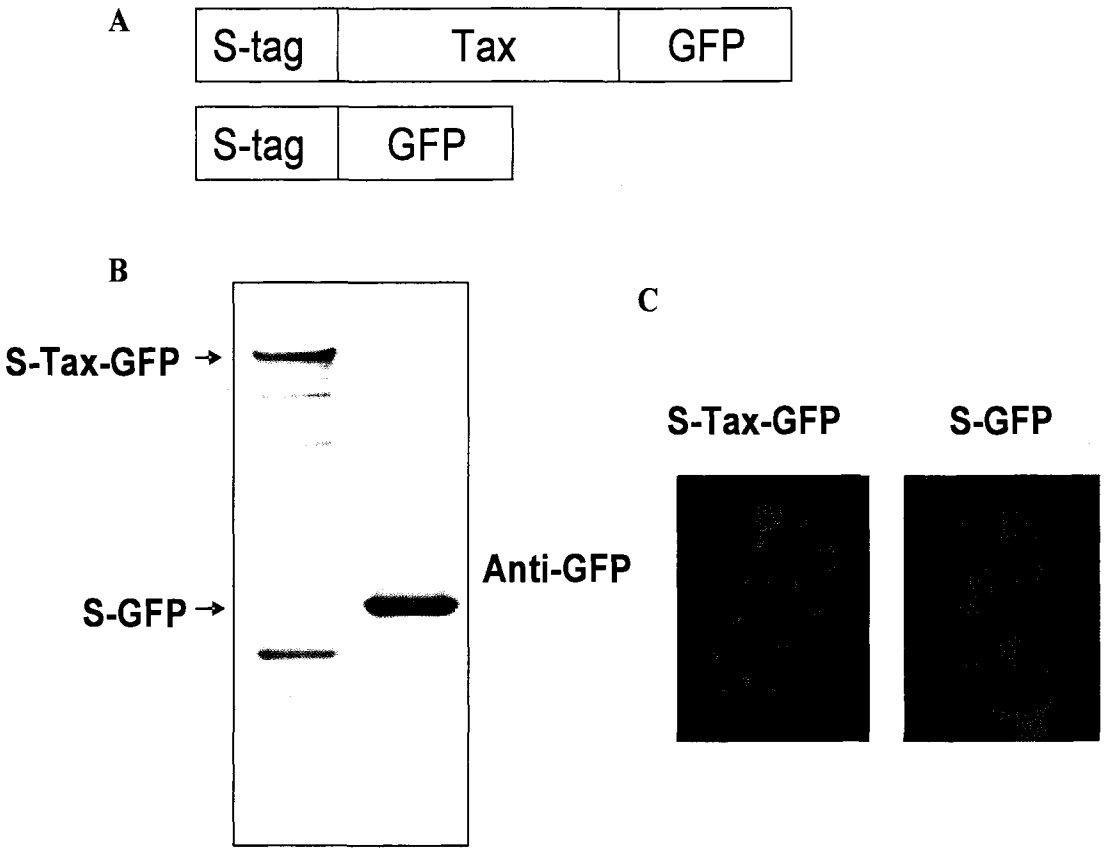

FIGURE 3. **Efficient expression of STaxGFP.** *A*, schematic representation of the plasmid used. *B*, cell lysates from 293T cells transiently transfected with *STaxGFP* and *SGFP* were subjected to SDS-PAGE and analysis by immunoblotting by the indicated antibodies. *C*, confocal microscopy images of an STaxGFP cell and an SGFP cell. Images are magnified ×63 with a ×4 zoom.

direct comparison of the amounts of both proteins in the cells. As shown in Fig. 3*B*, we could express both proteins at similar levels. Next, we wanted to determine the transfection efficiency of our plasmid. Using immunofluorescence, we determined that we could approximately transfect STaxGFP in 75% of the cells in one plate. Furthermore, STaxGFP formed the appropriate "Tax Speckled Structures" (TSS) (Fig. 3*C*), which is characteristic of the biologically active full-length Tax protein (68). SGFP was efficiently transfected in about 85% of the cells and, as expected, the protein was localized in both the nucleus and the cytoplasm (Fig. 3*C*).

Next, we purified the protein using the S-Tag purification system. Cells lysates from 293 T cells transiently expressing STaxGFP or SGFP were incubated with S protein immobilized on agarose beads. Fig. 4 shows that after affinity tag purification and stringent washes we isolated both STaxGFP and SGFP.

Identification of the proteins present in the Tax interactome

In order to identify the different proteins in the Tax interactome, we designed an experiment in which we tried to eliminate as many variables as possible (Fig. 5). First, we isolated both STaxGFP and SGFP from transiently transfected 293 T cells. Next, we stringently washed the beads in order to only have the S-tagged protein bound to the S-beads. Next, we incubated the S-tagged protein bound to the S-beads with a specific amount of commercially available pre-cleared Jurkat nuclear extract. HTLV-1 infects T cells, and Jurkat cells are an immortalized line of T lymphocytes, therefore it is appropriate to use Jurkat nuclear extract to identify Tax binding proteins. Furthermore, by only leaving the S-tagged proteins on the beads and incubating them with a

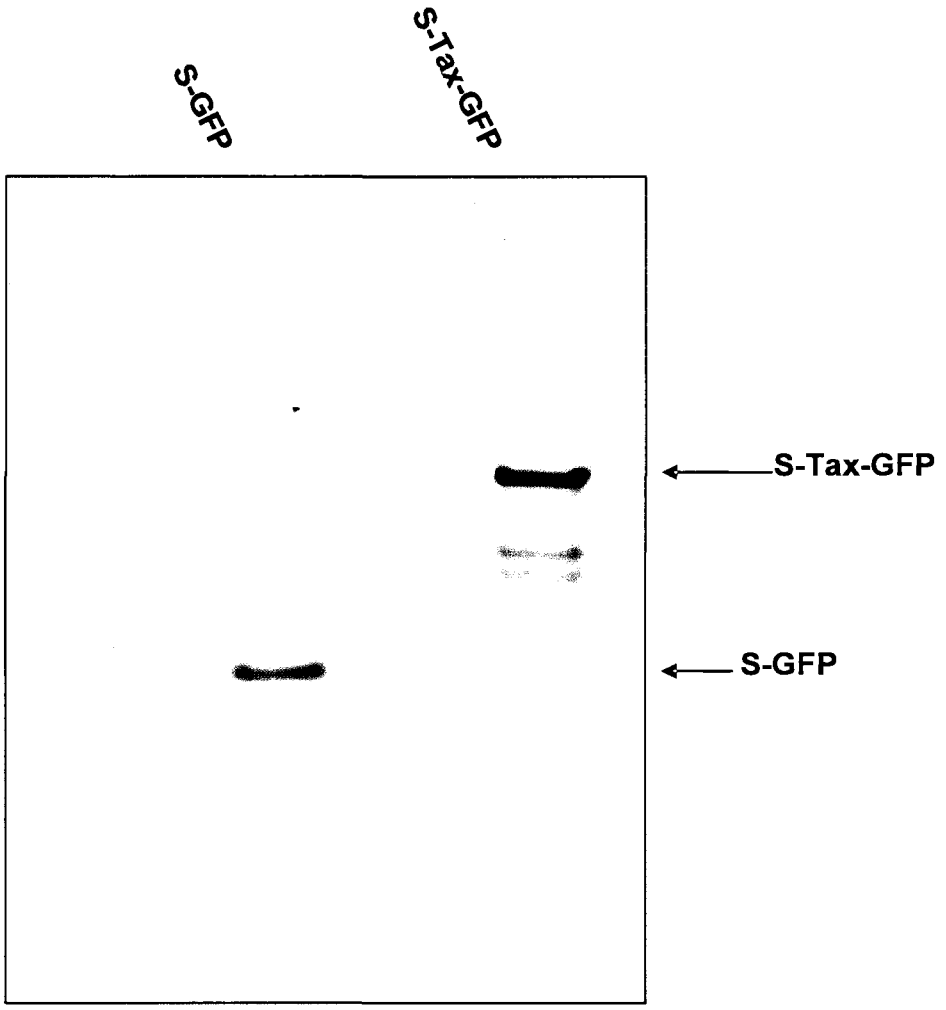

FIGURE 4. **Efficient purification of STaxGFP.** Whole cell lysate from 1000 μg of total protein in STaxGFP transfected cell or 400 μg of protein in SGFP transfected cells were pulled down by S-beads (120 μl), incubated O/N at 4°C. The beads pellet were washed by RIPA buffer for 3 times thoroughly. Approximately, 60 μl sample buffer were loaded on a 4-12% SDS-PAGE following boiling the beads. The gel (1.5 mm thick) were stained by Bio-Safe Coomassie Blue (Bio Rad) for 1 hr at RT.

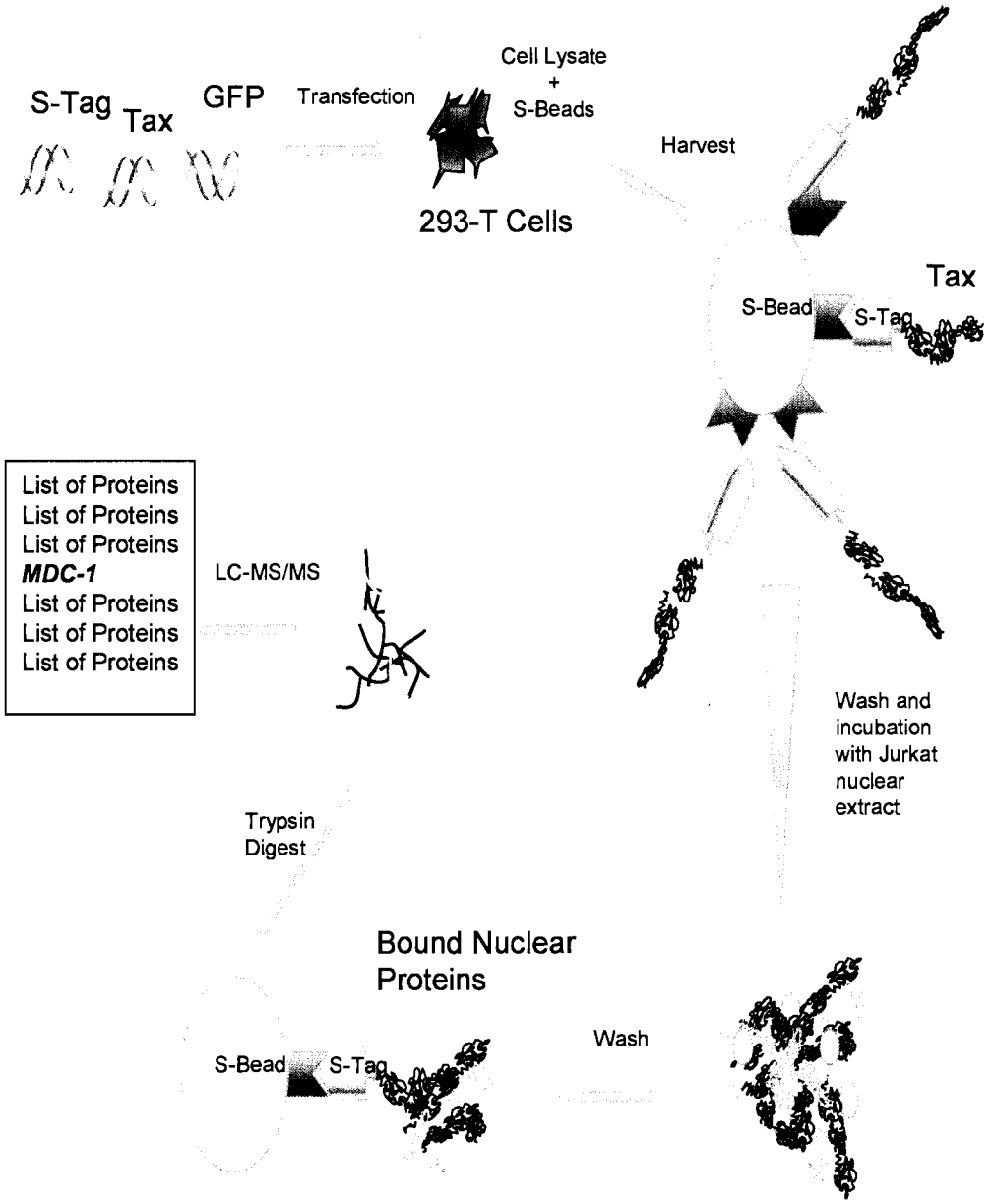

FIGURE 5. **Construction of the Tax interactome**

predetermined amount of proteins, we eliminated several variables. For instance, Tax *trans*-activates a variety of cellular genes and this might cause a dramatic increase in certain proteins in STaxGFP transfected cells compared to SGFP expressing cells, thus increasing potential unspecific binding. Using Jurkat nuclear extract from non-Tax expressing cells ensures that we have the same amount of each nuclear protein incubating with STaxGFP and SGFP. Therefore, if a protein is found to bind STaxGFP but not SGFP, we would be sure that it is due to an actual binding and not nonspecific binding caused by the increased amount of that protein in Tax expressing cells. Beads were then subject to trypsin digestion. Liquid chromatography-Mass spectrometry (LC-MS/MS) analysis was then performed. We selected the proteins that had at least two peptides hits, an expect score below 0.5 and an individual peptide score indicating at least homology. The experiment was performed three different times. Next, we generated a list in which the proteins were identified in all three experiments. Also, we generated the same list with the SGFP control and subtracted proteins that were found in the SGFP control from the list of the STaxGFP experiment. Repeating the experiment three times resulted in the elimination a large number of proteins from our final list. In fact, 406 proteins were found in a least one experiment, 315 were found in at least two experiments and only 76 proteins were presents in all 3 experiments. Proteins in the one out of three and two of three lists might still bind Tax, but we had higher confidence that the 76 proteins found in three out of three lists were indeed in the Tax interactome (see "Appendix A" for the list).

Classification of the Tax binding proteins according to their functions

Not surprisingly, we found in the Tax interactome, proteins that were already

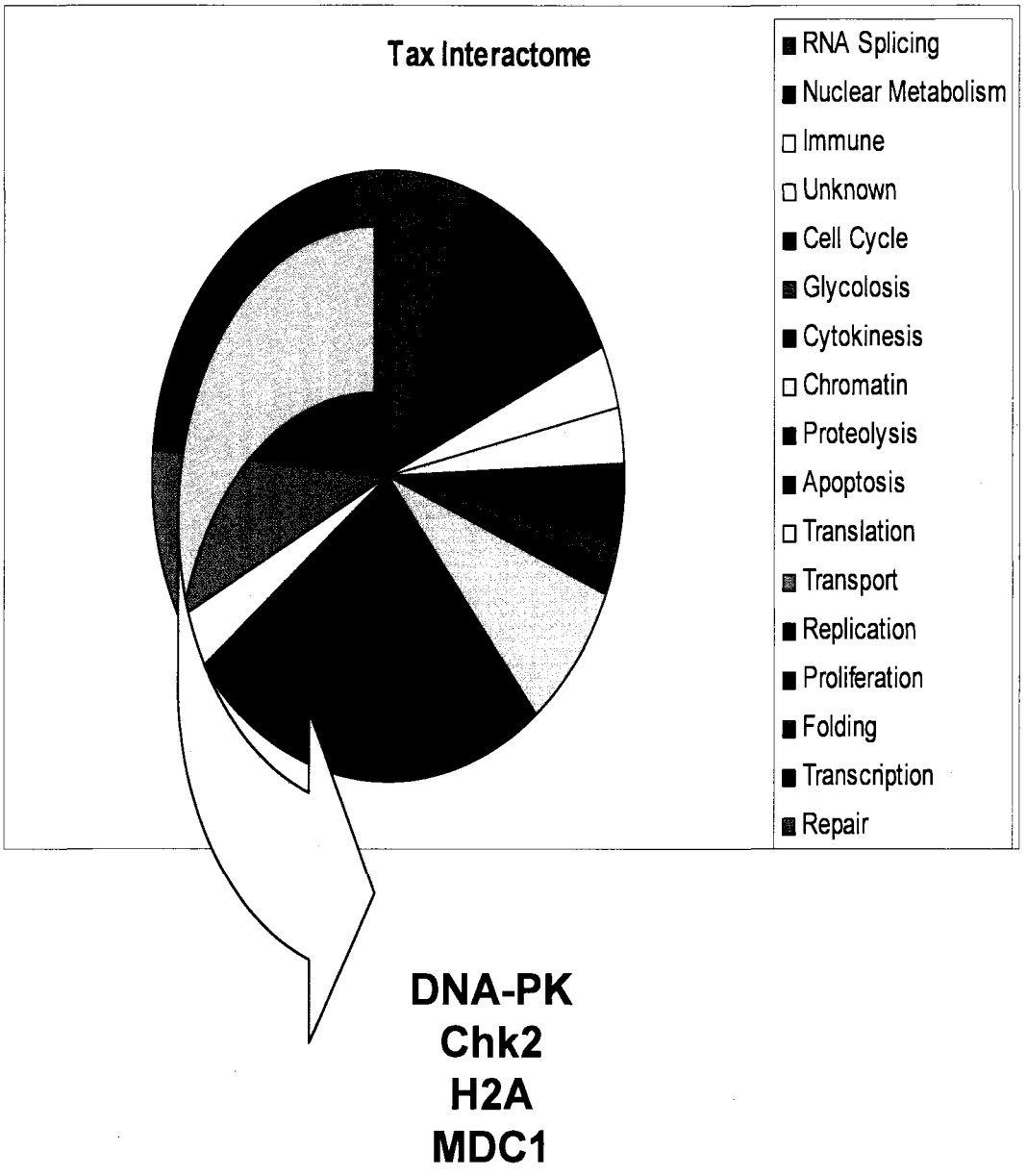

FIGURE 6. **Proteomic analysis of the Tax interactome.** Proteomic analysis showed the presence in the Tax interactome of a number of proteins involved in DNA repair such as DNA-PK, Chk2, H2A and MDC1.

known to bind Tax and that our laboratory studied extensively, such as DNA-PK and Chk2. DNA-PK was in the three out of three list whereas Chk2 was in the two out of three list. These two proteins are involved in the DNA damage repair pathway, and our laboratory previously showed that Tax causes the aberrant activation of both of these proteins in the absence of DNA damage. This causes the dysregulation of the DNA damage repair machinery that ultimately might lead to genomic instability (92, 98, 146). Due to the presence of Chk2, which is a known Tax binding protein, in the two out of three list, we decided to include these proteins in our classification of Tax binding proteins according to their cellular functions (Fig. 6). Many categories were created such as cell cycle, transcription and apoptosis. Next, we determined through literature search which proteins were studied in relation to Tax. In addition to DNA-PK and Chk2, we found other known Tax binding proteins such as the E3 SUMO- protein ligase Ran-binding protein 2 (RanBP2) (147), the Retinoblastoma protein (Rb) (142), the nuclear pore glycoprotein p62 (148) and SWI/SNF (130).

Additionally, we found several proteins that were not previously linked to Tax. For instance, both the interferon gamma-inducible protein 16 (IFI-16), a protein involved in p53 dependent apoptosis (149), and the minichromosome maintenance deficient protein 7 (MCM7), a protein implicated in DNA replication (150), were never reported to bind to Tax and both were present in three out of three list of the Tax interactome. Many Tax binding proteins have been reported to interact with Tax in the TSS (68, 115). This was determined by immunofluorescence studies showing colocalization of these proteins with Tax. Here, we looked at the localization of MCM7 and IFI16 in Tax expressing cells and determined that they both colocalized with Tax suggesting that it may be interesting

to pursue the relationships of Tax and these two proteins (Fig. 7).

Another new Tax binding protein we found in the three out of three list is the mediator of DNA damage checkpoint protein 1 (MDC1) (Fig. 8). MDC1 relates to both DNA-PK and Chk2. As a result of its ability to regulate several aspects of DNA damage response pathways. It is crucial for DNA-PK autophosphorylation and H2AX phosphorylation (107, 108, 111, 113). In addition to its role in H2AX phosphorylation, it has been shown that MDC1 is essential for H2AX and H2A ubiquitylation. H2AX and H2A ubiquitylation, which is a critical step in the DNA damage repair mechanism, is part of the chromatin remodeling process which "opens up" the DNA at the damage sites thus allowing the recruitment of more DNA damage repair proteins (110). It should be noted that several H2A subtypes were identified in our analysis of the Tax interactome. Therefore, we sought to determine whether Tax and H2AX interact. Overexpression of GFP tagged H2AX in Tax expressing cells, followed by immunoprecipitation confirmed that Tax and H2AX indeed interact (Fig. 9). This further strengthens the hypothesis that Tax forms a complex with several members of the DNA damage machinery.

In the LC-MS/MS analyses, MDC1 was identified by 6 unique peptides with significant MS/MS Mascot ion scores, expect scores and a sequence coverage of 4.7%. The low coverage is due to the large size of the protein which has 2,089 amino acids and molecular mass of about 226 kD (Fig. 8). Fig. 10 shows the MS/MS spectrum of a triply charged peptide with an m/z of 716.68 that identifies the MDC1 sequence HLAPPPLLSPLLPSIKPTVR from amino acid 1060 to 1079 with a molecular mass of 2147.04 Da. The high quality of the spectrum is illustrated by the presence of high number of both b and y ions. In the y ion series, the most intense peak is the y17

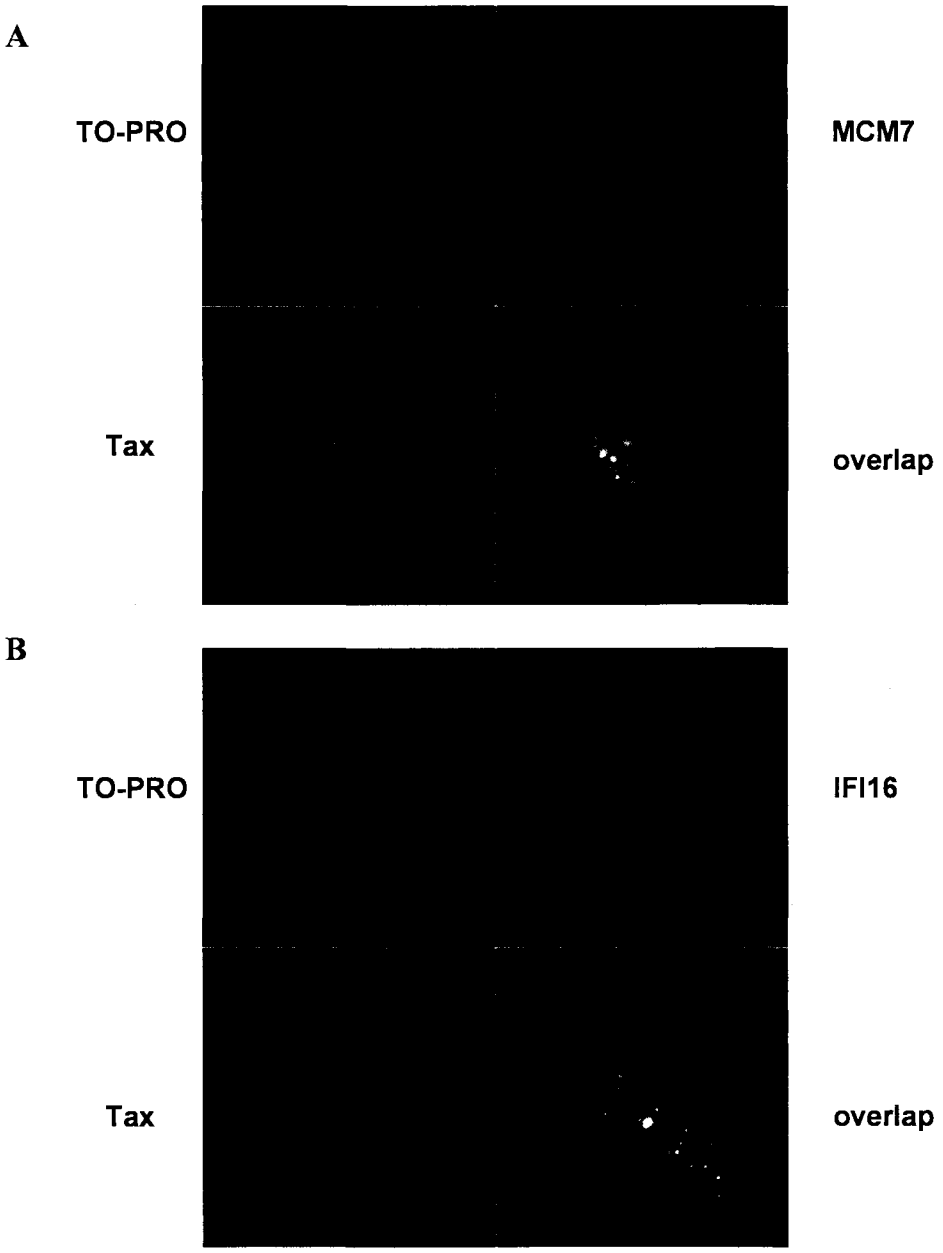

FIGURE 7. **Colocalization of Tax and novel Tax binding proteins.** STaxGFP was expressed in 293 FT cells. Endogenous MCM7 (*A*) and IFI116 (*B*) were detected with the indicated antibodies; Tax expression was detected via the GFP fusion. Nuclei were visualized by co-staining with TO-PRO-3 iodide. Three images were merged to visualized overlap. Confocal microscopy images are magnified ×63 with a ×4 zoom.

Observed	Mr(expt)	Mr(calc)	Score	Expect	Peptide
621.8162	1241.6178	1240.6412	32	0.095	R.NQLVTPEPTSR.A
675.7546	1349.4946	1348.6358	37	0.035	R.QTDVTGEEELTK.G
898.9407	1795.8668	1795.0859	52	0.00078	R.VGLPLLSPEFLLTGVLK.Q
716.6876	2147.0410	2145.3038	57	0.00021	K.HLAPPPLLSPLLPSIKPTVR.K
875.6605	2623.9597	2622.3177	47	0.0025	K.TPEPVVPTAPEPHPTTSTDQPVTPK.L
1026.8770	3077.6092	3076.5928	60	7.8e-05	K.TPETVVPTAPELQISTSTDQPVTPKPTSR.T

MDC1_HUMAN Mass: 226529 Score: 276 Queries matched: 7 emPAI: 0.13 coverage:4.7%

FIGURE 8. **MDC1 unique peptides.** In the LC-MS/MS analysis of the Tax interactome, MDC1 was identified by 6 unique peptides.

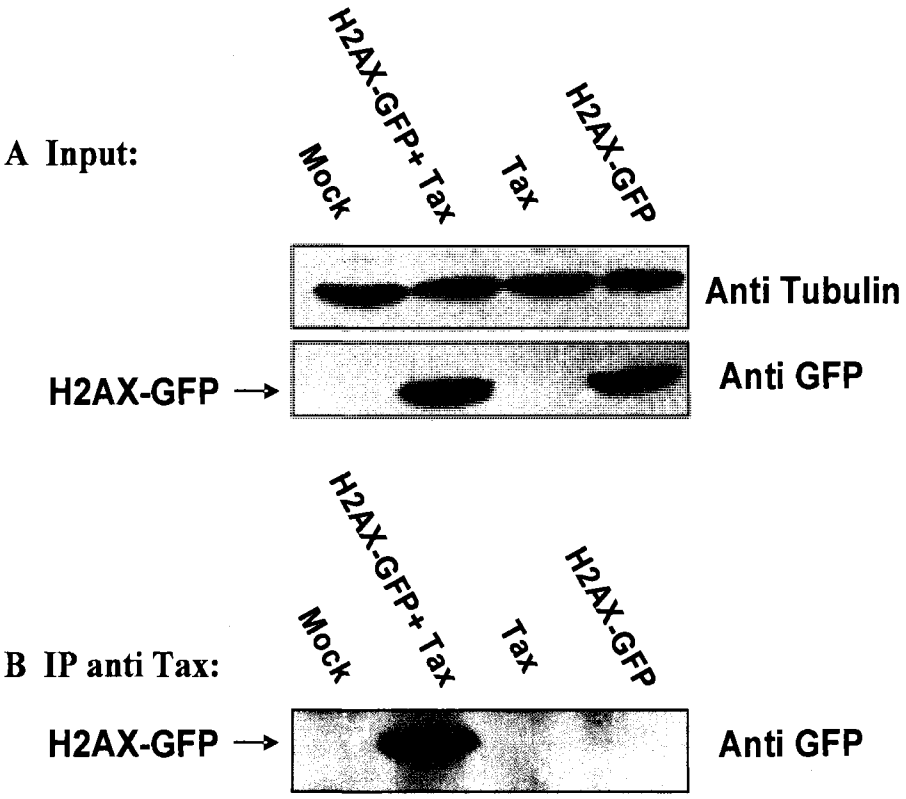

FIGURE 9. **H2AX co-purifies with Tax.** Cell lysates from 293T cells transiently co-transfected with *H2AX-GFP* and *Tax*, or transfected with *H2AX-GFP* alone or *Tax* alone or Mock transfected were (*A*) subjected to SDS-PAGE and analysis by immunoblotting by the indicated antibodies or (*B*) immunoprecipitated with anti-Tax antibody as described under "Experimental Procedures" and subjected to SDS-PAGE and analysis by immunoblotting with the indicated antibody.

A

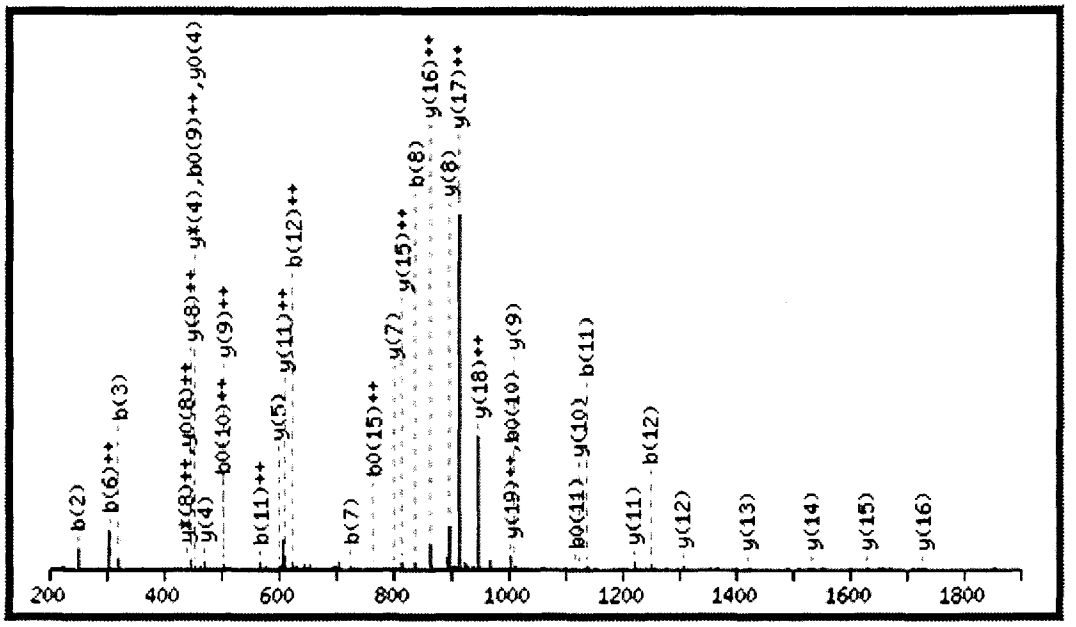

B

#	b	b++	Seq.	y	y++	#
1	138.0662	69.5367	H			20
2	**251.1503**	126.079	L	2009.252	**1005.13**	19
3	**322.1874**	161.597	A	1896.168	**948.5877**	18
4	419.2401	210.124	P	1825.131	**913.0691**	17
5	516.2929	258.65	P	**1728.078**	**864.5427**	16
6	613.3457	**307.177**	P	**1631.025**	**816.0164**	15
7	**726.4297**	363.719	L	**1533.973**	767.49	14
8	**839.5138**	420.261	L	**1420.889**	710.9479	13
9	926.5458	463.777	S	**1307.805**	654.4059	12
10	1023.599	512.303	P	**1220.773**	**610.8899**	11
11	**1136.683**	**568.845**	L	**1123.72**	562.3635	10
12	**1249.767**	**625.387**	L	**1010.636**	**505.8215**	9
13	1346.82	673.913	P	**897.5516**	**449.2795**	8
14	1433.852	717.429	S	**800.4989**	400.7531	7
15	1546.936	773.971	I	713.4668	357.2371	6
16	1675.031	838.019	K	**600.3828**	300.695	5
17	1772.083	886.545	P	**472.2878**	236.6475	4
18	1873.131	937.069	T	375.235	188.1212	3
19	1972.199	986.603	V	274.1874	137.5973	2
20			R	175.119	88.0631	1

FIGURE 10. **MDC1 peptide with sequence HLAPPPLLSPLLPSIKPTVR**. *A*, representative MS/MS fragmentation and the b and y ion annotation of a triply charged MDC1 peptide with sequence HLAPPPLLSPLLPSIKPTVR. *B*, table showing the y and b ions. Note the dominating high intensity proline y_{17} ion.

proline consistent with the high ionization efficiency and thus intensity of a proline containing fragment. This further validates the identification of the peptide sequence. The same observation is made in Fig. 11, in which the most intense peak of the MS/MS spectrum of the peptide TPETVVPTAPELQISTSTDQPVTPKPTSR from amino acid 1608 to 1636 is again a proline (y23). Fig. 12 is an example of doubly charged peptide with an m/z of 898.94 that identifies the sequence VGLPLLSPEFLLTGVLK from amino acid 2055 to 2071 with almost complete annotation of the b and y ions series including the proline (y10).

In addition, the exponentially modified protein abundance index (emPAi) score of MDC1, which indicates the relative amount of a protein in the mixture, was 0.13 (Fig. 8) and it is comparable to the emPAi scores of DNA-PK (0.27) and Chk2 (0.25). Both DNA–PK and Chk2 are known to bind Tax (92, 98) thus increasing our confidence that MDC1 is indeed present in the Tax interactome.

Discussion

We attempted to construct the Tax interactome using a specific experimental design that would decrease variability and false positives. First, we efficiently expressed STaxGFP and SGFP in mammalian cells. We then used the S-Tag purification system (Novagen) to pull down both STaxGFP and SGFP. After showing that we could successfully express and pull down both STaxGFP and SGFP, we then washed the beads stringently in order to only keep the S-tagged proteins bound to beads. We then incubated the beads with a predetermined amount of pre-cleared Jurkat nuclear extract. This step accomplished several goals. First, we could control the amount of proteins mixed with

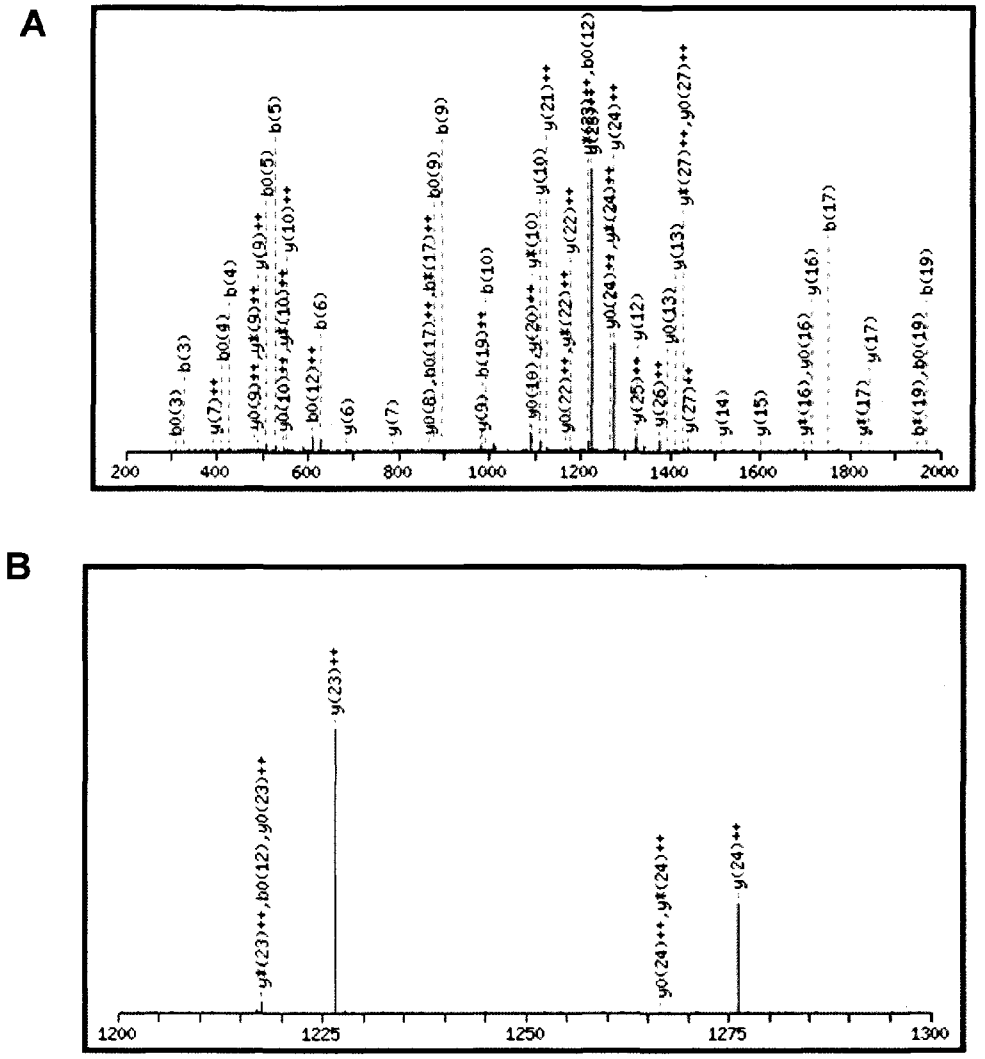

FIGURE 11. **MDC1 peptide with sequence TPETVVPTAPELQISTSTDQPVTPKPTSR.** *A*, representative MS/MS fragmentation and the b and y ion annotation of a triply charged MDC1 peptide with sequence TPETVVPTAPELQISTSTDQPVTPKPTSR. *B*, note the dominating high intensity proline y_{23} ion. *C*, table showing the y and b ions

C

#	b	b^{++}	Seq.	y	y^{++}	#
1	102.055	51.5311	T			29
2	199.1077	100.0575	P	2976.552	1488.78	28
3	**328.1503**	164.5788	E	2879.5	**1440.254**	27
4	**429.198**	215.1026	T	2750.457	**1375.732**	26
5	**528.2664**	264.6368	V	2649.409	**1325.208**	25
6	**627.3348**	314.171	V	2550.341	**1275.674**	24
7	724.3876	362.6974	P	2451.273	**1226.14**	23
8	825.4353	413.2213	T	2354.22	**1177.614**	22
9	**896.4724**	448.7398	A	2253.172	**1127.09**	21
10	**993.5251**	497.2662	P	2182.135	**1091.571**	20
11	1122.568	561.7875	E	2085.082	1043.045	19
12	1235.652	618.3295	L	1956.04	978.5235	18
13	1363.71	682.3588	Q	**1842.956**	921.9814	17
14	1476.794	738.9009	I	**1714.897**	857.9521	16
15	1563.827	782.4169	S	**1601.813**	801.4101	15
16	1664.874	832.9407	T	**1514.781**	757.8941	14
17	**1751.906**	876.4567	S	**1413.733**	707.3703	13
18	1852.954	926.9806	T	**1326.701**	663.8542	12
19	**1967.981**	**984.494**	D	1225.654	613.3304	11
20	2096.039	1048.523	Q	**1110.627**	**555.8169**	10
21	2193.092	1097.05	P	**982.568**	**491.7876**	9
22	2292.161	1146.584	V	885.5152	443.2613	8
23	2393.208	1197.108	T	**786.4468**	**393.7271**	7
24	2490.261	1245.634	P	**685.3991**	343.2032	6
25	2618.356	1309.682	K	588.3464	294.6768	5
26	2715.409	1358.208	P	460.2514	230.6293	4
27	2816.456	1408.732	T	363.1987	182.103	3
28	2903.488	1452.248	S	262.151	131.5791	2
29			R	175.119	88.0631	1

FIGURE 11. Continued.

A

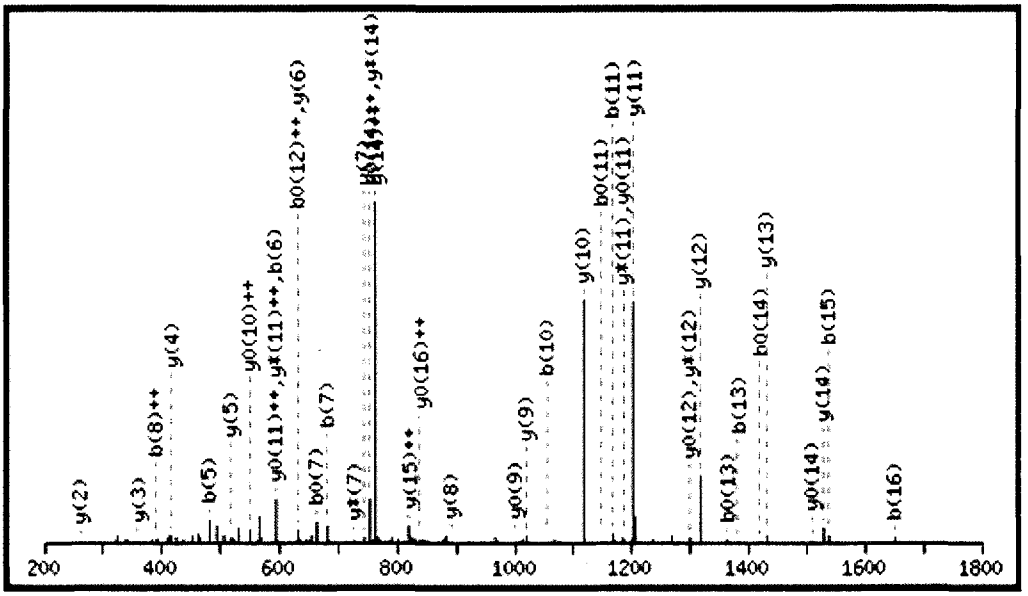

B

#	b	b*+	Seq.	y	y*+	#
1	100.0757	50.5415	V			17
2	157.0972	79.0522	G	1697.025	849.016	16
3	270.1812	135.5942	L	1640.003	**820.5053**	15
4	367.234	184.1206	P	**1526.919**	**763.9633**	14
5	**480.318**	240.6627	L	**1429.867**	715.4369	13
6	**593.4021**	297.2047	L	**1316.782**	658.8948	12
7	**680.4341**	340.7207	S	**1203.698**	602.3528	11
8	777.4869	**389.2471**	P	**1116.666**	558.8368	10
9	906.5295	453.7684	E	**1019.614**	510.3104	9
10	**1053.598**	527.3026	F	**890.571**	445.7891	8
11	**1166.682**	583.8446	L	**743.5026**	372.2549	7
12	1279.766	640.3867	L	**630.4185**	315.7129	6
13	**1380.814**	690.9105	T	**517.3344**	259.1709	5
14	1437.835	719.4212	G	**416.2867**	208.647	4
15	**1536.904**	768.9554	V	**359.2653**	180.1363	3
16	**1649.988**	825.4975	L	**260.1969**	130.6021	2
17			K	147.1128	74.06	1

FIGURE 12. **MDC1 peptide with sequence VGLPLLSPEFLLTGVLK.** *A*, representative MS/MS fragmentation and the b and y ion annotation of a doubly charged MDC1 peptide with sequence VGLPLLSPEFLLTGVLK.*B*, table showing the y and b ions.

the S-tagged proteins. We tried the experiment using several concentrations of nuclear extract and determined the optimal amount for LC-MS/MS analysis. Second, Jurkat cells are T cells therefore they are more biologically relevant to this study than 293 T cells which are derived from kidney cells. Using non-Tax transfected cells would eliminate bias due to Tax upregulation of cellular genes. Each protein found to bind Tax using our experimental design should be present at the same concentration in every Jurkat nuclear extract. This increases our confidence that a Tax-binding protein hit is really present in the Tax interactome and that it is not just a result of increased nonspecific binding due to increased expression. The experiment was repeated three separate times, and after LC-MS/MS analysis, we ended up with one list for each experiment. We eliminated the proteins found in the SGFP list and only chose in our final list the proteins that were found in at least two experiments. The higher the number of experiments a protein was found in, the more confident we were in the presence of that protein in the Tax interactome. Therefore, proteins that were found in all three experiments were considered the likeliest to interact with Tax. However, this does not mean that the proteins that were detected only once or twice do not bind Tax. In fact, we found proteins that were previously shown to bind Tax in the two of three list such as Chk2. For this reason, we decided to include in our final list, proteins from the two out of three list and the three out of three list.

Proteins in the final list could be classified in many different cellular processes such as cell cycle regulation, apoptosis and DNA replication. As expected, we found in the final list proteins that were already known to bind Tax such as DNA-PK. This was a good indicator that our experiment worked properly. Other interesting proteins that were

not known to bind Tax were also identified such as IFI16 and MCM7. One interesting protein that was identified in the Tax interactome is the mediator of DNA damage checkpoint protein 1 (MDC1). MDC1 interacts with numerous proteins involved in the checkpoint signaling and DNA damage repair pathway. Furthermore, following DNA damage MDC1 gets phosphorylated and translocates to DNA damage sites where it allows recruitment and accumulation of downstream DNA damage repair proteins (104). Our laboratory has been studying the relationship between Tax and other proteins involved in DNA damage repair such as DNA-PK, Chk2 and γ-H2AX (92, 98, 146). Our laboratory previously showed that Tax binds and activates DNA-PK causing phosphorylation of the H2AX histone protein (98). In a normal cell, H2AX phosphorylation by DNA-PK only occurs after induction of DNA damage, but in the presence of Tax, H2AX is constitutively hyperphosphorylated which does not allow the cell to detect newly formed damage. MDC1 is a crucial part of this process since it binds DNA-PK and seems to be important in the process of H2AX phosphorylation (111). In addition, MDC1 was also found to bind Chk2, which is another Tax binding protein, and is essential for Chk2-mediated DNA damage responses (112).

In this study, we designed an experiment that allowed us to identify with high confidence proteins that are present in the Tax interactome. We have identified new Tax-binding proteins, and their relationship to Tax should be studied further in the future. However, due to the identification of MDC1 in the Tax interactome and its central role in the DNA damage response pathway through its interaction with DNA-PK, Chk2 and H2AX, we decided to focus on the role of MDC1 in the Tax induced dysregulation of the DNA damage response pathway (92, 98, 146).

SECTION 4

STRUCTURAL CHARACTERIZATION OF MDC1 WITHIN THE TAX COMPLEXES

Introduction

Human T-cell leukemia virus-1 (HTLV-1) is a human transforming retrovirus which can cause adult T-cell Leukemia (ATL) and HTLV associated myelopathy/tropical spastic paraperisis (HAM/TSP) (19, 34). Tax is one of the HLTV-1 encoded proteins and plays an essential role in viral transcription as well as cellular transformation leading to ATL (20, 37, 114, 120, 121). The oncogenic potential of Tax is demonstrated by the fact it can induce neoplastic transformation of the rat fibroblast Rat-1 cell line (70) and the mouse fibroblast NIH/3T3 cell line (71). Furthermore, Tax expression immortalizes primary human T-cells (72, 151). Finally, expressing Tax *in vivo* induces tumors in transgenic mice (120, 152, 153). Tax induces cellular transformation by transcriptionally regulating cellular gene expression and also by functionally inactivating proteins involved in cell-cycle progression and DNA repair (75).

Impairment of the DNA damage repair by Tax greatly contributes to genomic instability (77). In a normal cell, the DNA damage repair pathway is essential to maintain the integrity of the genome. As cells divide, DNA can be damaged due to nucleotide misincorporation during replication or by environmental factors (75). Proper repair of damaged DNA ensures that mutations are not passed on to daughter cells. DNA damage can be repaired by several pathways such as base excision repair (BER), nucleotide excision repair (NER), mismatch repair (MMR), and double strand break (DSB) repair

(75). Examples of Tax interacting proteins involved in the DNA damage repair pathway are Rad51 (130), DNA topoisomerase 1 (143),Chk2 (92) and DNA-PK (98).

Previous studies from our laboratory investigated the relationship between Tax and DNA-PK (98). DNA-PK is a key enzyme in non-homologous end joining (NHEJ), the predominant DSB repair pathway in mammalian cells (99-102). We found that Tax not only binds DNA-PK, but that it induces DNA-PK hyperphosphorylation at S2056 and T2609, thus activating it. This leads to the activation of downstream targets of DNA-PK such as Chk2 and H2AX (98). Phosphorylation of H2AX (termed γ-H2AX) is an early event in the sensing of newly formed DNA damage and it causes changes in the chromatin conformation. This allows the recruitment of downstream DNA damage response (DDR) proteins either directly by γ-H2AX or by other repair proteins to the DNA damage sites, also called ionizing radiation-induced nuclear foci (IRIF) (104). Once the damage is repaired, γ-H2AX needs to be dephosphorylated in order to maintain the DNA damage repair machinery properly functioning (105, 106). Our laboratory has shown that there is dramatic increase in the level of γ-H2AX in Tax expressing cells compared to cells that do not express Tax (98). The constant H2AX phosphorylation in Tax expressing cells, taken together with the importance of γ-H2AX dephosphorylation in properly functioning DNA damage repair machinery, suggests that Tax interferes with the DNA damage repair machinery by not allowing the cell to detect and repair newly formed damage.

After isolation of the Tax complex from the cells and identification of the different Tax interacting proteins using liquid chromatography tandem mass spectrometry (LC-MS/MS), we identified a novel Tax-binding protein, mediator of DNA damage

checkpoint 1 (MDC1), a key enzyme in the DNA damage response pathway (104). MDC1 is a large protein (about 250 kD) that possesses two consecutive BRCA1 C-terminal (BRCT) motifs (118) and an N-terminal forkhead-associated (FHA) domain (107, 111, 118, 154-157). FHA domains are phosphoprotein binding domains usually found in signaling proteins (158); BRCT domains are also very common in many DNA damage repair proteins (159, 160). In addition, tandem BRCT (tBRCT) domains constitute phosphoprotein binding domains (159-161). It has been shown that MDC1 binds to phosphorylated histone H2AX near sites of DNA double-stranded breaks through its tBRCT motif, thus facilitating the recruitment of other DNA damage repair proteins to DNA damage foci (108). The MRE11–RAD50–NBS1 (MRN) complex, which is crucial for DNA damage repair, is recruited by MDC1 via the binding of the phosphorylated Ser-Asp-Thr (SDT) repeats of MDC1 to the N-terminal FHA domain of NBS1 (162, 163). The phosphorylation of the SDT repeats of MDC1 is mediated by casein kinase 2 (CK2) (163, 164). MDC1 is also essential for the accumulation of other DDR proteins within IRIF including BRCA1, 53BP1 and Chk2 (107, 112, 118, 119, 165). Another important role of MDC1 in response to DNA damage is the recruitment of RNF8, a RING-finger ubiquitin ligase, which in turn ubiquitylates H2AX (109). Ubiquitylation of H2AX causes changes in chromatin conformation at the DNA damage sites, thus "opening up" the DNA, similar to phoshorylation, allowing the recruitment of even more DDR proteins (109). Finally, DNA-PK also interacts with MDC1, and it was shown that MDC1 is crucial for DNA-PK autophosphorylation at T2609 in response to DNA damage (111).

Due to the presence of MDC1 in the Tax interactome and its central role in the DNA damage response pathway through its interaction with DNA-PK, Chk2 and H2AX, we focused on the role of MDC1 in the Tax induced dysregulation of the DNA damage response pathway. Once we confirmed the interaction between Tax and MDC1, it was important to determine the nature and the potential roles of that interaction. The *Objective* of this aim is to confirm and characterize the physical interaction between Tax and MDC1. We accomplished this objective using the following *experimental approaches.* (1) We confirmed binding using S-pull down assay and immunoblotting techniques; (2) Since Tax is a cellular transcriptional *trans*-activator we determined the effect of Tax on MDC1 expression levels in the cell; (3) We used immunohistochemistry technique to determine the localization of Tax and MDC1; (4) We knocked down MDC1 expression in Tax expressing cells using siRNA and looked at the effect on MDC1 downstream targets; (4) We also conducted structural studies on MDC1 and examined its phosphorylation pattern in Tax expressing cells since it is known that active MDC1 is hyperphosphorylated (163, 164).

Experimental Procedures

Cell culture and transient transfection

293T cells were maintained at 37°C in a humidified atmosphere of 5% CO_2 in air, in Iscove's modified Dulbecco's medium supplemented with 10% fetal bovine serum (Cambrex, East Rutherford, NJ) and 1% penicillin-streptomycin (Invitrogen, Carlsbad, CA).

Transfections of 293T cells were performed by standard calcium phosphate precipitation. Cells were plated at $1x10^5$ cells/ml. The following day, plasmid DNA in 2M $CaCl_2$ and 2X HBS were added dropwise to cells in fresh medium. Cells were incubated at 37°C overnight and fresh medium was added. The cells were harvested 48 h post-transfection, following a single wash with 1X PBS, in 500 µl M-Per mammalian protein extraction reagent (Pierce, Rockford, IL) with protease inhibitor cocktail (Roche, Palo Alto, CA) and immediately frozen at –80°C.

Plasmids

Generation of the *STaxGFP*, *STax* and *SGFP* plasmids have been described earlier (144). Briefly, the S-tagged expression vectors *STaxGFP*, *STax* and *SGFP* were constructed by inserting the *tax-EGFP* fusion or *EGFP* ORF, respectively, into the *Sma*I site of *pTriEx4-Neo* (Novagen, Madison, WI) in frame with the amino-terminal S-tag and His-tag.

HA-tagged human *MDC1* (pcDNA3-neo) was a gift from D. Lukas (Danish Cancer Society, Copenhagen, Denmark).

SiRNA transfection

Cells were plated at $2x10^5$ cells/ml in 60 mm plates and left to grow overnight. The following day medium was changed with serum free and antibiotic free media 1 hour prior to transfection. A total of 2 µg of *STaxGFP* or *pTriEx4-Neo* (empty vector) and 100 pmol of siRNA MDCI (Santa Cruz biotechnology inc. sc-43917) or siRNA control were diluted in 500 µl of Opti-MEM® I medium without serum. Next, lipofectamin™ 2000 was

gently mixed then 5 µl was diluted in 500 µl of Opti-MEM® I medium without serum in a separate tube. The mixture was mixed gently and incubated for 5 minutes at room temperature. After 5 minutes incubation, the diluted DNA and siRNA molecule were mixed with the diluted Lipofectamin™ 2000. The solution was mixed gently and incubated for 20 minutes at room temperature to allow complex formation to occur. The DNA-siRNA-lipofectamin™ 2000 complexes were then added to the plate. We then mixed gently by rocking the plate back and forth. We incubated the cells at 37°C in a CO_2 incubator for 6 hours. The media was replaced with media that had serum and antibiotic. Cells were left to grow for 48 hours and harvested.

Immunofluorescence

Cells that were plated on a coverslip were washed twice with ice cold PBS. Cells were then fixed with 4% paraformaldehyde for 12 minutes at room temperature. Next, cells were washed 3 times with PBS. Methanol was added and left on the cells for 2 minutes. Cells were washed 4 times with PBS. The primary antibody was diluted in 3% Bovine Serum Albumin (BSA) in PBS at the appropriate concentration. A 100 µl drop of the diluted primary antibody was then placed on parafilm in a wet chamber. The coverslip was then inverted onto the drop and left incubating at 4°C overnight. The next day, the coverslip was removed from the parafilm and placed back into the tissue culture dish. The cells were washed twice with PBS-1% Tween 20 and twice with PBS. The species-appropriate Alexa Fluor 594-conjugated secondary antibody (Molecular Probes) was diluted at 1/1000 in 3% BSA in PBS. Nuclei were counterstained with To-Pro-3 iodide (Molecular Probes) diluted 1/1,000 in the same BSA-PBS and secondary antibody

solution. A 100 µl drop of BSA-PBS solution containing both the secondary antibody and To-Pro-3 was placed onto parafilm in a wet chamber. The coverslip was inverted onto the drop and left incubating for 1 hour at room temperature in the dark. Next, the coverslip was put back into a tissue culture dish and washed twice with 3% BSA in PBS then twice with PBS. One drop of Vectashield mounting medium with DAPI (Vector Laboratories Inc, Burlingame, CA) was placed onto a slide. The coverslip was inverted onto the slide and left to air dry for one hour at room temperature in the dark. The coverslip was then sealed to the slide using nail polish. Confocal fluorescent images were acquired using a Zeiss LSM 510 confocal microscope at 63X magnification with a 2X zoom using Argon (488 nm), HeNe1 (543 nm), and HeNe2 (633 nm) lasers, and imaged with LSM Image Browser software (Carl Zeiss, Jena, Germany).

Immunoprecipitation

Whole cell lysate (1500 µg) in 1000 µl volume was incubated with 15 µl anti-HA rabbit polyclonal antibody (0.25 mg/ml, 71-5500, Zymed, San Francisco, CA) at 4°C for 4 hours, with constant rotation. The lysate was then incubated with 90 µl Protein A/G plus Agarose beads (Zymed, San Francisco, CA) while rotating for overnight at 4°C. The beads were washed 3 times with 1 ml of wash buffer (0.2 M NaCl, 0.5% Nonidet P-40, 20 mM Tris-HCl [pH 8.0], 1 mM EDTA) and pelleted by centrifugation at 4°C for 5 minutes each time at 500 *g* (2500 rpm). Proteins were eluted from beads by resuspension in 45 µl Laemmli sample buffer (Bio-Rad, Hercules, CA) with β-mercaptoethanol, and boiled for 10 minutes. The sample was the centrifuged at 4°C for 5 minutes at 500 *g*

(2500 rpm) and the supernatant was transferred to a sterile microcentrifuge tube. The sample was either ran in a gel directly or frozen at -20°C.

Immunoblot analysis

Proteins separated by electrophoresis were transferred to Immobilon-P membranes (Millipore, Billerica, MA) using the semidry transfer method with 20 V applied for 1 hour. The membranes were then blocked for 1 hour at room temperature in 1x Odyssey blocking buffer (Li-Cor Biosciences, Lincoln, NE). Primary antibodies diluted in 1x Odyssey blocking buffer were applied to the membranes and allowed to interact at 4°C overnight on an orbital shaker. Membranes were washed four times for 5 minutes with PBS-1% Tween. Li-Cor Odyssey secondary antibodies were diluted to a concentration of 1/20,000 in 1x Odyssey blocking buffer containing 0.5% SDS and 0.5% Tween and then incubated for 1 hour at room temperature on an orbital shaker protected from light. The membranes were washed four times for 5 minutes with PBS-1% Tween and then stored in PBS and in the dark until ready to be analyzed. Blots were scanned and analyzed with a Li-Cor Odyssey scanner and software (Li-Cor Biosciences, Lincoln, NE).

Antibodies

For the immunofluorescence analysis, anti-MDC1 goat polyclonal (1/100, Santa Cruz Biotechnology, Santa Cruz, CA) was used to detect the localization of MDC1. For immunoblot analysis, the following antibodies were used: anti-MDC1 goat polyclonal (1/200, Santa Cruz Biotechnology, Santa Cruz, CA), anti-GFP mouse monoclonal (1/500, Santa Cruz Biotechnology, Santa Cruz, CA), anti-HA rabbit polyclonal (1/1500, Zymed,

San Francisco, CA) , anti-Tubulin mouse monoclonal (1/2000, Sigma, St. Louis, MO), anti-Tax-pep3 rabbit polyclonal (1/2000), anti-ORC2 rabbit polyclonal (1/400, Santa Cruz Biotechnology, Santa Cruz, CA), anti-γ-H2AX (1/2000, R&D systems, Minneapolis, MN).

Chromatin fractionation

Before harvest, the cells were rinsed twice with ice cold PBS. A total of $5x10^6$ cells were harvested in 1.5 ml eppendorf tube using a cell scraper with cold PBS (1 ml). The cells were then spun at 1500rpm for 2 minutes and the supernatant was discarded. The cell pellet was washed with cold PBS and spun down at 1500 rpm for 2 minutes. The cell pellet was then resuspended in 200 μl of buffer A (100 mM HEPES, pH 7.9, 10 mM KCl, 1.5 mM $MgCl_2$, 0.34 M Sucrose, 10% glycerol, 10 mM NaF, 1 mM Na_2VO_3, 1 mM DTT and protease inhibitor cocktail) with a blunt 1000 μl tip. Triton X-100 was added to a final concentration of 0.1%. The solution was mixed well and incubated on ice for 5 minutes. The tube was then centrifuged at 1,300 *g* (4000 rpm) at 4°C for 5 minutes. The supernatant (fraction S1) was separated from the pellet (fraction P1) which contains the nuclei. The fraction S1 was clarified by high speed centrifugation at 20,000 *g* (14,000 rpm) at 4°C for 5 minutes. The supernatant (fraction S2), which represents the cytosolic fraction, was collected and the pellet P2 was discarded. Fraction S2 was stored at -80°C until ready to use. Pellet P1 was washed once with buffer A (0.6 ml per tube) by centrifugation again at 4000 rpm at 4°C for 5 minutes. Pellet P1 was resuspended in 100 μl of buffer B (3 mM EDTA, 0.2 mM EGTA, 1 mM DTT, protease inhibitor cocktail) with blunt 1000 μl tip and lysed for 30 minutes on ice. The sample was then centrifuged

at 1,700 *g* (5000 rpm) at 4°C for 5 minutes. The supernatant (fraction S3), which contains the soluble nuclear proteins, was separated from the pellet (fraction P2) which contains the chromatin. S3 was stored at -80°C until ready to use. Fraction P2 was washed once with Buffer B (0.6 ml per tube) and the pellet was collected after centrifugation at 10,000 *g* (11,000 rpm) at 4°C for 1 minute. Fraction P2 was then resuspended in M-PER (Mammalian protein extraction reagent) protein extraction buffer (180 µl per sample) which was followed by a short sonication. Fraction P2 was clarified by high-speed centrifugation at 20,000 *g* (14,000 rpm) at 4°C for 5 minutes. The supernatant (fraction P3), which contains the chromatin bound proteins, was collected and kept at -80°C until ready to use.

Trypsin in-gel digestion and LC-MS/MS analysis

Coomassie blue stained protein band was excised with a scalpel on a glass plate. The band was transferred to a 0.5 ml polypropylene eppendorf tube and the excess water was removed. The band was briefly washed with 100 µl solution A (50 mM NH_4HCO_3, pH 8.0) to make sure that the piece is at the correct pH. The gel piece was then incubated with 200 µl of solution B (50 mM NH_4HCO_3/50% acetonitrile) for 10 minutes. The liquid was removed and the same step was repeated twice. The liquid was removed and the gel piece was incubated for 5 minutes in solution C (100 % acetonitrile). Solution C was removed and evaporated briefly for 5 minutes in a vacuum concentrator. Next, the gel piece was covered with 10 mM DTT in 50 mM NH_4HCO_3. The proteins were reduced for 45 minutes at 56°C in the thermocycler. The sample was cooled to room temperature and the DTT was removed and 50 µl of 55 mM iodoacetamide in 50 mM NH_4HCO_3 was

added and left to incubate for 45 minutes in the dark at room temperature. Iodoacetamide was the removed and the gel piece was washed with 100 µl of solution A for 5 minutes with shaking and then washed twice with 100 µl of solution B for 5 minutes. Next, the gel piece was dehydrated with 100 µl solution C. The remaining liquid was removed and the sample was dried in a vacuum concentrator. The gel piece was rehydrated in an ice bath for 30 minutes with 50 µl of 12 µg/µl of trypsin in solution D (50 mM NH_4HCO_3/10% acetonitrile). This was done to get as much active trypsin absorbed by the gel piece as possible before the digestion started. Trypsin was carefully removed and 50 µl of solution D was added to the gel piece. The gel piece was digested overnight at 37°C. The next day, the digest solution supernatant was transferred into a clean 0.5 ml tube. 50 µl of solution E (50% Acetonitrile/0.1% formic acid) was added to the gel piece and the tube was centrifuged at room temperature at 8000 *g* (10,000 rpm) for 1 minute followed by static incubation for 5 minutes. This was repeated twice. The supernatant was then removed and combined with the initial digest solution supernatant. The extracted digest was then vortexed and placed in a speed vacuum until dry. The sample was stored at -20°C until ready to use. For LC-MS/MS analysis the sample was resuspended in 11 µl of 5% acetonitrile, 0.1% formic acid and 0.005% heptafluorobutyric acid (HFBA). LC-ESI-MS-MS analyses of MDC1 tryptic peptides were done on a linear trap quadrupole (LTQ) mass spectrometer (Thermo Finnigan, Waltham, MA). The acquired MS/MS data was submitted to an in-house Mascot daemon search engine (www.matrixscience.com) for searches against the human protein sequences in the SwissProt database for protein and post translational modification identification. The following parameters were used in the searches: carbamidomethylation of cysteines as a fixed modification; oxidation of

methionines, deamidation of asparagines and glutamine, phosphorylation of serine, threonine and tyrosine as variable modifications.

Results

Tax interacts with MDC1

Our goal was to identify the different cellular proteins within the Tax interactome *in vivo* using the previously described *STaxGFP* vector which expresses the biologically active full length Tax protein with an amino-terminal S-tag and a carboxy-terminal green fluorescent protein (GFP). The S-Tag allowed purification of the protein, and GFP facilitated monitoring of protein expression and localization. After purification of the Tax protein followed by incubation with Jurkat nuclear extract, the bound proteins were subjected to on-bead trypsin digest and LC-MS/MS analysis. The same experiment was done using the *SGFP* vector as a control. Proteins that were known to bind Tax were found in the Tax interactome such as DNA-PK and Chk2. One new protein that found in the Tax interactome is the mediator of DNA damage checkpoint 1 (MDC1) protein.

We next sought to confirm that Tax interacts with MDC1 by pulling down Tax using the S-tax purification system. Detecting endogenous MDC1 in the whole cell lysate using the available antibodies is difficult. Therefore, we decided to overexpress both MDC1 and Tax to confirm their interaction. *HA-MDC1* was co-transfected with *STaxGFP* into 293T cells and we determined that we could efficiently co-express Tax and MDC1 (Fig. 13). Next, Tax complexes were isolated from whole cell lysates with S-agarose beads and an immunoblot with anti-HA antibody revealed that MDC1 is present in the Tax complex. When SGFP was co-expressed with HA-MDC1 and pulled down

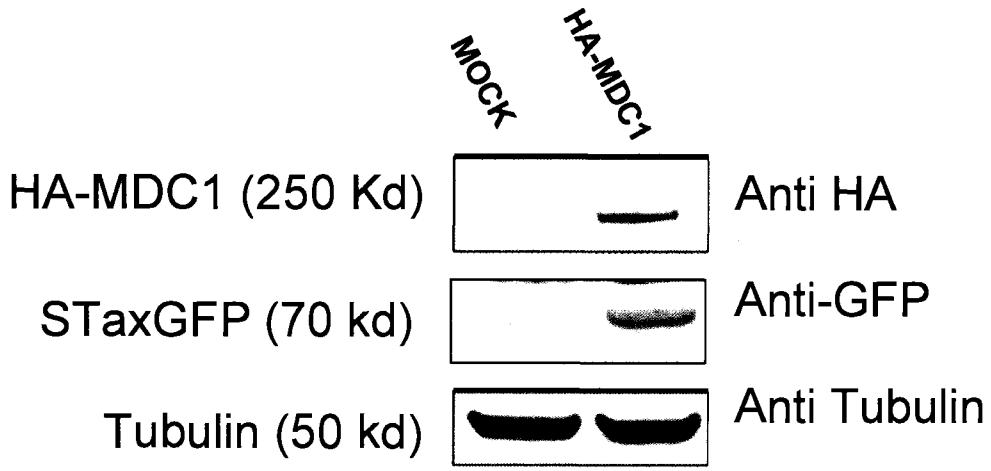

FIGURE 13 . **Efficient co-expression of STaxGFP and HA-MDC1.** Cell lysates from 293T cells transiently mock transfected or co-transfected with *HA-MDC1* and *STaxGFP* were subjected to SDS-PAGE and analysis by immunoblotting by the indicated antibodies

using S-agarose beads, we could not detect MDC1 which indicated the specificity of the Tax-MDC1 interaction (Fig. 14). In the same experiment, in addition to STaxGFP, we also pulled down STax to assay whether the GFP tag was interfering with the MDC1 interaction, which was not the case.

Next, we looked at the localization of endogenous MDC1 in the cell in the presence of Tax. Previous studies have shown that Tax forms discrete nuclear foci termed "Tax speckled structures" (TSS) (68, 115). TSS overlap with interchromatin granules and contain various proteins such as transcription factor NF-κB (115), spliceosome component 35 (SC35) (68, 115) and DNA damage factors 53BP1 (92), Chk2 (92) and DNA-PK (98). The proximity between Tax and cellular machineries involved in splicing, transcription, checkpoint activation and DNA damage repair support the concept that Tax interferes with these different pathways (92). Immunofluorescence analysis of MDC1 in Tax expressing cells determined that it colocalizes with Tax in the TSS (Fig. 15). This result, together with pull down experiment, indicates that Tax binds MDC1 and specifically co-localizes with it at discrete nuclear foci.

Tax recruits MDC1 to the chromatin in absence of DNA damage

Tax can also *trans*-activate various cellular genes through complex interaction with cyclic AMP-responsive element binding protein (CREB), CREB-response elements (CRE), and transcriptional coactivators CREB-binding protein (CBP), p300 and P300/CBP-associated factor (PCAF) (62-66). It has been shown that Tax is able to deregulate the expression of more than one hundred genes (122). Therefore, we sought to determine its effect on MDC1 expression using Western blot analysis. Our immunoblot

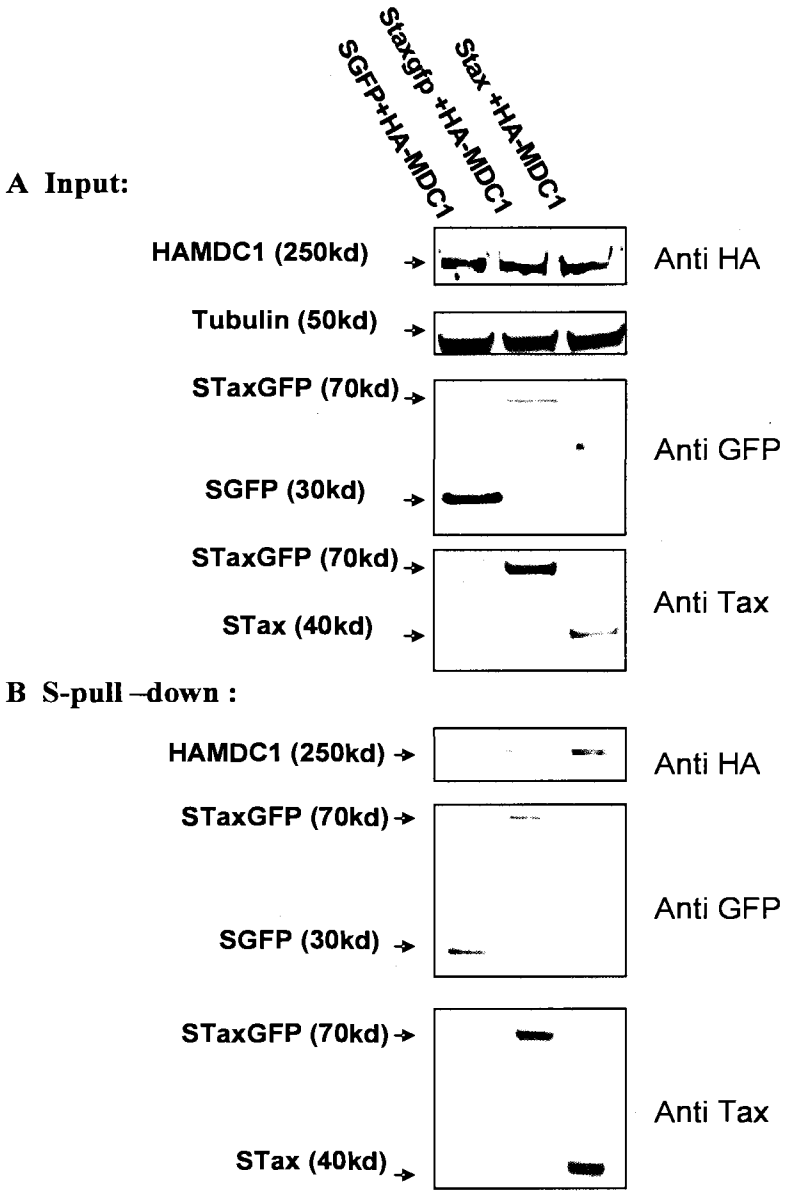

FIGURE 14. **Tax co-purifies with MDC1.** Cell lysates from 293T cells transiently co-transfected with *HA-MDC1* and *SGFP* , *STaxGFP* or *STax* (indicated) were (*A*) subjected to SDS-PAGE and analysis by immunoblotting by the indicated antibodies or (*B*) affinity purified on S-protein agarose beads as described under "Experimental Procedures" and subjected to SDS-PAGE and analysis by immunoblotting with the indicated antibody

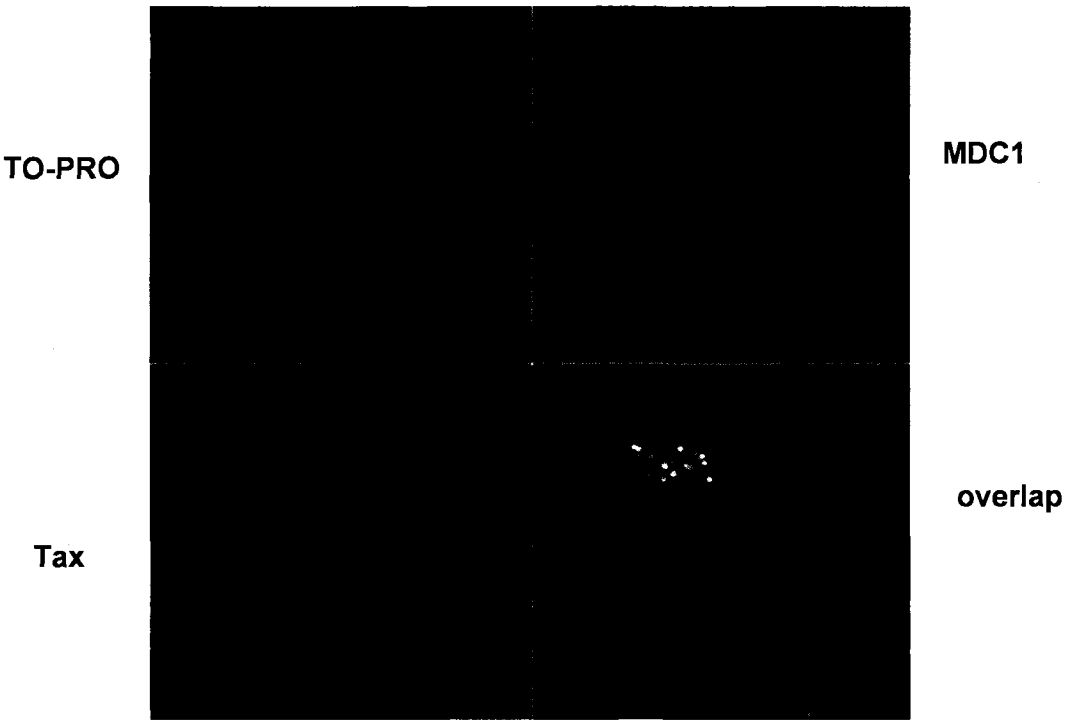

FIGURE 15. **Colocalization of Tax and MDC1.** STaxGFP was expressed in 293 FT cells. Endogenous MDC1 was detected with anti-MDC1 antibody (red, 1/200, rabbit, Santa Cruz); Tax expression was detected via the GFP fusion. Nuclei were visualized by co-staining with TO-PRO-3 iodide . Three images were merged to visualized overlap. Confocal microscopy images are magnified ×63 with a ×4 zoom.

experiments indicate that overall MDC1 protein expression was unaffected by Tax (Fig. 16*A*). It should be noted that multiple isoforms of MDC1 were detected. In addition, our laboratory previously showed that in the absence of DNA damage, Tax recruits both hyperphosphorylated DNA-PK and Chk2 to the chromatin (98, 146). Similarly, upon DNA damage, DDR proteins, such as phosphorylated DNA-PK, accumulate at the site of damage and, consequently, their levels increase in the cellular chromatin faction (119, 166-168). Recruitment of active DNA-PK to the chromatin by either Tax or in response to DNA damage leads to an increase in H2AX phosphorylation (98). MDC1 is another DDR protein that was reported to increase in the chromatin fraction following DNA damage (169). However, the effect of Tax on the level of MDC1 in the chromatin bound fraction has not been yet investigated. Immunoblot analysis of chromatin bound fractions indicated that MDC1 is increased in the chromatin in Tax expressing cells (Fig. 16*B*). This result correlates with our previous findings which suggested that Tax induces constitutive signaling of the DNA-PK pathway thus causing the impairment of the cellular response to new damage (98).

Activation of MDC1 by Tax

In the DNA-PK pathway MDC1 is a downstream target of DNA-PK. Previously, our laboratory determined that Tax recruits DNA-PK phosphorylated at Ser-2056 and Thr-2609 to the TSS suggesting that DNA-PK is active (98). Furthermore, an *in vitro* kinase assay for DNA-PK using p53 peptide as a substrate, a known target of DNA-PK, showed an increase in DNA-PK activity in the presence of Tax (98). Taken together, these results showed that Tax recruited active DNA-PK to the TSS. Similarly, we

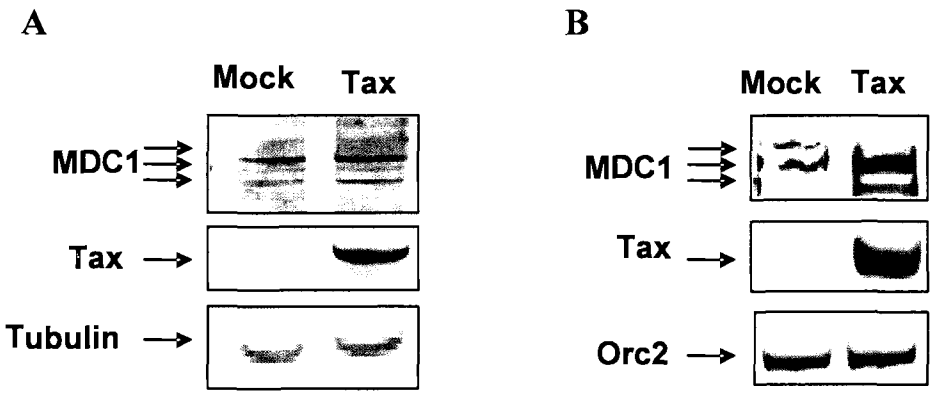

FIGURE 16. **Tax recruits MDC1 to the chromatin.** *A*, cell lysates from 293T cells transiently transfected with *Tax* or MOCK transfected were subjected to SDS-PAGE and analysis by immunoblotting by the indicated antibodies . *B*, chromatin fractions from 293T cells transiently transfected with *Tax* or Mock transfected were subjected to SDS-PAGE and analysis by immunoblotting by the indicated antibodies .

attempted to determine the activation state of the MDC1 recruited to the TSS. One simple way to determine whether MDC1 is active is to look at the level of the mono-ubiquitylated form of γ-H2AX (mono-ub-γ-H2AX) (109). In a normal cell following DNA damage, activated MDC1 recruits RNF8, a RING-finger ubiquitin ligase, which in turn ubiquitylates H2AX (Fig. 17*A*). This causes a change in chromatin conformation, thus "opening up" the DNA and allowing the recruitment of downstream DDR proteins (109). Earlier studies have been able to detect mono-ub-γ-H2AX using γ-H2AX antibodies in immunoblot experiments. The mono-ub-γ-H2AX band appeared at 25 kD, which is about 9 kD (the size of one ubiquitin) above the 16.5 kD γ-H2AX band (170, 171). Therefore, using a γ-H2AX antibody in an immunoblot analysis of chromatin fractions, we attempted to detect mono-ub-γ-H2AX. In the presence of Tax alone, we saw an increase in γ-H2AX at 16.5 kD as well as an increase in intensity of a 25 kD band which corresponds to mono-ub-γ-H2AX (Fig. 17*C*). These results suggest that, in Tax expressing cells, active MDC1 recruits RNF8, leading to ubiquitylation of γ-H2AX.

In order to make sure that MDC1 activation is responsible for ubiquitylation of γ-H2AX, we conducted a siRNA experiment in which we knocked down MDC1 expression. Immunoblot analysis of whole cell lysates showed that we could efficiently knock down MDC1 (Fig. 17*B*). When looking at the chromatin fractions, we determined that siRNA to MDC1 did not change the levels of chromatin-bound MDC1 in non-Tax expressing cells which can be explained by the already low amount of MDC1 in the chromatin (Fig. 17*C*). On the other hand, we saw a decrease in chromatin-bound MDC1 in Tax expressing cells following siRNA MDC1 treatment, confirming that MDC1 expression was knocked down (Fig. 17*C*). In parallel, we also showed a decrease in the

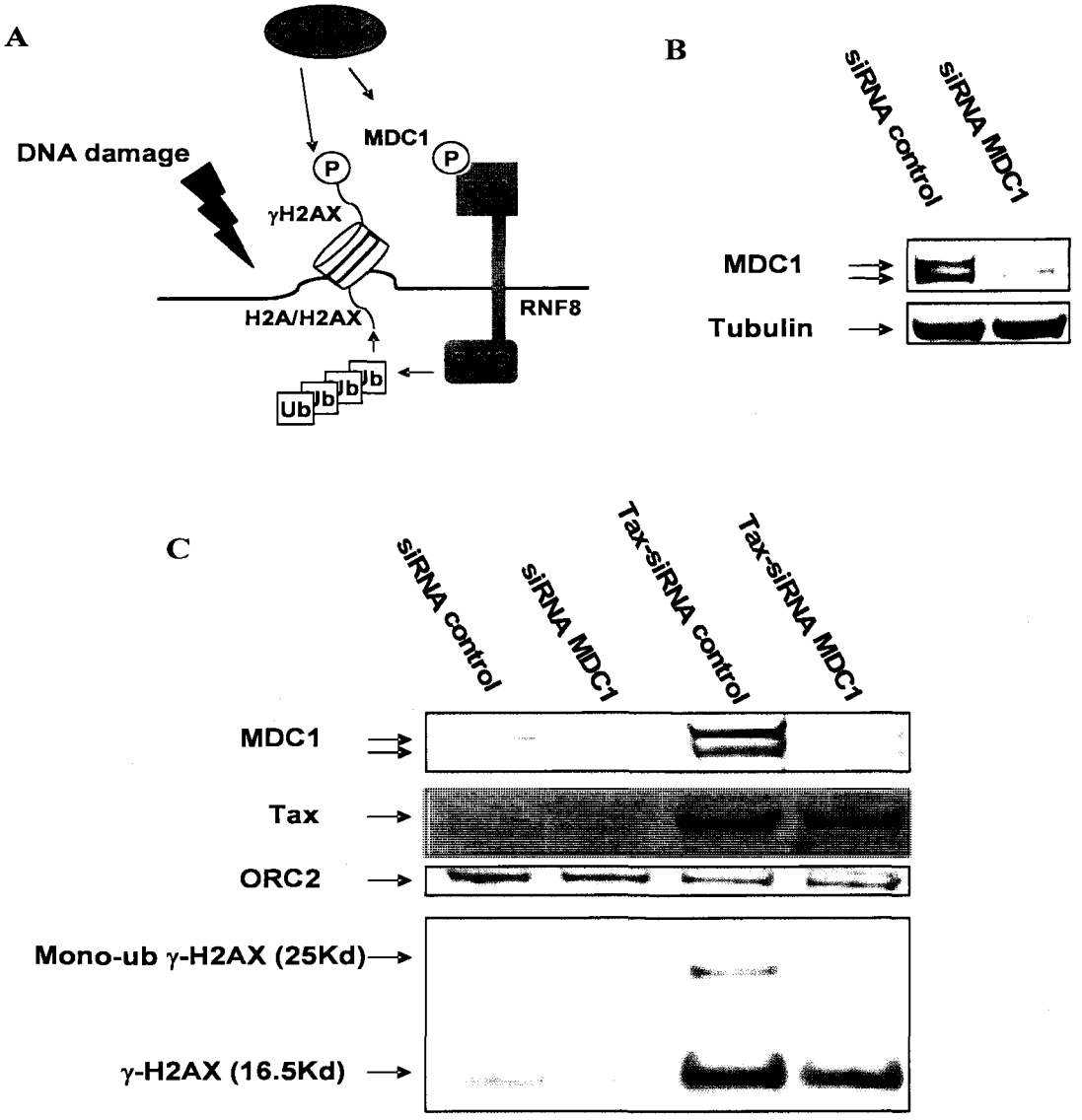

FIGURE 17. **MDC1 is activated in Tax expressing cells.** *A*, a schematic representation of the DNA-PK-MDC1 signaling pathway following DNA damage. *B*, siRNA control or SiRNA MDC1 was co-transfected with Tax in 293 T cells. Whole cell lysates were extracted and subjected to SDS-PAGE and analysis by immunoblotting by the indicated antibodies. *C*, siRNA control or SiRNA MDC1 was co-transfected with Tax in 293 T cells. Chromatin fractions were extracted as described under "Experimental Procedures" and were subjected to SDS-PAGE and analysis by immunoblotting by the indicated antibodies

Level of mono-ub-γ-H2AX in cells co-transfected with Tax and siRNA against MDC1, thus demonstrating that MDC1 is active in Tax expressing cells (Fig. 17*C*).

Phosphorylation analysis of MDC1

Following DNA damage, MDC1 is phosphorylated. Phospo-peptide mapping of MDC1 has not been done thoroughly due to the size and complexity of the protein (163). However, a few phosphorylation sites have been identified in MDC1 following DNA damage (172) and we wanted to determine whether Tax induced phosphorylation of any of these sites. In this experiment, we overexpressed and immunoprecipitated HA-MDC1 in Tax expressing cells and non-Tax expressing cells, in the presence and absence of ionizing radiation (Fig. 18). Following excision and tryptic digestion of the HA-MDC1 bands, LC-ESI-MS-MS analyses of MDC1 tryptic peptides was done on a linear trap quadrupole (LTQ) mass spectrometer (Thermo Finnigan, Waltham, MA). The results show that MDC1 is phosphorylated at several sites in the presence of Tax alone. These sites are S-372, S-780, T-579, S-793, T-1157 and S-1175. S-372 is a site that was previously reported to be phosphorylated in MDC1 following ionizing radiation (172). Fig. 19 shows an example of a MS/MS spectrum of a phosphorylated peptide with a dominant neutral loss peak of a H_3PO_4 group from the +3 parent ion. The search identifies the MDC1 peptide IFHGVGTRGPGAPGLAHLQESQAGSDTDVEEGKAPQ AVPLEK phosphorylated at S-372. This result suggests that MDC1 is activated in Tax-expressing cells. It should be noted that there are 216 possible phosphorylation sites in MDC1 and earlier studies have unsuccessfully attempted to do a complete phosphopeptide mapping of the protein (163). This has been a challenge due to the

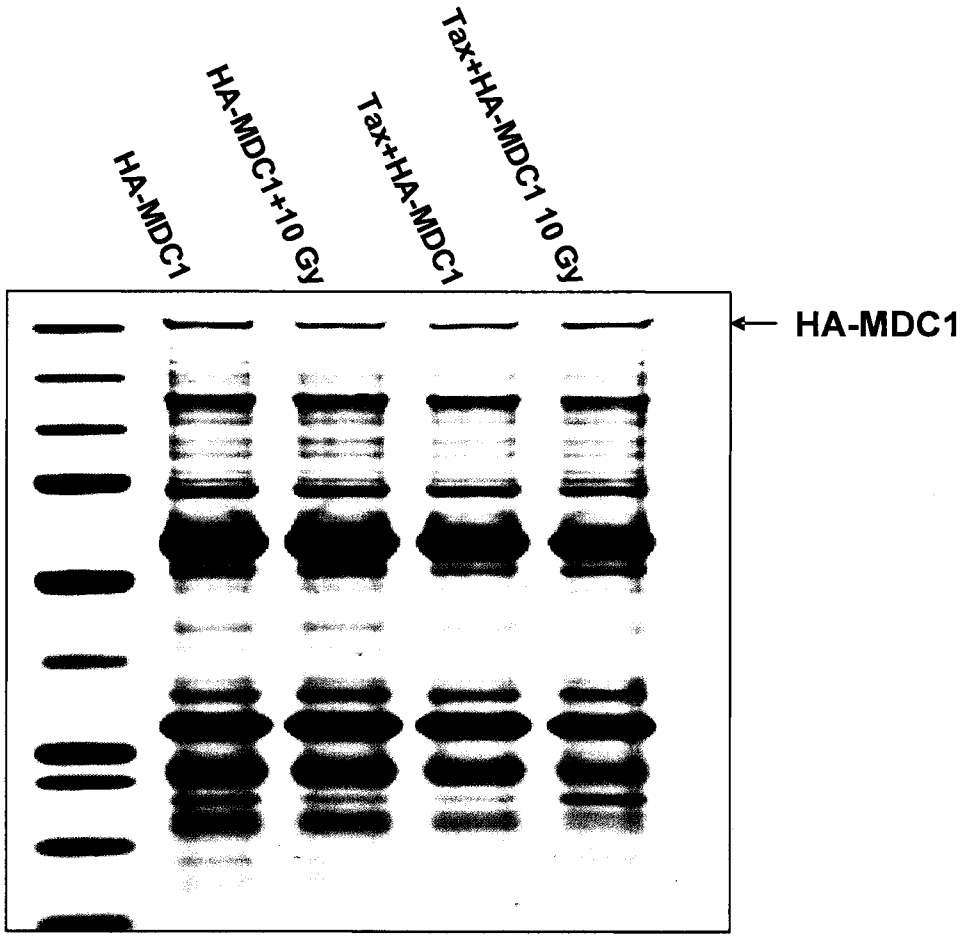

FIGURE 18. **HA-MDC1 immunoprecipitation.** Whole cell lysates from cells transfected with *HA-MDC1* or *HA-MDC1* and *Tax* treated with 10 Gy or no ionizing radiation were immunoprecipitated with anti-HA rabbit as described under "Experimental Procedures". Samples were loaded on a 4-12% SDS-PAGE. The gel (1.5 mm thick) were stained by Bio-Safe Coomassie Blue (Bio Rad) for 1 hr at RT.

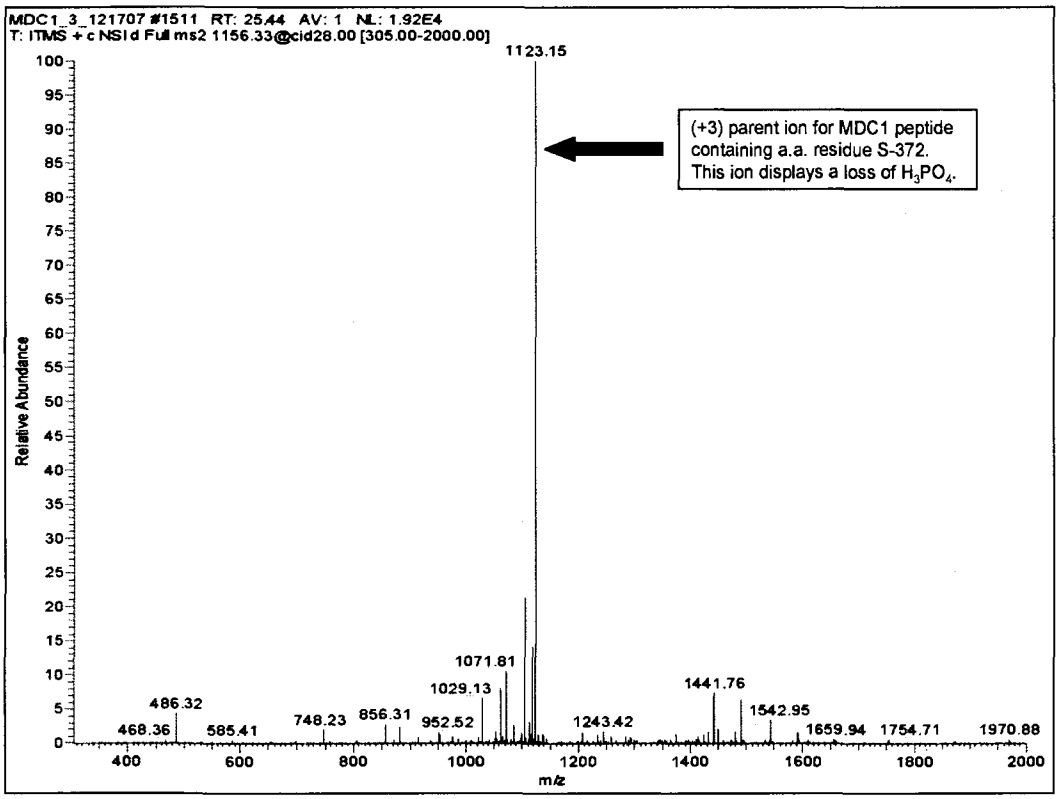

FIGURE 19. **MS/MS spectra of MDC1 peptide from amino acid 360 to amino acid 393 with a neutral loss of a phosphate group.** MS/MS spectrum of a phosphorylated peptide with m/z 1156.33 with a loss of H_3PO_4 forming a dominant 1123.15 peak.

complexity of the protein and the high number of phosphorylation sites. Phosphorylation of MDC1 at S-372 is yet another indication that it is active in the Tax expressing cells, but a more extensive phosphorylation analysis needs to be done to confirm the observed phosphorylation sites.

Discussion

Cellular transformation caused by the HTLV-1 Tax oncoprotein is partly achieved by the induction of genomic instability. One piece of evidence of Tax induced genomic instability is the fact that the presence of Tax alone leads to micronuclei formation, which represents fragmented chromosomes indicative of DNA damage, or defects in DNA repair or in chromosomal segregation (76). Maintenance of the integrity of the genome depends greatly on a properly functioning DNA damage repair pathway. During the cell cycle, DNA can be damaged by various sources, such as environmental factors, and needs to be repaired (75). Failure to repair the damage can lead to the mother cell passing on mutations to its daughter cells which can have catastrophic consequences (75).

Tax was first linked to the DNA repair pathway when it was shown that it represses the transcription of the human DNA polymerase β (pol β) promoter (93), an enzyme involved in base excision repair (BER) and mismatch repair (MMR) (94). Tax is also able to suppress nucleotide excision repair (NER) (95), correlating with its ability to activate the transcription of the proliferating cell nuclear antigen (PNCA) (96, 97). In addition, Tax also interferes with the non-homologous end-joining (NHEJ) repair pathway which is crucial in the repair of DNA double strand breaks (DSB) (98). DNA double strand breaks (DSB) are one the most hazardous types of damage because they

can cause genome rearrangement (173). Our laboratory previously showed that Tax dysregulates the DSB repair pathway by directly interacting with DNA-PK (98) and Chk2 (92). In addition to binding DNA-PK, Tax induces its hyperphosphorylation at S2056 and T2609, thus activating it. This, in turn, leads to an increase in γ-H2AX (98). It was hypothesized that constitutive H2AX phosphorylation in Tax expressing cells was interfering with the DNA damage repair machinery by not allowing the cell to detect and repair newly formed damage (98, 105, 106).

Previously, we identified MDC1 as part of the Tax interactome using LC-MS/MS. MDC1 is essential in the repair of DSB. Following DNA damage, activated MDC1 binds to the phosphorylated serine 139 of H2AX, and in turn recruits the RING-finger ubiquitin ligase RNF8 to the IRIF. Next, RNF8 ubiquitylates γ-H2AX, thus leading to a change in chromatin conformation and allowing the recruitment of more DDR proteins (109). The central role of MDC1 is illustrated by the fact that MDC1 -/- mice demonstrate many phenotypes of H2AX -/- mice, including growth retardation, male infertility, immune defects, chromosome instability, DNA repair and radiation sensitivity (113).

In the current study, we first confirmed the interaction between the HTLV-1 oncoprotein Tax and MDC1 using pull down and immunoblotting assays. Furthermore, several Tax binding proteins are known to colocalize with Tax in the TSS (92, 98). Therefore, we decided to investigate using immunohistochemistry the localization of MDC1 in Tax expressing cells. We determined that Tax does indeed colocalize with MDC1. Taken together, these results show that Tax binds MDC1 and recruits it to the TSS. This correlates with the presence of phosphorylated DNA-PK hyperphosphorylation at S2056 and T2609 in the TSS (98). Furthermore, Tax alters cellular pathways by either

directly binding proteins involved in those pathways or by *trans*-activating transcription of cellular genes (62-66). Therefore, we looked at the total expression level of MDC1 in Tax-expressing cells. The total amount of MDC1 did not change suggesting that Tax does not activate or repress MDC1 expression.

MDC1 was also reported to increase in the chromatin fraction after DNA damage (169) and we made the same observation in Tax expressing cells. Furthermore, using siRNA experiment we found evidence that MDC1 activity is increased in Tax-expressing cells. An increase in mono-ub-γ-H2AX in the presence of Tax suggests that MDC1 is active. This was further confirmed by the decrease in mono-ub-γ-H2AX seen after MDC1 knock down in Tax expressing cells.

Finally, we also attempted to do a phosphopeptide mapping of MDC1 and found that is was phosphorylated at several sites in the presence of Tax alone, including a site that was reported to be phosphorylated following ionizing radiation. This result is another indication that MDC1 is active in the presence of Tax. In the future, a comprehensive phosphopeptide mapping can be done by using different approaches. For example targeted MRM targeted analyses of tryptic peptides from the protein. The stoichiometry between phosphorylated and non-phosphorylated peptides is usually low but this can be overcome by using phosphopeptide specific affinity purification strategies, for example IMAC (immobilized metal affinity chromatography) using gallium beads, titanium dioxide, and Fe^{3+} to enrich the phosphopeptide before MS analysis.

SECTION 5

DETERMINE THE FUNCTIONAL SIGNIFICANCE OF THE INTERACTION OF TAX AND MDC1

Introduction

The transforming retrovirus human T-cell leukemia virus type 1 (HTLV-1) is the etiological agent of adult T-cell leukemia (ATL) and HTLV-1 associated myelopathy/tropical spastic paraparesis (HAM/TSP) (19, 34). The HLTV-1 Tax protein plays a central role in viral transcription and cellular transformation (20, 37, 114, 120, 121). The oncogenic potential of Tax is illustrated by the fact that its expression can alone cause cellular transformation (114). Tax binds and interferes with several proteins involved in cell cycle and DNA damage repair. This is thought to be a major cause of the Tax induced genomic instability, which ultimately leads to oncogenesis (75, 84, 92, 114, 174, 175).

A previous study from our laboratory determined that Tax interacts with DNA-dependent Protein Kinase (DNA-PK), a protein involved in the repair of DNA double strand breaks (DSB) (98). In addition, it was shown that Tax induces the phosphorylation of DNA-PK at Ser-2056 (DNA-PK pS2056) and Thr-2609 (DNAP-PK pT2609) suggesting that DNA-PK is active. This was further confirmed by an *in vitro* kinase assay which showed an increased DNA-PK activity in the presence of Tax (98). Activation of DNA-PK in Tax expressing cells leads to the phosphorylation of the histone protein H2AX (termed γ-H2AX) (98). In a normal cell, γ-H2AX is considered as an early marker of DNA damage. In addition, we have shown in this work that Tax binds and induces the

activation of another DNA damage repair (DDR) protein called the mediator of DNA damage checkpoint 1 (MDC1). MDC1 regulates various aspects of DNA damage response pathways such as DNA-PK auto-phosphorylation (111) and the Chk2-mediated DNA damage responses (112). MDC1 also binds γ-H2AX at the phosphorylated serine 139 and recruits RNF8, a RING-finger ubiquitin ligase, which in turn ubiquitylates H2AX. This induces a change in chromatin conformation causing the DNA to "open up", thus allowing the recruitment of downstream DDR proteins (109, 110). Taken together, these results showed that Tax binds and activates several proteins involved in the DNA damage repair pathway.

Previous studies have shown that Tax forms discrete nuclear foci termed "Tax speckled structures" (TSS) (68, 115). TSS overlap with interchromatin granules and contain various proteins such as transcription factor NF-κB (115), and spliceosome component 35 (SC35) (68, 115). Our laboratory also determined that Tax recruits several DDR to the TSS, including phosphorylated DNA-PK at Ser-2056 and Thr-2609 (98) and MDC1. In a normal cell, following DNA damage, DDR proteins get recruited to the DNA damage sites called ionizing radiation-induced nuclear foci (IRIF) (104). Our findings show a lot of similarities between IRIF and TSS. There are two possible explanations for this resemblance. The first hypothesis is that Tax causes DNA damage thus inducing the recruitment of DDR in the TSS. The second possibility is that Tax causes aberrant activation of DDR proteins at the TSS in the absence of DNA damage, which could lead to the dysregulation of the DNA damage repair machinery. To answer this question, we needed to determine whether there is an increase in DNA damage in Tax-expressing cells. Several DDR proteins such as γ-H2AX have been used to detect

newly formed DNA damage. However, in this study, due to the similarities between TSS and IRIF, it was crucial to use an assay that directly detects the DNA breaks rather than a protein involved in the signaling of the repair.

Here, we hypothesized that the impairment of the DNA damage repair machinery by Tax does not allow the cell to detect and repair newly formed DNA damage. Therefore, we also designed experiments in which we looked at DDR proteins in the presence of both Tax and DNA damage. In addition, our laboratory previously generated a Tax deletion mutant which corresponds the to minimum sequence requirement to be targeted to the TSS. It was determined that the mutant had both the Nuclear localization signaling (NLS) as well as the Tax TSS localization signal (TSS) (69). Therefore, we attempted to test the mutant's ability to recruit DDR to the TSS. Finally, we sought to assess the role of MDC1 in TSS formation. To do so, we used a MDC1 knock out cell line and determined whether it had any effect on the TSS and the recruitment of other DDR proteins.

The objective of this aim is to determine the role of MDC1 in the Tax induced genomic instability. We will accomplish this objective using the following *experimental approaches*. (1) We will measure DNA damage in Tax expressing cells in the presence and absence of ionizing radiations using a BrdU assay; (2) We will use immunohistochemistry techniques to determine the effect of both Tax and IR on the localization MDC1 and other DDR proteins in the cell; (3) We will express a Tax deletion mutant which corresponds to the minimum sequence requirement to be targeted to the TSS and determine if it is sufficient to recruit DDR proteins; (4) We will use a MDC1 knockout cell line and determine the role of MDC1 in TSS formation.

Experimental Procedures

Cell culture and transient transfection

293T cells were maintained at 37°C in a humidified atmosphere of 5% CO_2 in air, in Iscove's modified Dulbecco's medium supplemented with 10% fetal bovine serum (Cambrex, East Rutherford, NJ) and 1% penicillin-streptomycin (Invitrogen, Carlsbad, CA).

Transfections of 293T cells were performed by standard calcium phosphate precipitation. Cells were plated at $1x10^5$ cells/ml. The following day, plasmid DNA in 2M $CaCl_2$ and 2X HBS were added dropwise to cells in fresh medium. Cells were incubated at 37°C overnight and fresh medium was added. The cells were harvested 48 h post-transfection, following a single wash with 1X PBS, in 500 µl M-Per mammalian protein extraction reagent (Pierce, Rockford, IL) with protease inhibitor cocktail (Roche, Palo Alto, CA) and immediately frozen at –80°C.

Mouse embryonic fibroblast MDC1 knockout cells were a gift from Dr. Lou, Mayo Clinic, Rochester, MN. The cells were maintained at 37°C in a humidified atmosphere of 5% CO_2 in air, in Dulbecco's modified Eagle medium supplemented with 10% fetal bovine serum (Cambrex, East Rutherford, NJ) and 1% penicillin-streptomycin (Invitrogen, Carlsbad, CA). For transient transfection, cells were plated on coverslip at $1x10^5$ cells/ml in 6 well plates and left to grow overnight. The following day medium was changed with serum free and antibiotic free media 1 hour prior to transfection. A total of 6 µg of *STaxGFP* was diluted in 250 µl of Opti-MEM® I medium without serum. Next, Lipofectamine™ 2000 was gently mixed then 5 µl was diluted in 250 µl of Opti-MEM® I

medium without serum in a separate tube. The mixture was mixed gently and incubated for 5 minutes at room temperature. After 5 minutes incubation, the diluted DNA was mixed with the diluted Lipofectamine™ 2000. The solution was mixed gently and incubated for 20 minutes at room temperature to allow complex formation to occur. The DNA-Lipofectamine™ 2000 complexes were then added to the plate. We then mixed gently by rocking the plate back and forth. We incubated the cells at 37°C in a CO_2 incubator for 6 hours. The media was replaced with media that had serum and antibiotic. Cells were left to grow for 48 hours.

Plasmids

Generation of the *STaxGFP*, *STax* and *SGFP* plasmids have been described earlier (144). Briefly, the S-tagged expression vectors *STaxGFP*, *STax* and *SGFP* were constructed by inserting the *tax-EGFP* fusion or *EGFP* ORF, respectively, into the *Sma*I site of *pTriEx4-Neo* (Novagen, Madison, WI) in frame with the amino-terminal S-tag and His-tag.

BrdU Assay

Mock transfected and *STaxGFP* transfected cells were labeled with 10 μg/ml of 5' bromo 2' deoxyuridine (BrdU, Sigma, St. louis , MO) for 30 h, then treated with 15 Gy of X-rays or left untreated. After ionizing radiation, cells were left to grow for 16 hours, fixed with methanol for 5 minutes at -20°C and blocked with 3% BSA for 30 minutes. Cells were immunolabelled with anti BrdU followed by anti mouse Alexa Fluor 594-

conjugated secondary antibody (Molecular Probes). Nuclei were counterstained with To-Pro-3 iodide (Molecular Probes) diluted at 1/1,000.

Immunoblot analysis

Proteins separated by electrophoresis were transferred to Immobilon-P membranes (Millipore, Billerica, MA) using the semidry transfer method with 20 V applied for 1 hour. The membranes were then blocked for 1 hour at room temperature in 1X Odyssey blocking buffer (Li-Cor Biosciences, Lincoln, NE). Primary antibodies diluted in 1x Odyssey blocking buffer were applied to the membranes and allowed to interact at 4°C overnight on an orbital shaker. Membranes were washed four times for 5 minutes with PBS-1% Tween. Li-Cor Odyssey secondary antibodies were diluted to a concentration of 1/20,000 in 1x Odyssey blocking buffer containing 0.5% SDS and 0.5% Tween and then incubated for 1 hour at room temperature on an orbital shaker in the dark. The membranes were washed four times for 5 minutes with PBS-1% Tween and then stored in PBS and in the dark until ready to be analyzed. Blots were scanned and analyzed with a Li-Cor Odyssey scanner and software (Li-Cor Biosciences, Lincoln, NE).

Immunofluorescence

Cells were plated on a coverslip and treated with 10 Gy of X-rays or left untreated. After 4 hours, cells were washed twice with ice-cold PBS. Cells were then fixed with 4% paraformaldehyde for 12 minutes at room temperature. Next, cells were washed 3 times with PBS. Methanol was added and left on the cells for 2 minutes. Cells were washed 4 times with PBS. The primary antibody was diluted in 3% bovine serum

albumin (BSA) in PBS at the appropriate concentration. A 100 µl drop of the diluted primary antibody was then placed on parafilm in a wet chamber. The coverslip was then inverted onto the drop and left incubating at 4°C overnight. The next day, the coverslip was removed from the parafilm and placed back into the tissue culture dish. The cells were washed twice with PBS-1% Tween 20 and twice with PBS. The species-appropriate Alexa Fluor 594-conjugated secondary antibody (Molecular Probes) was diluted at 1/1000 in 3% BSA in PBS. Nuclei were counterstained with To-Pro-3 iodide (Molecular Probes) diluted 1/1,000 in the same BSA-PBS and secondary antibody solution. A 100 µl drop of BSA-PBS solution containing both the secondary antibody and To-Pro-3 was placed onto parafilm in a wet chamber. The coverslip was inverted onto the drop and left incubating for 1 hour at room temperature in the dark. Next, the coverslip was put back into a tissue culture dish and washed twice with 3% BSA in PBS then twice with PBS. One drop of Vectashield mounting medium with DAPI (Vector Laboratories Inc, Burlingame, CA) was placed onto a slide. The coverslip was inverted onto the slide and left to air dry for one hour at room temperature in the dark. The coverslip was then sealed to the slide using nail polish. Confocal fluorescent images were acquired using a Zeiss LSM 510 confocal microscope at 63X magnification with a 2X zoom using Argon (488 nm), HeNe1 (543 nm), and HeNe2 (633 nm) lasers, and imaged with LSM Image Browser software (Carl Zeiss, Jena, Germany).

Antibodies

For immunofluorescence analysis, we used the following antibodies: anti-MDC1 goat polyclonal (1/100, Santa Cruz Biotechnology, Santa Cruz, CA), anti-BrdU mouse

monoclonal (1/50, BD Biosciences, San Jose, CA), anti-BRCA1 mouse monoclonal (1/100, Santa Cruz Biotechnology, Santa Cruz, CA), anti-NBS1 rabbit polyclonal (1/400, Novus Biologicals, Littleton, CO), anti-DNA-PK pT2609 mouse monoclonal (1/400, Abcam, Cambridge, MA).

Results

Tax does not induce DNA breaks

Compelling data from our laboratory suggests that Tax activates and recruits several DDR proteins to the TSSs such as DNA-PK (98), Chk2 (92) and MDC1. In other words, TSS seem to mimic IRIF. Therefore, we attempted to determine whether the recruitment of DDR proteins to the TSS is the result of actual DNA damage. To do so, we needed to use an assay that can directly detect the DNA breaks. Therefore, we used a BrdU staining protocol that allows the visualization of single-stranded DNA breaks after ionizing radiation (IR) (176). Briefly, Tax expressing cells were pulsed with BrdU for 30 hours before ionizing radiation treatment, to completely label the DNA. No denaturation step was used before anti-BrdU staining, therefore the only accessible BrdU epitopes occur at sites of single-stranded DNA breaks (SSBs). Ionizing radiation mainly causes DSBs, but as the damage sites are being repaired, DNA DSBs are processed into single stranded DNA (ssDNA) (176, 177). If TSS are in fact sites of DNA damage and DDR proteins are recruited to these sites then these damage sites should be getting repaired. Thus at least some of them, if not all, should be converted to ssDNA. The BrdU experiment was conducted in Tax expressing cells in the absence of DNA damage, and our data show that the TSS are not sites of DNA damage since they did not stain for

BrdU (Fig. 20*A*). This result supports the idea that Tax recruits several DDR proteins to the TSS such as Chk2 (92), DNA-PK (98) and MDC1 and aberrantly activates them. Ultimately, this may lead to the dysregulation of DNA damage repair pathway.

IRIF and TSS are distinct structures

The same BrdU assay was also conducted on Tax expressing cells treated with IR. This allowed us to determine the location of the TSS relative to the IRIF. The majority of IRIF do not colocalize with the TSS following IR (Fig. 20*A*). In addition, we counted the number of DNA damage sites in cells that express and do not express Tax before and after IR (Fig. 20*B*). We found that the average number of foci is generally the same regardless of the presence or absence of Tax. This result shows that Tax does not induce an increase in DNA damage following IR.

Characterization of the IRIF and the TSS

We determined that the TSS and IRIF are distinct from each other. We also showed that Tax does not induce an increase in IRIF when cells are treated with IR. Still, the dysregulation of the DNA damage repair machinery via the recruitment of DDR proteins to the TSS seem to be a crucial mechanism by which Tax induces genomic instability. Next, we investigated the effect of IR on MDC1 and phosphorylated DNA-PK localization in Tax expressing cells (Fig. 21). Immunofluorescence analysis showed that DNA-PK pT2609 is located in both IRIF and TSS following IR. On the other hand, MDC1 seems to leave the TSS and is relocalized to the IRIF. This suggests that there is a

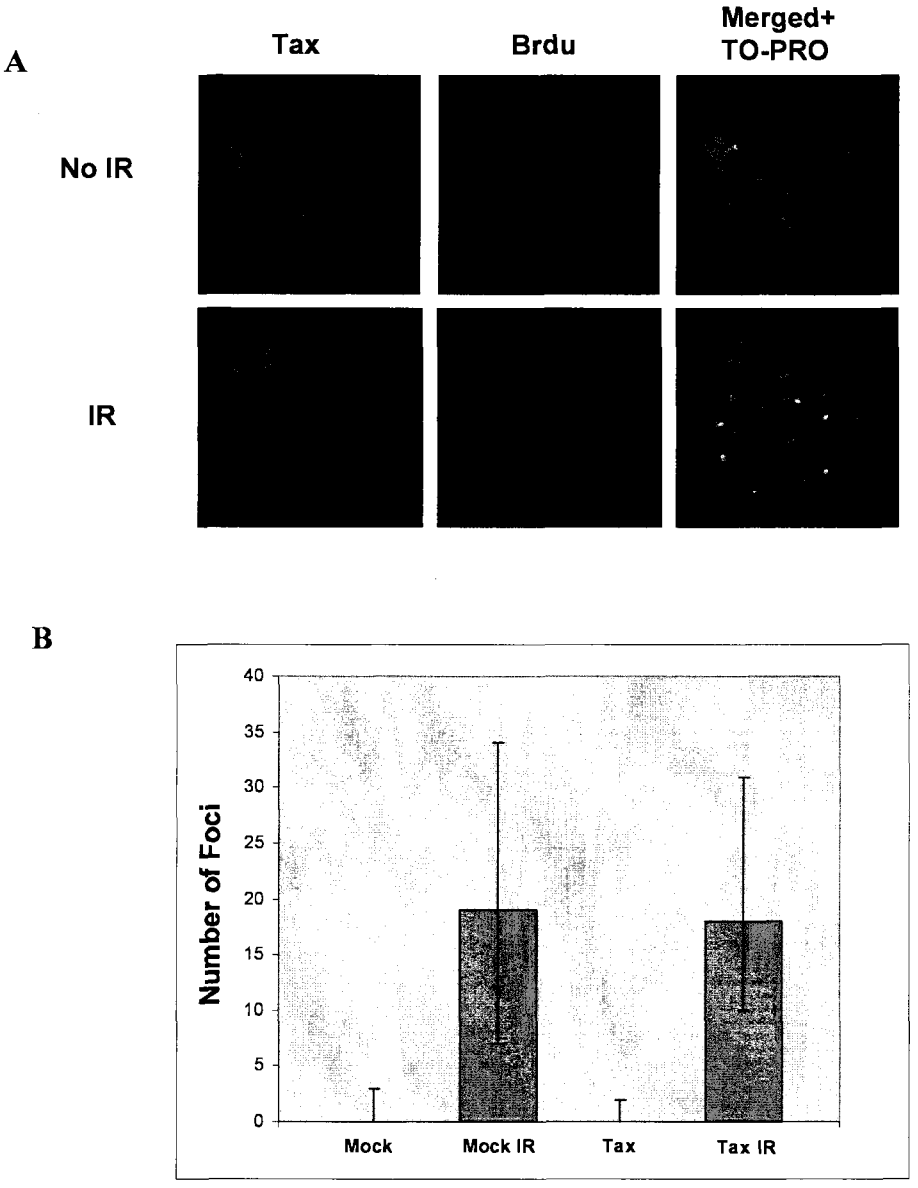

FIGURE 20. **Tax does not induce DNA breaks.** *A*, STaxGFP was expressed in 293 T cells and the cells were pulsed with BrdU for 30 hours. When indicated, cells were treated with ionizing radiation and fixed with methanol 16 hours post-Ionizing radiation. BrdU was detected with the indicated antibody. Tax expression was detected via the GFP fusion. Nuclei were visualized by co-staining with TO-PRO-3 iodide. Three images were merged to visualized overlap. Confocal microscopy images are magnified ×63 with a ×4 zoom. *B*, mean number of BrdU foci per cell. Foci were counted in 30 cells for each condition and averaged.

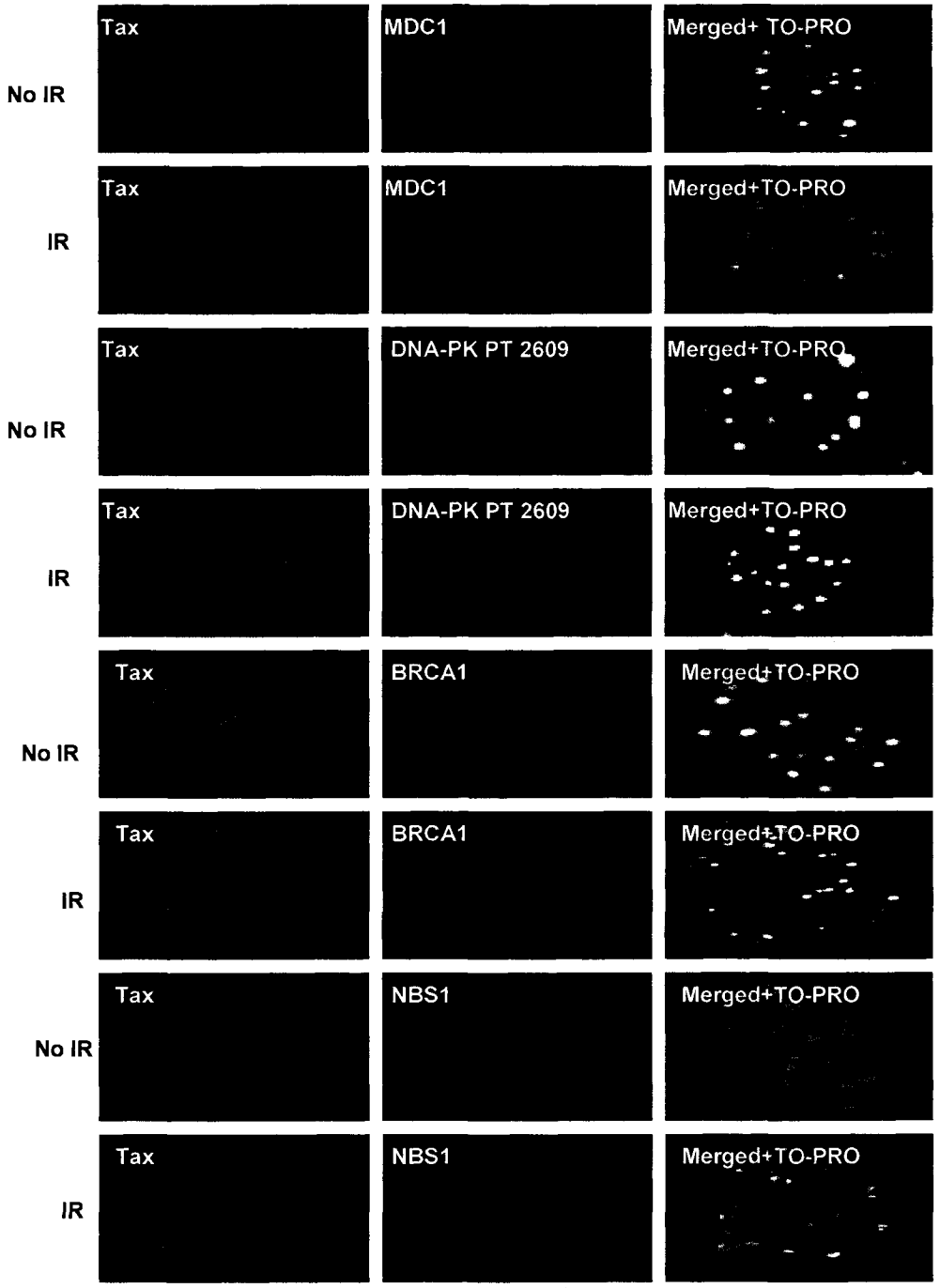

FIGURE 21. **Characterization of IRIF and TSS .** STaxGFP was expressed in 293 T cells. Cells were treated with Ionizing radiation when indicated. Endogenous MDC1, DNA-PK- pT2609, BRCA1 and NBS1 were detected with the indicated antibodies; Tax expression was detected via the GFP fusion. Nuclei were visualized by co-staining with TO-PRO-3 iodide. Three images were merged to visualized overlap. Confocal microscopy images are magnified ×63 with a ×4 zoom.

limited amount of MDC1 in the nucleus and that it is competed for between TSS and IRIF. DNA-PK levels may be high enough in the cells so that it is sufficient to be present in both TSS and IRIF. This finding demonstrates that MDC1, contrary to DNA-PK, is a limiting factor and that the competition for MDC1 between TSS and IRIF may play a role in the dysregulation the DNA damage machinery by Tax.

In addition, we decided to further characterize the IRIF and the TSS by looking at DDR proteins that were not previously known to colocalize with Tax. BRCA1 is a DDR protein that interacts indirectly with Rad51 (178) and directly with SWI/SNF (179) which are both known to bind Tax (130). A colocalization study of BRCA1 determined that this protein follows the same pattern as pT 2609-DNA-PK (Fig. 21). In other words, in the absence of DNA damage, it is present in the TSS and following IR it is located in both the TSS and IRIF, suggesting TSS and IRF do not compete for BRCA1. Another DDR protein that we investigated is NBS1 which is part of the MRE11–RAD50–NBS1 (MRN) complex. This complex is crucial for DNA damage repair and it is recruited to the DNA damage site by MDC1 via the binding of the phosphorylated Ser-Asp-Thr (SDT) repeats of MDC1 to the N-terminal FHA domain of NBS1 (162, 163). Interestingly, immunofluorescence analysis shows that NBS1 is not present in the TSS (Fig. 21). This result suggests that when present in the TSS, MDC1 is unable to recruit NBS1. More importantly, this also highlights a significant difference between TSS and IRIF, demonstrating that even though these two entities are similar, they are not identical.

Tax protein bridges the recruitment of DDR proteins to the TSS

Tax is present in both the nucleus and the cytoplasm and needs to be targeted to the TSS. Our laboratory determined that in addition to the nuclear localization signal (NLS) that targets Tax to the nucleus, there is a TSS localization signal (TSLS) that is needed for Tax to be directed to the TSS (69). The TSLS was mapped to a region containing amino acids 50 to 75 (Fig. 22*A*). The NLS is adjacent to the TSLS and is between amino acid 18 and 52 (69, 180). In that same study, it was determined that the minimum sequence requirement for the targeting of Tax to the TSS was from amino acid 1-75 (69). Here, we investigated whether targeting Tax to the TSS is sufficient for the recruitment of DRR proteins. Our results shows that the Tax mutant does not colocalize with DNA-PK pT2609 and MDC1 (Fig. 22*B*), demonstrating that the 1-75 region is responsible for the targeting and that the rest of the protein, from amino acid 75 to 353, is required for the recruitment and activation of DDR proteins. This result suggests that Tax bridges the recruitment process.

MDC1 is not required for TSS formation

In order to investigate the role of MDC1 in the formation of TSS, we used MDC1 mouse embryonic fibroblast (MEF) knockout cells. Alternatively, we could have used siRNA technique to knockdown MDC1. However, this technique would leave a small amount of MDC1 in some cells which might still be sufficient for proper TSS formation. The use of MDC1 knockout cell lines insures the total absence of MDC1 in all the cells. In other words, if we can see TSS in MDC1 knockout cells, it would mean that Tax does not require MDC1 to form the TSS. Results from our immunofluorescence studies

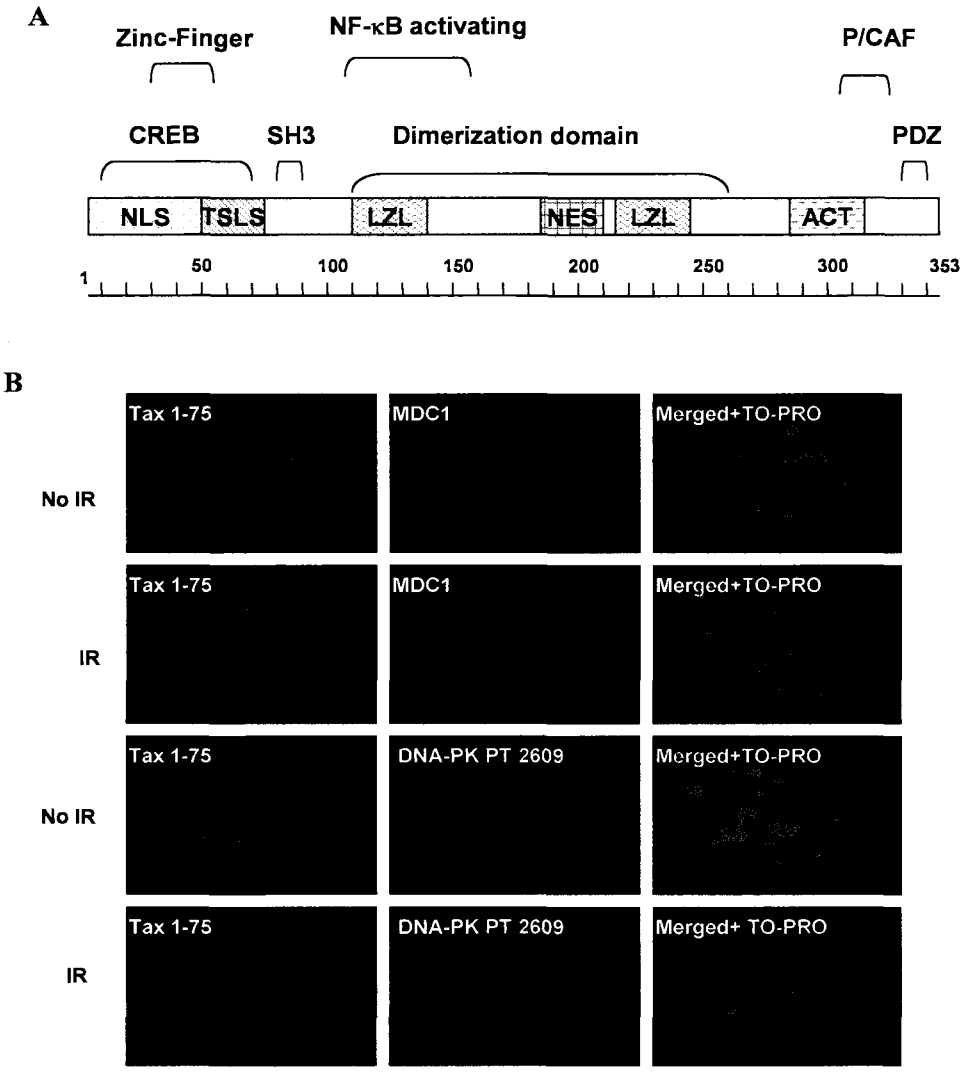

FIGURE 22. **Tax 1-75 does not recruit DDR proteins to the TSS.** *A*, diagram of Tax showing the relative positions of the nuclear Localization signal (NLS), TSS localization signal (TSLS), leucine zipper region (LZL), nuclear export signal (NES), activation domain (ACT). Also indicated are the CREB-interacting, zinc finger, SH3 binding, PDZ binding, dimerization, and P/CAF binding domains. *B*, S-Tax-1-75-GFP was expressed in 293 T cells. Cells were treated with Ionizing radiation when indicated. Endogenous MDC1 and DNA-PK-pT2609 were detected with the indicated antibodies; Tax expression was detected via the GFP fusion. Nuclei were visualized by co-staining with TO-PRO-3 iodide. Three images were merged to visualized overlap. Confocal microscopy images are magnified ×63 with a ×4 zoom.

showed that TSS could efficiently form in the MDC1 knockout cells (Fig. 23). This suggests that TSS first form, next MDC1 is recruited and activated.

Discussion

Tax is known to interact and interfere with several DDR proteins. These interactions are though to be a major cause of the Tax induced genomic instability, which ultimately leads to oncogenesis (75, 84, 92, 114, 174, 175). Our laboratory showed the interaction of Tax with the DDR protein MDC1. MDC1 regulates various aspects of DNA damage response pathways (109-112). Interestingly, it seems that Tax not only recruits MDC1 and other DDR proteins to the TSS but it also induces their activation (98, 146). These data suggested that TSS might mimic IRIF. To investigate this hypothesis, we attempted to further characterize these two entities.

Here, we demonstrated that, contrary to IRIF, TSS are not sites of DNA damage. This result allows us to clearly distinguish between TSS and IRIF. In addition, we saw that following IR treatment, the DNA damage sites were localized away from the TSS. This correlates with our immunofluorescence studies when looking at the localization of different DDR proteins. In fact, following IR, some DDR proteins such as MDC1 seem to be relocalized from the TSS to the IRIF. On the other hand, other DDR proteins like DNA-PK pT2609 and BRCA1 are located in both TSS and IRIF. We hypothesized that this difference might be due to the level of each protein in the cell. DNA-PK and BRCA1 may be abundant enough that they can be recruited to both the IRIF and TSS. However, levels of MDC1 in the cell, which we have previously shown to not change in the presence of Tax, might be too low for MDC1 to be recruited to both TSS and IRIF.

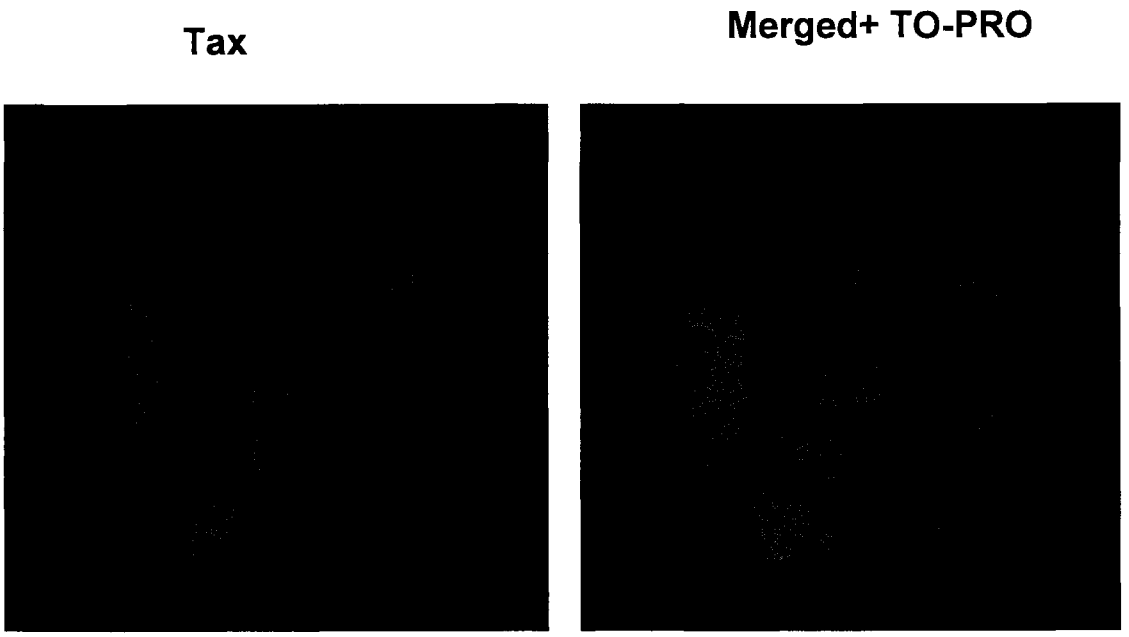

FIGURE 23. **Tax is able to form TSS in MDC1 knockout cells.** STaxGFP was expressed in MEF MDC1 -/- cells. Tax expression was detected via the GFP fusion. Nuclei were visualized by co-staining with TO-PRO-3 iodide. Confocal microscopy images are magnified ×63 with a ×4 zoom.

Therefore, MDC1 may be a limiting factor in the competition between IRIF and TSS for DDR proteins. This competition could result in the dysregulation of the DNA damage repair pathway thus leading to Tax induced genomic instability. In addition, we found that NBS1 is not present in the TSS. This showed a significance difference between TSS and IRIF demonstrating that even though they are similar, they are not identical. Finally, we determined that TSS can be formed in MDC1 knockout cell line, thus suggesting that the chronological arrangement of the complex involves first the formation of the TSS followed by the recruitment of MDC1. Next, we investigated the ability of TSS to recruit DDR proteins using a Tax mutant that has the minimum sequence requirement for targeting it to the TSS (Tax 1-75). Our results showed that even though Tax1-75 is able to form TSS, it is unable to recruit DDR proteins. This suggests that the region of Tax responsible for the recruitment of DDR proteins is different from the one responsible for its targeting to the TSS.

Our laboratory previously showed that Tax increases DNA-PK's activity, thus leading to an increase in γ-H2AX (98). It was hypothesized that constitutive H2AX phosphorylation in Tax expressing cells was interfering with the DNA damage repair machinery by not allowing the cell to detect and repair newly formed damage (98, 105, 106). In light of our results in this study, we can extend our model further. In our model of Tax induced genomic instability, Tax is targeted to the TSS via its 1-75 amino acid region. Next, it recruits and aberrantly activates several DDR proteins such MDC1, DNA-PK pT2609 via the 75-353 region. When DNA damage occurs in Tax expressing cells, DDR proteins need to be recruited to the IRIF in order to repair the newly formed DNA breaks. Some proteins such as DNA-PK may be abundant enough to be present in

both the TSS and IRIF. Others, such as MDC1, may only be available at a limited amount thus creating a competition between IRIF and TSS. In some cases, MDC1 may not be properly recruited to the IRIF, which could cause an improper formation of the DNA damage repair complex. Ultimately, this might initiate an inappropriate repair of the damage leading to mutations and genomic instability.

SECTION 6

CONCLUSIONS

Summary

In this study, we have engineered an assay in which we isolated the Tax interactome and studied it using mass spectrometry. We have found many known Tax binding proteins and some novel ones. One of the new Tax interacting proteins is MDC1, a DNA damage repair protein. Tax is known to interfere with the DNA damage repair pathway; therefore we decided to focus on its interaction with MDC1. Pull down experiments confirmed the interaction between MDC1 and Tax, and a siRNA study determined that MDC1 is active in Tax expressing cells. In addition, immunofluorescence analysis showed that MDC1 is present in the TSS. This correlates with a study previously done by our laboratory that showed that DNA-PK pT2609 is also present in the TSS.

Our data indicated that the TSS and IRIF share a lot of similarities. Therefore, we decided to further characterize these two complexes. First, we determined that TSS are not sites of DNA breaks which clearly distinguish them from IRIF. Secondly, we looked at the different DDR proteins and their localization in Tax expressing cells before and after ionizing radiation (IR). BRCA1, MDC1 and DNA-PK pT2609 were all present in the TSS, but NBS1, another DDR proteins associated with IRIF, was not found in the TSS. Due to the central role of NBS1 in the DNA damage repair pathway, this result highlighted a striking difference between TSS and IRIF. In addition, following IR treatment, DNA-PK pT2609 and BRCA1 were present in both TSS and IRIF whereas

MDC1 seemed to be relocalized from the TSS to the IRIF. We hypothesized that there might be a competition between IRIF and TSS for MDC1 which could be available only in a limited amount in the cell. Finally, we investigated the mechanism by which Tax and the DDR are recruited to the TSS. We determined that the presence of MDC1 is not necessary for the formation of the TSS, suggesting that Tax is first recruited to the TSS which then leads to the recruitment of the different DDR proteins. In addition, we showed that the sequence responsible for the targeting of Tax to the TSS is not sufficient for the recruitment of the DNA-PK pT2609 and MDC1, suggesting that the rest of the Tax sequence is responsible for the recruitment of the several DDR proteins found in the TSS.

Taken these results together, we formulated a model of Tax induced genomic instability (Fig. 24). In our model, Tax gets recruited to the TSS via its 1-75 region. Next, Tax recruits several DDR proteins. When DNA damage occurs, DDR proteins need to be recruited to the IRIF in order to repair the DNA breaks. This leads to a competition between the IRIF and TSS. Tax may be able to prevent some DDR proteins, such as MDC1, to be recruited to the IRIF which could lead to inappropriate repair of DNA breaks. This could induce an accumulation of mutations and ultimately cause genomic instability.

Significance of Findings

Human T-cell leukemia virus type 1 (HTLV-1) is a retrovirus that infects 20 million people worldwide (20). It is endemic in southwestern Japan, Africa, the Caribbean islands and South America. In Japan alone, there are approximately 1.2 million infected individuals (20). The main modes of transmission are from mother to

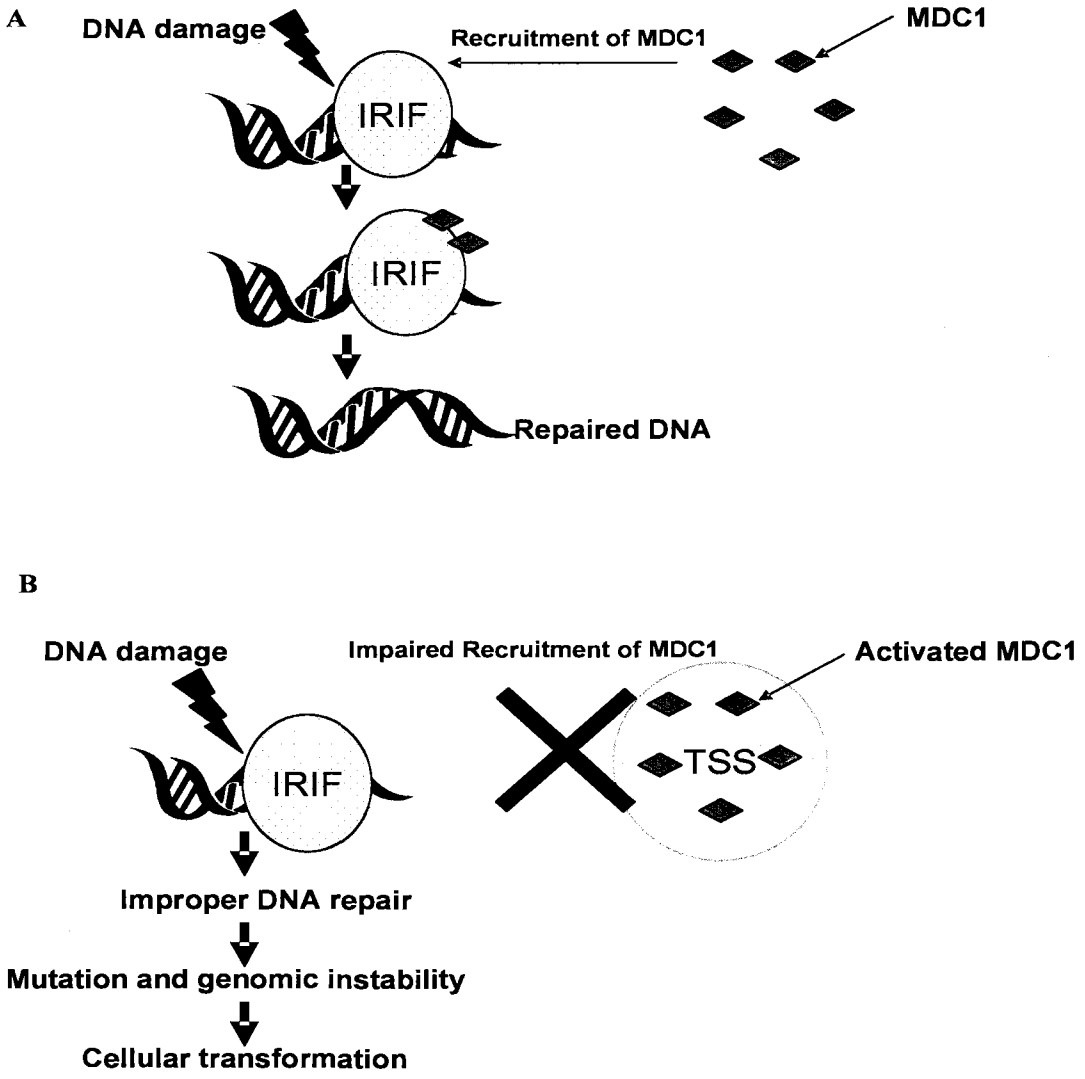

FIGURE 24. **A model of Tax induced genomic instability.** *A*, in a normal cell, MDC1 is recruited to the IRIF following DNA damage, leading to the recruitment of more DDR proteins and the repair of the damage. *B*, in a Tax expressing cell, Tax sequesters MDC1 away from the IRIF that form following DNA damage. This leads to improper repair of the damage and accumulation of mutations. Ultimately, this causes genomic instability and cellular transformation.

infant via breastfeeding, sexual contact and parenteral transmission (181). It was the first retrovirus to be shown to cause a human cancer, adult T-cell leukemia (ATL) (19). In addition, it can also induce another incurable life threatening disease called HTLV-1 – associated myelopathy and tropical spastic parapesis (HAM/TSP) (34). Soon after infection the virus goes into a latent state, making the infected individuals asymptomatic seropositive carriers. About 5% of these individuals develop one of the viral associated diseases 10 to 40 years after infection (37). In Japan, 800 to 1000 new ATL cases are diagnosed every year (20). ATL is an extremely aggressive disease with a poor prognosis, and it is also resistant to chemotherapeutic treatment (38). Study of the molecular pathogenesis of HTLV-1-mediated T-cell transformation is crucial to improve ATL treatment. The viral Tax protein is considered to play a central role in the process leading to ATL (37). It is thought that Tax causes transformation through various mechanisms that are not yet fully understood such as chromosomal instability and the abrogation of DNA repair (20).

Tax is known to interact with a wide variety of cellular proteins and it is believed that it may interfere with their functions (67). In this study, we successfully isolated the Tax interactome and analyzed it using mass spectrometry. This study adds a tremendous amount of knowledge to the proteins already known to bind Tax. In addition, with this assay we detected several known Tax binding proteins thus confirming the fidelity of our approach. We were also able to find several new Tax binding proteins that are involved in various pathways that are known to be affected by Tax. Results from this experiment are therefore a good starting point for the study of these proteins in relation to Tax. In addition, we confirmed that MDC1, which is a novel Tax interacting protein found in our

mass spectrometry data, did in fact interact with Tax thus highlighting the efficiency of our assay in identifying new Tax binding patterns.

In addition, we further investigated the relationship between TSS and IRIF. To our knowledge, our study is the first one that clearly shows that TSS are not sites of DNA breaks. This finding is significant because just like IRIF, which are sites of DNA breaks, TSS recruits several DDR proteins. This similarity could lead to the assumption that TSS recruits DDR proteins because they are also site of DNA breaks that need to be repaired. Here, we show that that assumption is false. Another important contribution to the field that was made is the introduction of a novel model of Tax induced genomic instability, thus giving us a better understanding of HTLV-1-mediated T-cell transformation. In our model, there is a competition between IRIF and TSS for DDR proteins which could lead to improper repair of some damaged DNA. *In vivo*, Tax levels are low and the amounts of DNA damage experienced by cells are also much lower to what we see in our experimental model. In other words, the competition between the TSS and IRIF *in vivo* is much more discrete which would explain the low level of HTLV-1 infected patients that develop ATL and the long time of onset of the disease.

Our model correlates with the findings of an earlier study that showed that, in HTLV-1 infected cells, MDC1 and γ-H2AX did not colocalize after IR, suggesting that Tax may interfere with the recruitment of MDC1 to the DNA damage sites (182). Our findings give a potential mechanism to would explain this phenomenon.

Future Directions

The experimental model used to identify Tax interacting proteins is a valuable

tool to study other novel Tax binding proteins. Using mass spectrometry, we already identified several proteins that we think should be studied further. One example of such protein is the interferon gamma-inducible protein 16 (IFI-16). IFI-16 is involved in p53 dependent apoptosis (149). The tumor suppressor p53 protein is involved in several cellular pathways such as cell cycle (183), apoptosis (184, 185) and DNA repair (186). It has been shown that the loss of IFI-16 causes the dysregulation of p53 mediated apoptosis, leading to cellular transformation (149). In addition, Tax is known to interfere with p53 function. It is believed that Tax inactivates it thus inhibiting apoptosis. The mechanism by which this happens is not yet fully understood, but it has been determined that the two proteins do not to interact directly (187-191). Therefore, the binding of Tax to IFI-16 could play a role in Tax-induced p53 inactivation. We can speculate that Tax might be sequestering IFI-16 from p53 thus interfering with its function. This hypothesis should be further investigated by first confirming the binding of Tax to IFI-16.

Another protein identified using mass spectrometry is the minichromosome maintenance deficient protein 7 (MCM7). This protein is implicated in DNA replication (150). Tax expressing cells exhibit an increase in DNA replication which combined with an enhancement of cell cycle progression contribute to cellular transformation (192-197). One proposed mechanism is that Tax *trans*-activates PCNA which enables the cell to bypass the p21-dependent in DNA replication in the presence of DNA damage (97, 197). The interaction with MCM7 could be another way by which Tax enhances DNA replication.

Studies that further characterize the relationship between DDR proteins and Tax should also be pursued. A recent study showed that the activation of DDR does not

require DNA damage (198). In that study, DDR proteins were fused to the E. coli lac-repressor (lacR) and tagged with Cherry-Red fluorescent protein. The fusion proteins were introduced into a NIH-3T3 cell line which contains 256 repeats of the lac operator sequence (lacO) stably integrated on chromosome 3. This causes the fusion proteins to accumulate at the lacO array as distinct nuclear foci. Interestingly, the stable association of single repair factors to the chromatin was sufficient for the activation of the DNA damage repair pathway. For instance, when LacR-MDC1-Cherry was expressed, it was targeted to chromatin and formed a distinct nuclear focus. After staining for γ-H2AX, it was shown that a γ-H2AX focus also formed and that it colocalized with LacR-MDC1-Cherry. This result suggests that the DNA damage repair pathway can be activated by just targeting MDC1 to the chromatin. Our laboratory recently received the LacR-MDC1-Cherry vector as well as the NIH-3T3 cell line and we were able to successfully reproduce the same results (data not shown). In a future study, we will clone a Tax mutant that lacks the TSLS and NLS sequence into the LacR-Cherry vector. Introduction of that plasmid should target Tax to the chromatin and we should investigate its ability to recruit DDR proteins. This experiment would allow us to confirm that Tax recruits DDR proteins in the absence of DNA damage.

REFERENCES

1. Coffin, J. M., Hughes, S. H., and Varmus, H. (1997) *Retroviruses*, Cold Spring Harbor Laboratory Press, Plainview, N.Y.

2. Yeager, M., Wilson-Kubalek, E. M., Weiner, S. G., Brown, P. O., and Rein, A. (1998) *Proc Natl Acad Sci U S A* **95**(13), 7299-7304

3. Leis, J., Baltimore, D., Bishop, J. M., Coffin, J., Fleissner, E., Goff, S. P., Oroszlan, S., Robinson, H., Skalka, A. M., Temin, H. M., and et al. (1988) *J Virol* **62**(5), 1808-1809

4. Gallo, R. C. (2005) *Retrovirology* **2**, 17

5. Matsuoka, M. (2003) *Oncogene* **22**(33), 5131-5140

6. Seiki, M., Hattori, S., Hirayama, Y., and Yoshida, M. (1983) *Proc Natl Acad Sci U S A* **80**(12), 3618-3622

7. Yoshida, M. (2005) *Oncogene* **24**(39), 5931-5937

8. Nam, S. H., Kidokoro, M., Shida, H., and Hatanaka, M. (1988) *J Virol* **62**(10), 3718-3728

9. Nicot, C., Harrod, R. L., Ciminale, V., and Franchini, G. (2005) *Oncogene* **24**(39), 6026-6034

10. Varmus, H. (1988) *Genes Dev* **2**(9), 1055-1062

11. Koyanagi, Y., Itoyama, Y., Nakamura, N., Takamatsu, K., Kira, J., Iwamasa, T., Goto, I., and Yamamoto, N. (1993) *Virology* **196**(1), 25-33

12. Manel, N., Kim, F. J., Kinet, S., Taylor, N., Sitbon, M., and Battini, J. L. (2003) *Cell* **115**(4), 449-459

13. Yasunaga, J., Sakai, T., Nosaka, K., Etoh, K., Tamiya, S., Koga, S., Mita, S., Uchino, M., Mitsuya, H., and Matsuoka, M. (2001) *Blood* **97**(10), 3177-3183

14. Matsuoka, M. (2005) *Retrovirology* **2**, 27

15. Bangham, C. R. (2003) *J Gen Virol* **84**(Pt 12), 3177-3189

16. Igakura, T., Stinchcombe, J. C., Goon, P. K., Taylor, G. P., Weber, J. N., Griffiths, G. M., Tanaka, Y., Osame, M., and Bangham, C. R. (2003) *Science* **299**(5613), 1713-1716

17. Yamamoto, N., Okada, M., Koyanagi, Y., Kannagi, M., and Hinuma, Y. (1982) *Science* **217**(4561), 737-739

18. Edlich, R. F., Arnette, J. A., and Williams, F. M. (2000) *J Emerg Med* **18**(1), 109-119

19. Takatsuki, K. (2005) *Retrovirology* **2**, 16

20. Matsuoka, M., and Jeang, K. T. (2007) *Nat Rev Cancer* **7**(4), 270-280

21. Kinoshita, K., Hino, S., Amagaski, T., Ikeda, S., Yamada, Y., Suzuyama, J., Momita, S., Toriya, K., Kamihira, S., and Ichimaru, M. (1984) *Gann* **75**(2), 103-105

22. Ando, Y., Nakano, S., Saito, K., Shimamoto, I., Ichijo, M., Toyama, T., and Hinuma, Y. (1987) *Jpn J Cancer Res* **78**(4), 322-324

23. Hino, S., Sugiyama, H., Doi, H., Ishimaru, T., Yamabe, T., Tsuji, Y., and Miyamoto, T. (1987) *Lancet* **2**(8551), 158-159

24. Tsuji, Y., Doi, H., Yamabe, T., Ishimaru, T., Miyamoto, T., and Hino, S. (1990) *Pediatrics* **86**(1), 11-17

25. Hirata, M., Hayashi, J., Noguchi, A., Nakashima, K., Kajiyama, W., Kashiwagi, S., and Sawada, T. (1992) *Int J Epidemiol* **21**(5), 989-994

26. Tajima, K., Tominaga, S., Suchi, T., Kawagoe, T., Komoda, H., Hinuma, Y., Oda, T., and Fujita, K. (1982) *Gann* **73**(6), 893-901

27. Nakano, S., Ando, Y., Ichijo, M., Moriyama, I., Saito, S., Sugamura, K., and Hinuma, Y. (1984) *Gann* **75**(12), 1044-1045

28. Gotoh, Y. I., Sugamura, K., and Hinuma, Y. (1982) *Proc Natl Acad Sci U S A* **79**(15), 4780-4782

29. Maeda, Y., Furukawa, M., Takehara, Y., Yoshimura, K., Miyamoto, K., Matsuura, T., Morishima, Y., Tajima, K., Okochi, K., and Hinuma, Y. (1984) *Int J Cancer* **33**(6), 717-720

30. Miyamoto, K., Tomita, N., Ishii, A., Nishizaki, T., Kitajima, K., Tanaka, T., Nakamura, T., Watanabe, S., and Oda, T. (1984) *Int J Cancer* **33**(6), 721-725

31. Jason, J. M., McDougal, J. S., Cabradilla, C., Kalyanaraman, V. S., and Evatt, B. L. (1985) *Am J Hematol* **20**(2), 129-137

32. Sato, H., and Okochi, K. (1986) *Int J Cancer* **37**(3), 395-400

33. Minamoto, G. Y., Gold, J. W., Scheinberg, D. A., Hardy, W. D., Chein, N., Zuckerman, E., Reich, L., Dietz, K., Gee, T., Hoffer, J., and et al. (1988) *N Engl J Med* **318**(4), 219-222

34. Bangham, C. R., and Osame, M. (2005) *Oncogene* **24**(39), 6035-6046

35. Hinuma, Y., Nagata, K., Hanaoka, M., Nakai, M., Matsumoto, T., Kinoshita, K. I., Shirakawa, S., and Miyoshi, I. (1981) *Proc Natl Acad Sci U S A* **78**(10), 6476-6480

36. Yoshida, M., Miyoshi, I., and Hinuma, Y. (1982) *Proc Natl Acad Sci U S A* **79**(6), 2031-2035

37. Azran, I., Schavinsky-Khrapunsky, Y., and Aboud, M. (2004) *Retrovirology* **1**, 20

38. Yasunaga, J., and Matsuoka, M. (2007) *Cancer Control* **14**(2), 133-140

39. Uchiyama, T., Yodoi, J., Sagawa, K., Takatsuki, K., and Uchino, H. (1977) *Blood* **50**(3), 481-492

40. Shimoyama, M. (1991) *Br J Haematol* **79**(3), 428-437

41. Yamaguchi, K., Nishimura, H., Kohrogi, H., Jono, M., Miyamoto, Y., and Takatsuki, K. (1983) *Blood* **62**(4), 758-766

42. Kawano, F., Yamaguchi, K., Nishimura, H., Tsuda, H., and Takatsuki, K. (1985) *Cancer* **55**(4), 851-856

43. Takatsuki, K., Matsuoka, M., and Yamaguchi, K. (1996) *J Acquir Immune Defic Syndr Hum Retrovirol* **13 Suppl 1**, S15-19

44. Gessain, A., Barin, F., Vernant, J. C., Gout, O., Maurs, L., Calender, A., and de The, G. (1985) *Lancet* **2**(8452), 407-410

45. Osame, M., Usuku, K., Izumo, S., Ijichi, N., Amitani, H., Igata, A., Matsumoto, M., and Tara, M. (1986) *Lancet* **1**(8488), 1031-1032

46. Osame, M., Janssen, R., Kubota, H., Nishitani, H., Igata, A., Nagataki, S., Mori, M., Goto, I., Shimabukuro, H., Khabbaz, R., and et al. (1990) *Ann Neurol* **28**(1), 50-56

47. Uchiyama, T. (1997) *Annu Rev Immunol* **15**, 15-37

48. Mochizuki, M., Watanabe, T., Yamaguchi, K., Takatsuki, K., Yoshimura, K., Shirao, M., Nakashima, S., Mori, S., Araki, S., and Miyata, N. (1992) *Jpn J Cancer Res* **83**(3), 236-239

49. Kitajima, I., Yamamoto, K., Sato, K., Nakajima, Y., Nakajima, T., Maruyama, I., Osame, M., and Nishioka, K. (1991) *J Clin Invest* **88**(4), 1315-1322

50. Verdonck, K., Gonzalez, E., Van Dooren, S., Vandamme, A. M., Vanham, G., and Gotuzzo, E. (2007) *Lancet Infect Dis* **7**(4), 266-281

51. Wiktor, S. Z., Pate, E. J., Weiss, S. H., Gohd, R. S., Correa, P., Fontham, E. T., Hanchard, B., Biggar, R. J., and Blattner, W. A. (1991) *Lancet* **338**(8765), 512-513

52. Thorstensson, R., Albert, J., and Andersson, S. (2002) *Transfusion* **42**(6), 780-791

53. Gallo, D., Hoffman, M. N., Cossen, C. K., Diggs, J. L., Hurst, J. W., and Penning, L. M. (1988) *J Clin Microbiol* **26**(8), 1487-1491

54. Larsen, O., Andersson, S., da Silva, Z., Hedegaard, K., Sandstrom, A., Naucler, A., Dias, F., Melbye, M., and Aaby, P. (2000) *J Acquir Immune Defic Syndr* **25**(2), 157-163

55. Mangano, A. M., Remesar, M., del Pozo, A., and Sen, L. (2004) *J Med Virol* **74**(2), 323-327

56. Vandamme, A. M., Van Laethem, K., Liu, H. F., Van Brussel, M., Delaporte, E., de Castro Costa, C. M., Fleischer, C., Taylor, G., Bertazzoni, U., Desmyter, J., and Goubau, P. (1997) *J Med Virol* **52**(1), 1-7

57. Matsuzaki, T., Nakagawa, M., Nagai, M., Usuku, K., Higuchi, I., Arimura, K., Kubota, H., Izumo, S., Akiba, S., and Osame, M. (2001) *J Neurovirol* **7**(3), 228-234

58. Kamihira, S., Dateki, N., Sugahara, K., Hayashi, T., Harasawa, H., Minami, S., Hirakata, Y., and Yamada, Y. (2003) *Clin Lab Haematol* **25**(2), 111-117

59. Olindo, S., Lezin, A., Cabre, P., Merle, H., Saint-Vil, M., Edimonana Kaptue, M., Signate, A., Cesaire, R., and Smadja, D. (2005) *J Neurol Sci* **237**(1-2), 53-59

60. Dehee, A., Cesaire, R., Desire, N., Lezin, A., Bourdonne, O., Bera, O., Plumelle, Y., Smadja, D., and Nicolas, J. C. (2002) *J Virol Methods* **102**(1-2), 37-51

61. Lee, T. H., Chafets, D. M., Busch, M. P., and Murphy, E. L. (2004) *J Clin Virol* **31**(4), 275-282

62. Lenzmeier, B. A., Giebler, H. A., and Nyborg, J. K. (1998) *Mol Cell Biol* **18**(2), 721-731

63. Kwok, R. P., Laurance, M. E., Lundblad, J. R., Goldman, P. S., Shih, H., Connor, L. M., Marriott, S. J., and Goodman, R. H. (1996) *Nature* **380**(6575), 642-646

64. Giebler, H. A., Loring, J. E., van Orden, K., Colgin, M. A., Garrus, J. E., Escudero, K. W., Brauweiler, A., and Nyborg, J. K. (1997) *Mol Cell Biol* **17**(9), 5156-5164

65. Jiang, H., Lu, H., Schiltz, R. L., Pise-Masison, C. A., Ogryzko, V. V., Nakatani, Y., and Brady, J. N. (1999) *Mol Cell Biol* **19**(12), 8136-8145

66. Harrod, R., Kuo, Y. L., Tang, Y., Yao, Y., Vassilev, A., Nakatani, Y., and Giam, C. Z. (2000) *J Biol Chem* **275**(16), 11852-11857

67. Boxus, M., Twizere, J. C., Legros, S., Dewulf, J. F., Kettmann, R., and Willems, L. (2008) *Retrovirology* **5**, 76

68. Semmes, O. J., and Jeang, K. T. (1996) *J Virol* **70**(9), 6347-6357

69. Fryrear, K. A., Durkin, S. S., Gupta, S. K., Tiedebohl, J. B., and Semmes, O. J. (2009) *J Virol* **83**(11), 5339-5352

70. Matsumoto, K., Shibata, H., Fujisawa, J. I., Inoue, H., Hakura, A., Tsukahara, T., and Fujii, M. (1997) *J Virol* **71**(6), 4445-4451

71. Tanaka, A., Takahashi, C., Yamaoka, S., Nosaka, T., Maki, M., and Hatanaka, M. (1990) *Proc Natl Acad Sci U S A* **87**(3), 1071-1075

72. Grassmann, R., Dengler, C., Muller-Fleckenstein, I., Fleckenstein, B., McGuire, K., Dokhelar, M. C., Sodroski, J. G., and Haseltine, W. A. (1989) *Proc Natl Acad Sci U S A* **86**(9), 3351-3355

73. Akagi, T., and Shimotohno, K. (1993) *J Virol* **67**(3), 1211-1217

74. Dahlke, M. B., and Nowell, P. C. (1975) *Br J Haematol* **31**(1), 111-116

75. Marriott, S. J., and Semmes, O. J. (2005) *Oncogene* **24**(39), 5986-5995

76. Majone, F., Semmes, O. J., and Jeang, K. T. (1993) *Virology* **193**(1), 456-459

77. Lemoine, F. J., and Marriott, S. J. (2002) *Oncogene* **21**(47), 7230-7234

78. Felber, B. K., Paskalis, H., Kleinman-Ewing, C., Wong-Staal, F., and Pavlakis, G. N. (1985) *Science* **229**(4714), 675-679

79. Chu, Z. L., Shin, Y. A., Yang, J. M., DiDonato, J. A., and Ballard, D. W. (1999) *J Biol Chem* **274**(22), 15297-15300

80. Harhaj, E. W., and Sun, S. C. (1999) *J Biol Chem* **274**(33), 22911-22914

81. Jin, D. Y., Giordano, V., Kibler, K. V., Nakano, H., and Jeang, K. T. (1999) *J Biol Chem* **274**(25), 17402-17405

82. Elledge, S. J. (1996) *Science* **274**(5293), 1664-1672

83. Lemoine, F. J., Wycuff, D. R., and Marriott, S. J. (2001) *Dis Markers* **17**(3), 129-137

84. Haoudi, A., and Semmes, O. J. (2003) *Virology* **305**(2), 229-239

85. Liu, B., Hong, S., Tang, Z., Yu, H., and Giam, C. Z. (2005) *Proc Natl Acad Sci U S A* **102**(1), 63-68

86. Kibler, K. V., and Jeang, K. T. (2001) *J Virol* **75**(5), 2161-2173

87. Liang, M. H., Geisbert, T., Yao, Y., Hinrichs, S. H., and Giam, C. Z. (2002) *J Virol* **76**(8), 4022-4033

88. Haller, K., Wu, Y., Derow, E., Schmitt, I., Jeang, K. T., and Grassmann, R. (2002) *Mol Cell Biol* **22**(10), 3327-3338

89. Fraedrich, K., Muller, B., and Grassmann, R. (2005) *Retrovirology* **2**, 54

90. Schmitt, I., Rosin, O., Rohwer, P., Gossen, M., and Grassmann, R. (1998) *J Virol* **72**(1), 633-640

91. Iwanaga, R., Ohtani, K., Hayashi, T., and Nakamura, M. (2001) *Oncogene* **20**(17), 2055-2067

92. Haoudi, A., Daniels, R. C., Wong, E., Kupfer, G., and Semmes, O. J. (2003) *J Biol Chem* **278**(39), 37736-37744

93. Jeang, K. T., Widen, S. G., Semmes, O. J. t., and Wilson, S. H. (1990) *Science* **247**(4946), 1082-1084

94. Wilson, S., Abbotts, J., and Widen, S. (1988) *Biochim Biophys Acta* **949**(2), 149-157

95. Kao, S. Y., and Marriott, S. J. (1999) *J Virol* **73**(5), 4299-4304

96. Lemoine, F. J., Kao, S. Y., and Marriott, S. J. (2000) *AIDS Res Hum Retroviruses* **16**(16), 1623-1627

97. Ressler, S., Morris, G. F., and Marriott, S. J. (1997) *J Virol* **71**(2), 1181-1190

98. Durkin, S. S., Guo, X., Fryrear, K. A., Mihaylova, V. T., Gupta, S. K., Belgnaoui, S. M., Haoudi, A., Kupfer, G. M., and Semmes, O. J. (2008) *J Biol Chem* **283**(52), 36311-36320

99. Meek, K., Gupta, S., Ramsden, D. A., and Lees-Miller, S. P. (2004) *Immunol Rev* **200**, 132-141

100. Collis, S. J., DeWeese, T. L., Jeggo, P. A., and Parker, A. R. (2005) *Oncogene* **24**(6), 949-961

101. Burma, S., and Chen, D. J. (2004) *DNA Repair (Amst)* **3**(8-9), 909-918

102. Smith, G. C., and Jackson, S. P. (1999) *Genes Dev* **13**(8), 916-934

103. Li, J., and Stern, D. F. (2005) *J Biol Chem* **280**(12), 12041-12050

104. Stucki, M., and Jackson, S. P. (2006) *DNA Repair (Amst)* **5**(5), 534-543

105. Chowdhury, D., Keogh, M. C., Ishii, H., Peterson, C. L., Buratowski, S., and Lieberman, J. (2005) *Mol Cell* **20**(5), 801-809

106. Keogh, M. C., Kim, J. A., Downey, M., Fillingham, J., Chowdhury, D., Harrison, J. C., Onishi, M., Datta, N., Galicia, S., Emili, A., Lieberman, J., Shen, X., Buratowski, S., Haber, J. E., Durocher, D., Greenblatt, J. F., and Krogan, N. J. (2006) *Nature* **439**(7075), 497-501

107. Stewart, G. S., Wang, B., Bignell, C. R., Taylor, A. M., and Elledge, S. J. (2003) *Nature* **421**(6926), 961-966

108. Stucki, M., Clapperton, J. A., Mohammad, D., Yaffe, M. B., Smerdon, S. J., and Jackson, S. P. (2005) *Cell* **123**(7), 1213-1226

109. Mailand, N., Bekker-Jensen, S., Faustrup, H., Melander, F., Bartek, J., Lukas, C., and Lukas, J. (2007) *Cell* **131**(5), 887-900

110. Yan, J., and Jetten, A. M. (2008) *Cancer Lett*

111. Lou, Z., Chen, B. P., Asaithamby, A., Minter-Dykhouse, K., Chen, D. J., and Chen, J. (2004) *J Biol Chem* **279**(45), 46359-46362

112. Lou, Z., Minter-Dykhouse, K., Wu, X., and Chen, J. (2003) *Nature* **421**(6926), 957-961

113. Lou, Z., Minter-Dykhouse, K., Franco, S., Gostissa, M., Rivera, M. A., Celeste, A., Manis, J. P., van Deursen, J., Nussenzweig, A., Paull, T. T., Alt, F. W., and Chen, J. (2006) *Mol Cell* **21**(2), 187-200

114. Grassmann, R., Aboud, M., and Jeang, K. T. (2005) *Oncogene* **24**(39), 5976-5985

115. Bex, F., McDowall, A., Burny, A., and Gaynor, R. (1997) *J Virol* **71**(5), 3484-3497

116. Chan, D. W., Chen, B. P., Prithivirajsingh, S., Kurimasa, A., Story, M. D., Qin, J., and Chen, D. J. (2002) *Genes Dev* **16**(18), 2333-2338

117. Chen, B. P., Chan, D. W., Kobayashi, J., Burma, S., Asaithamby, A., Morotomi-Yano, K., Botvinick, E., Qin, J., and Chen, D. J. (2005) *J Biol Chem* **280**(15), 14709-14715

118. Goldberg, M., Stucki, M., Falck, J., D'Amours, D., Rahman, D., Pappin, D., Bartek, J., and Jackson, S. P. (2003) *Nature* **421**(6926), 952-956

119. Bekker-Jensen, S., Lukas, C., Kitagawa, R., Melander, F., Kastan, M. B., Bartek, J., and Lukas, J. (2006) *J Cell Biol* **173**(2), 195-206

120. Nerenberg, M., Hinrichs, S. H., Reynolds, R. K., Khoury, G., and Jay, G. (1987) *Science* **237**(4820), 1324-1329

121. Pozzatti, R., Vogel, J., and Jay, G. (1990) *Mol Cell Biol* **10**(1), 413-417

122. Ng, P. W., Iha, H., Iwanaga, Y., Bittner, M., Chen, Y., Jiang, Y., Gooden, G., Trent, J. M., Meltzer, P., Jeang, K. T., and Zeichner, S. L. (2001) *Oncogene* **20**(33), 4484-4496

123. Ego, T., Ariumi, Y., and Shimotohno, K. (2002) *Oncogene* **21**(47), 7241-7246

124. Kamoi, K., Yamamoto, K., Misawa, A., Miyake, A., Ishida, T., Tanaka, Y., Mochizuki, M., and Watanabe, T. (2006) *Retrovirology* **3**, 5

125. Gray, S. G., Iglesias, A. H., Lizcano, F., Villanueva, R., Camelo, S., Jingu, H., Teh, B. T., Koibuchi, N., Chin, W. W., Kokkotou, E., and Dangond, F. (2005) *J Biol Chem* **280**(31), 28507-28518

126. Caron, C., Rousset, R., Beraud, C., Moncollin, V., Egly, J. M., and Jalinot, P. (1993) *Embo J* **12**(11), 4269-4278

127. Caron, C., Mengus, G., Dubrowskaya, V., Roisin, A., Davidson, I., and Jalinot, P. (1997) *Proc Natl Acad Sci U S A* **94**(8), 3662-3667

128. Clemens, K. E., Piras, G., Radonovich, M. F., Choi, K. S., Duvall, J. F., DeJong, J., Roeder, R., and Brady, J. N. (1996) *Mol Cell Biol* **16**(9), 4656-4664

129. Cho, W. K., Zhou, M., Jang, M. K., Huang, K., Jeong, S. J., Ozato, K., and Brady, J. N. (2007) *J Virol* **81**(20), 11179-11186

130. Wu, K., Bottazzi, M. E., de la Fuente, C., Deng, L., Gitlin, S. D., Maddukuri, A., Dadgar, S., Li, H., Vertes, A., Pumfery, A., and Kashanchi, F. (2004) *J Biol Chem* **279**(1), 495-508

131. Higuchi, M., Tsubata, C., Kondo, R., Yoshida, S., Takahashi, M., Oie, M., Tanaka, Y., Mahieux, R., Matsuoka, M., and Fujii, M. (2007) *J Virol* **81**(21), 11900-11907

132. Sun, S. C., and Yamaoka, S. (2005) *Oncogene* **24**(39), 5952-5964

133. Xiao, G., Cvijic, M. E., Fong, A., Harhaj, E. W., Uhlik, M. T., Waterfield, M., and Sun, S. C. (2001) *Embo J* **20**(23), 6805-6815

134. Yin, M. J., Christerson, L. B., Yamamoto, Y., Kwak, Y. T., Xu, S., Mercurio, F., Barbosa, M., Cobb, M. H., and Gaynor, R. B. (1998) *Cell* **93**(5), 875-884

135. Wu, X., and Sun, S. C. (2007) *EMBO Rep* **8**(5), 510-515

136. Jin, D. Y., Teramoto, H., Giam, C. Z., Chun, R. F., Gutkind, J. S., and Jeang, K. T. (1997) *J Biol Chem* **272**(41), 25816-25823

137. Peloponese, J. M., Jr., and Jeang, K. T. (2006) *J Biol Chem* **281**(13), 8927-8938

138. Lee, D. K., Kim, B. C., Brady, J. N., Jeang, K. T., and Kim, S. J. (2002) *J Biol Chem* **277**(37), 33766-33775

139. Arnulf, B., Villemain, A., Nicot, C., Mordelet, E., Charneau, P., Kersual, J., Zermati, Y., Mauviel, A., Bazarbachi, A., and Hermine, O. (2002) *Blood* **100**(12), 4129-4138

140. Haller, K., Ruckes, T., Schmitt, I., Saul, D., Derow, E., and Grassmann, R. (2000) *AIDS Res Hum Retroviruses* **16**(16), 1683-1688

141. Neuveut, C., Low, K. G., Maldarelli, F., Schmitt, I., Majone, F., Grassmann, R., and Jeang, K. T. (1998) *Mol Cell Biol* **18**(6), 3620-3632

142. Kehn, K., Fuente Cde, L., Strouss, K., Berro, R., Jiang, H., Brady, J., Mahieux, R., Pumfery, A., Bottazzi, M. E., and Kashanchi, F. (2005) *Oncogene* **24**(4), 525-540

143. Suzuki, T., Uchida-Toita, M., Andoh, T., and Yoshida, M. (2000) *Virology* **270**(2), 291-298

144. Durkin, S. S., Ward, M. D., Fryrear, K. A., and Semmes, O. J. (2006) *J Biol Chem* **281**(42), 31705-31712

145. Kim, J. S., and Raines, R. T. (1993) *J Biol Chem* **268**(23), 17392-17396

146. Gupta, S. K., Guo, X., Durkin, S. S., Fryrear, K. F., Ward, M. D., and Semmes, O. J. (2007) *J Biol Chem* **282**(40), 29431-29440

147. Jain, P., Mostoller, K., Flaig, K. E., Ahuja, J., Lepoutre, V., Alefantis, T., Khan, Z. K., and Wigdahl, B. (2007) *J Biol Chem* **282**(47), 34581-34593

148. Tsuji, T., Sheehy, N., Gautier, V. W., Hayakawa, H., Sawa, H., and Hall, W. W. (2007) *J Biol Chem* **282**(18), 13875-13883

149. Aglipay, J. A., Lee, S. W., Okada, S., Fujiuchi, N., Ohtsuka, T., Kwak, J. C., Wang, Y., Johnstone, R. W., Deng, C., Qin, J., and Ouchi, T. (2003) *Oncogene* **22**(55), 8931-8938

150. Lei, M., and Tye, B. K. (2001) *J Cell Sci* **114**(Pt 8), 1447-1454

151. Grassmann, R., Berchtold, S., Radant, I., Alt, M., Fleckenstein, B., Sodroski, J. G., Haseltine, W. A., and Ramstedt, U. (1992) *J Virol* **66**(7), 4570-4575

152. Hinrichs, S. H., Nerenberg, M., Reynolds, R. K., Khoury, G., and Jay, G. (1987) *Science* **237**(4820), 1340-1343

153. Grossman, W. J., Kimata, J. T., Wong, F. H., Zutter, M., Ley, T. J., and Ratner, L. (1995) *Proc Natl Acad Sci U S A* **92**(4), 1057-1061

154. Shang, Y. L., Bodero, A. J., and Chen, P. L. (2003) *J Biol Chem* **278**(8), 6323-6329

155. Motoyama, N., and Naka, K. (2004) *Curr Opin Genet Dev* **14**(1), 11-16

156. Lou, Z., Chini, C. C., Minter-Dykhouse, K., and Chen, J. (2003) *J Biol Chem* **278**(16), 13599-13602

157. Xu, X., and Stern, D. F. (2003) *J Biol Chem* **278**(10), 8795-8803

158. Durocher, D., Smerdon, S. J., Yaffe, M. B., and Jackson, S. P. (2000) *Cold Spring Harb Symp Quant Biol* **65**, 423-431

159. Yu, X., Chini, C. C., He, M., Mer, G., and Chen, J. (2003) *Science* **302**(5645), 639-642

160. Manke, I. A., Lowery, D. M., Nguyen, A., and Yaffe, M. B. (2003) *Science* **302**(5645), 636-639

161. Rodriguez, M., Yu, X., Chen, J., and Songyang, Z. (2003) *J Biol Chem* **278**(52), 52914-52918

162. Spycher, C., Miller, E. S., Townsend, K., Pavic, L., Morrice, N. A., Janscak, P., Stewart, G. S., and Stucki, M. (2008) *J Cell Biol* **181**(2), 227-240

163. Melander, F., Bekker-Jensen, S., Falck, J., Bartek, J., Mailand, N., and Lukas, J. (2008) *J Cell Biol* **181**(2), 213-226

164. Chapman, J. R., and Jackson, S. P. (2008) *EMBO Rep* **9**(8), 795-801

165. Bekker-Jensen, S., Lukas, C., Melander, F., Bartek, J., and Lukas, J. (2005) *J Cell Biol* **170**(2), 201-211

166. Bewersdorf, J., Bennett, B. T., and Knight, K. L. (2006) *Proc Natl Acad Sci U S A* **103**(48), 18137-18142

167. Park, E. J., Chan, D. W., Park, J. H., Oettinger, M. A., and Kwon, J. (2003) *Nucleic Acids Res* **31**(23), 6819-6827

168. Yaneva, M., Kowalewski, T., and Lieber, M. R. (1997) *EMBO J* **16**(16), 5098-5112

169. Lukas, C., Melander, F., Stucki, M., Falck, J., Bekker-Jensen, S., Goldberg, M., Lerenthal, Y., Jackson, S. P., Bartek, J., and Lukas, J. (2004) *EMBO J* **23**(13), 2674-2683

170. Huen, M. S., Grant, R., Manke, I., Minn, K., Yu, X., Yaffe, M. B., and Chen, J. (2007) *Cell* **131**(5), 901-914

171. Shao, G., Lilli, D. R., Patterson-Fortin, J., Coleman, K. A., Morrissey, D. E., and Greenberg, R. A. (2009) *Proc Natl Acad Sci U S A* **106**(9), 3166-3171

172. Matsuoka, S., Ballif, B. A., Smogorzewska, A., McDonald, E. R., 3rd, Hurov, K. E., Luo, J., Bakalarski, C. E., Zhao, Z., Solimini, N., Lerenthal, Y., Shiloh, Y., Gygi, S. P., and Elledge, S. J. (2007) *Science* **316**(5828), 1160-1166

173. Burma, S., Chen, B. P., and Chen, D. J. (2006) *DNA Repair (Amst)* **5**(9-10), 1042-1048

174. Majone, F., and Jeang, K. T. (2000) *J Biol Chem* **275**(42), 32906-32910

175. Majone, F., Luisetto, R., Zamboni, D., Iwanaga, Y., and Jeang, K. T. (2005) *Retrovirology* **2**(1), 45

176. Raderschall, E., Golub, E. I., and Haaf, T. (1999) *Proc Natl Acad Sci U S A* **96**(5), 1921-1926

177. Adams, K. E., Medhurst, A. L., Dart, D. A., and Lakin, N. D. (2006) *Oncogene* **25**(28), 3894-3904

178. Scully, R., Chen, J., Plug, A., Xiao, Y., Weaver, D., Feunteun, J., Ashley, T., and Livingston, D. M. (1997) *Cell* **88**(2), 265-275

179. Bochar, D. A., Wang, L., Beniya, H., Kinev, A., Xue, Y., Lane, W. S., Wang, W., Kashanchi, F., and Shiekhattar, R. (2000) *Cell* **102**(2), 257-265

180. Smith, M. R., and Greene, W. C. (1992) *Virology* **187**(1), 316-320

181. Proietti, F. A., Carneiro-Proietti, A. B., Catalan-Soares, B. C., and Murphy, E. L. (2005) *Oncogene* **24**(39), 6058-6068

182. Chandhasin, C., Ducu, R. I., Berkovich, E., Kastan, M. B., and Marriott, S. J. (2008) *J Virol* **82**(14), 6952-6961

183. Stewart, Z. A., and Pietenpol, J. A. (2001) *Chem Res Toxicol* **14**(3), 243-263

184. Fridman, J. S., and Lowe, S. W. (2003) *Oncogene* **22**(56), 9030-9040

185. Yu, J., and Zhang, L. (2005) *Biochem Biophys Res Commun* **331**(3), 851-858

186. Ford, J. M. (2005) *Mutat Res* **577**(1-2), 195-202

187. Pise-Masison, C. A., Jeong, S. J., and Brady, J. N. (2005) *Arch Immunol Ther Exp (Warsz)* **53**(4), 283-296

188. Pise-Masison, C. A., and Brady, J. N. (2005) *Front Biosci* **10**, 919-930

189. Pise-Masison, C. A., Choi, K. S., Radonovich, M., Dittmer, J., Kim, S. J., and Brady, J. N. (1998) *J Virol* **72**(2), 1165-1170

190. Akagi, T., Ono, H., Tsuchida, N., and Shimotohno, K. (1997) *FEBS Lett* **406**(3), 263-266

191. Ariumi, Y., Kaida, A., Lin, J. Y., Hirota, M., Masui, O., Yamaoka, S., Taya, Y., and Shimotohno, K. (2000) *Oncogene* **19**(12), 1491-1499

192. Mesnard, J. M., and Devaux, C. (1999) *Virology* **257**(2), 277-284

193. Neuveut, C., and Jeang, K. T. (2000) *Prog Cell Cycle Res* **4**, 157-162

194. Neuveut, C., and Jeang, K. T. (2002) *Front Biosci* **7**, d157-163

195. Hatta, Y., and Koeffler, H. P. (2002) *Leukemia* **16**(6), 1069-1085

196. Yoshida, M. (2001) *Annu Rev Immunol* **19**, 475-496

197. Gatza, M. L., Watt, J. C., and Marriott, S. J. (2003) *Oncogene* **22**(33), 5141-5149

198. Soutoglou, E., and Misteli, T. (2008) *Science* **320**(5882), 1507-1510

APPENDIX A

LIST OF THE 76 PROTEINS FOUND IN THE TAX INTERACTOME

Identified proteins
60 kDa heat shock protein, mitochondrial precursor - Homo sapiens (Human)
DNA-dependent protein kinase catalytic subunit - Homo sapiens (Human)
Vimentin - Homo sapiens (Human)
Tubulin beta-2C chain - Homo sapiens (Human)
Gamma-interferon-inducible protein Ifi-16 - Homo sapiens (Human)
Tubulin alpha-4A chain - Homo sapiens (Human)
ATP-dependent RNA helicase A - Homo sapiens (Human)
Stress-70 protein, mitochondrial precursor - Homo sapiens (Human)
Heterogeneous nuclear ribonucleoprotein A1 - Homo sapiens (Human)
Heat shock protein HSP 90-alpha - Homo sapiens (Human)
Lamina-associated polypeptide 2 isoform alpha - Homo sapiens (Human)
DNA topoisomerase 2-alpha - Homo sapiens (Human)
Core histone macro-H2A.1 - Homo sapiens (Human)
Matrin-3 - Homo sapiens (Human)
GMP synthase [glutamine-hydrolyzing] - Homo sapiens (Human)
DNA replication licensing factor MCM7 - Homo sapiens (Human)
Heterogeneous nuclear ribonucleoprotein R - Homo sapiens (Human)
F-box only protein 22 - Homo sapiens (Human)
Heterogeneous nuclear ribonucleoproteins C1/C2 - Homo sapiens (Human)
ATP-dependent DNA helicase 2 subunit 1 - Homo sapiens (Human)
Heterogeneous nuclear ribonucleoprotein H - Homo sapiens (Human)
Splicing factor, proline- and glutamine-rich - Homo sapiens (Human)
Heat shock 70 kDa protein 6 - Homo sapiens (Human)
Heterogeneous nuclear ribonucleoprotein A3 - Homo sapiens (Human)
60S acidic ribosomal protein P2 - Homo sapiens (Human)
Lymphoid enhancer-binding factor 1 - Homo sapiens (Human)
Histone H2A type 2-A - Homo sapiens (Human)
Far upstream element-binding protein 2 - Homo sapiens (Human)
Nucleolar protein 5A - Homo sapiens (Human)
Stomatin-like protein 2 - Homo sapiens (Human)
Histone H2AV - Homo sapiens (Human)
78 kDa glucose-regulated protein precursor - Homo sapiens (Human)
Peptidyl-prolyl cis-trans isomerase A - Homo sapiens (Human)
Protein-L-isoaspartate(D-aspartate) O-methyltransferase - Homo sapiens (Human)
60S ribosomal protein L4 - Homo sapiens (Human)
ATP-dependent RNA helicase DDX3X - Homo sapiens (Human)
Protein Tax-1 - Human T-cell leukemia virus 1 (strain Japan ATK-1 subtype A) (HTLV-1)
Calnexin precursor - Homo sapiens (Human)
Replication protein A 70 kDa DNA-binding subunit - Homo sapiens (Human)
Splicing factor 3B subunit 1 - Homo sapiens (Human)
Mediator of DNA damage checkpoint protein 1 - Homo sapiens (Human)

APPENDIX A, Continued

Identified proteins (continued)
Interleukin enhancer-binding factor 3 - Homo sapiens (Human)
Cell division control protein 2 homolog - Homo sapiens (Human)
Prolow-density lipoprotein receptor-related protein 1 precursor - Homo sapiens (Human)
Histone H3.1 - Homo sapiens (Human)
Myosin-11 - Homo sapiens (Human)
Probable global transcription activator SNF2L4 - Homo sapiens (Human)
Histone-binding protein RBBP4 - Homo sapiens (Human)
Splicing factor 3B subunit 2 - Homo sapiens (Human)
Annexin A2 - Homo sapiens (Human)
Poly(rC)-binding protein 1 - Homo sapiens (Human)
Far upstream element-binding protein 1 - Homo sapiens (Human)
40S ribosomal protein S15a - Homo sapiens (Human)
Single-stranded DNA-binding protein, mitochondrial precursor - Homo sapiens (Human)
ATP-dependent RNA helicase DDX18 - Homo sapiens (Human)
Spectrin beta chain, brain 1 - Homo sapiens (Human)
Tubulin gamma-1 chain - Homo sapiens (Human)
U5 small nuclear ribonucleoprotein 200 kDa helicase - Homo sapiens (Human)
Replication factor C subunit 4 - Homo sapiens (Human)
Delta-1-pyrroline-5-carboxylate synthetase - Homo sapiens (Human)
40S ribosomal protein S10 - Homo sapiens (Human)
N-acetyltransferase 10 - Homo sapiens (Human)
RNA-binding protein Raly - Homo sapiens (Human)
DNA ligase 3 - Homo sapiens (Human)
Nuclear pore complex protein Nup93 - Homo sapiens (Human)
Thioredoxin - Homo sapiens (Human)
T-complex protein 1 subunit beta - Homo sapiens (Human)
Cell growth-regulating nucleolar protein - Homo sapiens (Human)
Ran GTPase-activating protein 1 - Homo sapiens (Human)
PC4 and SFRS1-interacting protein - Homo sapiens (Human)
14-3-3 protein zeta/delta - Homo sapiens (Human)
T-complex protein 1 subunit gamma - Homo sapiens (Human)
Exportin-1 - Homo sapiens (Human)
RNA-binding protein 34 - Homo sapiens (Human)
Ras-related protein Rab-5C - Homo sapiens (Human)
Chromodomain-helicase-DNA-binding protein 7 - Homo sapiens (Human)

VITA

SIDI MEHDI BELGNAOUI

Eastern Virginia Medical School
Department of Microbiology and Molecular Cell Biology
700 West Olney Road
Norfolk, Virginia 23507

Education:

Doctor of Philosophy, Biomedical Sciences (December 2009)
Eastern Virginia Medical School and Old Dominion University
Norfolk, Virginia

Bachelor of Science, Biology (July 2004)
Albright College
Reading, Pennsylvania

Professional Experience:

Graduate Research Assistant (August 2005 – December 2009)
Eastern Virginia Medical School
Norfolk, Virginia

Research Assistant (November 2004 – July 2005)
Eastern Virginia Medical School
Norfolk, Virginia

Publications:

Sarah S. Durkin, Xin Guo, Kimberly A. Fryrear, Valia T. Mihaylova, Saurabh K. Gupta, **S. Mehdi Belgnaoui** , Abdelali Haoudi, Gary M. Kupfer, and O. John Semmes. HTLV-1 Tax oncoprotein subverts the cellular DNA damage response via binding to DNA-dependent protein kinase. Journal of Biological Chemistry 283(52):36311-20, 2008.

S. Mehdi Belgnaoui, Roger G. Gosden, O. John Semmes and Abdelali Haoudi. Human LINE-1 retrotransposon induces DNA damage and apoptosis in cancer cells. Cancer Cell International 6:13-22, 2006.